Modeling and Simulation of The CERTS Microgrid: A Comparative Study Using PSCAD and MATLAB SIMSCAPE

by

Muhammad Umar

B. Eng. University of Ontario Institute of Technology, Canada, 2016

A thesis submitted to the

School of Graduate and Postdoctoral Studies in partial

fulfillment of the requirements for the degree of

Master of Applied Science

in

The Faculty of Engineering and Applied Science

Electrical and Computer Engineering

University of Ontario Institute of Technology (Ontario Tech University)

April 2020

© Muhammad Umar, 2020

THESIS EXAMINATION INFORMATION

Submitted by: **Muhammad Umar**

Master of Applied Science (MASc) in Electrical and Computer Engineering

Thesis title: MODELING AND SIMULATION OF THE CERTS MICROGRID: A COMPARATIVE STUDY USING PSCAD AND MATLAB SIMSCAPE

An oral defense of this thesis took place on April 9th, 2020 in front of the following examining committee:

Examining Committee:

Chair of Examining Committee	Dr. Ying Wang
Research Supervisor	Dr. Walid Morsi Ibrahim
Research Co-supervisor	Dr. Tarlochan Sidhu
Examining Committee Member	Dr. Vijay Sood
Examining Committee Member	Dr. Mikael Eklund
Thesis Examiner	Dr. Xianke Lin

The above committee determined that the thesis is acceptable in form and content and that a satisfactory knowledge of the field covered by the thesis was demonstrated by the candidate during an oral examination. A signed copy of the Certificate of Approval is available from the School of Graduate and Postdoctoral Studies.

Abstract

The legacy electric power system has grown in magnitude and complexity since its conception. This was a result of various advancements, such as the need to match the increase in power demand, and to address the shortage of conventional sources (e.g. oil and gas). This led to the integration of Distributed Generators (DGs) into the legacy grid, thereby facilitating the incorporation of microgrids. An adverse effect can be seen with the large-scale penetration of various distributed generation (DGs) caused by the utilization of switching devices and inconsistent performance of the DGs. The effects of incorporating switching devices has led to issues such as an increase in harmonics, voltage, frequency regulation, power quality degradation, and reverse power flow.

A cost-effective approach to study the abovementioned impacts is via modelling and simulating the system in well-known simulating platforms such as Power System Computer Aided Design (PSCAD) and MATLAB Matlab-Simscape. To that note, the fundamental difference between the two simulation environments is that Matlab-Simscape is based on solving a system of ordinary differential equations (ODEs) represented in the form of matrices using ODE45 and its variations, while PSCAD utilizes electromagnetic transient including DC (EMTDC). EMTDC represents the system as differential equations for both electromagnetic and electromechanical systems in the time domain. Solutions are based on a fixed time step and the results are solved as instantaneous values in time. Therefore, modelling the same component in either of them can result in some inconsistencies in the output quantities.

In this work, the modeling of the microgrid in both simulation platforms is studied and the model transformation approach is introduced, which highlights the procedure to

model any component in the two simulation environments to generate consistent results. Additionally, both simulation platforms are studied in detail utilizing a standardized microgrid benchmark system, known as the Consortium for Electric Reliability Technology Solution (CERTS) microgrid. This CERTS configuration defines the framework necessary to measure and adjust the performance of both simulation platforms in a quantitative and qualitative manner. Furthermore, a methodology is proposed to model the various components of the microgrid in a uniform and interchangeable manner. Ultimately, the proposed methodology overcomes the differences in modelling some electrical components in each platform. In addition, the properties of each component in both software have been highlighted in detail to facilitate the transition between each platform.

Finally, this work introduces a comparative study between PSCAD and Matlab-Simscape based on the CERTS microgrid. The performance of both simulating platforms is studied in both the grid connected mode of operation and in the island mode of operation. The performance of both simulating platforms is evaluated, and the results are presented to demonstrate the validity of the modeling techniques. The results have shown that the difference between the quantities measured at the same point of measurement in both simulation platforms are less than 1%, which verifies that the modeling technique results in uniform outcomes in both PSCAD and Matlab-Simscape.

AUTHOR'S DECLARATION

I hereby declare that this thesis consists of original work of which I have authored. This is a true copy of the thesis, including any required final revisions, as accepted by my examiners.

I authorize the University of Ontario Institute of Technology (Ontario Tech University) to lend this thesis to other institutions or individuals for the purpose of scholarly research. I further authorize University of Ontario Institute of Technology (Ontario Tech University) to reproduce this thesis by photocopying or by other means, in total or in part, at the request of other institutions or individuals for the purpose of scholarly research. I understand that my thesis will be made electronically available to the public.

STATEMENT OF CONTRIBUTIONS

The primary contribution of this thesis is to develop a methodology to model the CERTS microgrid. The objective is to uniformly model the CERTS microgrid in PSCAD and Matlab-Simscape, which enables the evaluation of the performance of both simulation environments. Such a study is crucial in identifying the pros and cons of each simulation environment when modeling and simulating microgrids given the complexities which arise when integrating renewable distributed energy resources.

I hereby certify that I am the sole author of this thesis and that no part of this thesis has been published or submitted for publication. I have used standard referencing practices to acknowledge ideas, research techniques, or other materials that belong to others. Furthermore, I hereby certify that I am the sole source of the creative works and/or inventive knowledge described in this thesis.

Acknowledgements

I would like to express my sincere gratitude to my supervisors Dr. Walid Morsi Ibrahim and Dr. Tarlochan Sidhu for their guidance and support throughout the duration of my graduate studies. I would like to sincerely thank my colleagues in my research group in the Smart Grid and Electric Vehicles Research Laboratory. I would also like to thank the University of Ontario Institute of Technology for providing me with the opportunity to carry on with my graduate studies. Lastly, I would like to thank my parents for all the love, support and the guidance. My parents provided me with enough resources and training to conquer any challenges life presents.

No two things have been combined better than knowledge and patience.

- Prophet Muhammad (Peace and Blessings Be Upon Him)

Dedication

This dissertation is dedicated to my Parents Muhammad Arshad & Saima Shaheen, who instilled in me the virtues of perseverance and commitment and relentlessly encouraged me to strive for excellence.

Table of Contents

Thesis Examination Information……..……....i
Abstract……..……..ii
Author's Declaration……...iv
Statement of Contributions……..v
Acknowledgements……..…….....vi
Dedication……..vii
List of tables…….x
List of figures…….....xi
Nomenclature……...xvii
1. Introduction 1
1.1. Background 1
1.1.1 Legacy Grid 1
1.1.2 Smart Grid 2
1.1.3 Microgrid System 4
1.2. Problem Statement and Motivation 8
1.3. Research Objectives 10
1.4. Contribution 10
1.5. Thesis Organization 11
2. Literature Review 13
2.1. Introduction 13
2.2. Previous Work on Modelling and Simulation of Microgrids 13
2.2.1 PSCAD and MATLAB Matlab-Simscape 13
2.3. Consortium for Electric Reliability Technology Solutions (CERTS) 18
2.4. Research Gaps 25
2.5. Summary 26
3. CERTS Micro-Grid Testbed System 28
3.1. Introduction 28
3.2. CERTS Micro-Grid Testbed System 28
3.3. Modelling of the CERTS Microgrid Testbed System 33
3.3.1 Discrepancies Between the Two Simulation Platforms 34

3.3.2 Reduced CERTS System with no Distributed Generation 34
3.3.3 Source of Inconsistency 36
3.3.4 Load Modelling Methodology 38
3.4. Voltage Source Converter Control Methodologies 41
3.4.1 Current-Mode Control 41
3.4.2 Modified Current-Mode Control with DC Link Voltage 43
3.4.3 Frequency Mode Control 45
3.5. Data Acquisition and the Recorded Parameters 47
3.6. Summary 51
4. Results and Evaluation 53
4.1. Introduction 53
4.2. Test System Description 54
4.3. Grid Connected Mode 57
4.3.1 PSCAD Simulation Grid Connected Mode 58
4.3.2 Matlab-Simscape Simulation Grid Connected Mode 76
4.3.3 PSCAD and Simulink in Grid Connected Mode Comparative Study 94
4.4. Island Mode of Operation 102
4.4.1 PSCAD Simulation Island Mode of Operation 103
4.4.2 Matlab-Simscape Simulation Island Mode of Operation 119
4.4.3 PSCAD and Simulink in Island Mode Comparative Study 135
5. Conclusion and Recommendations 141
5.1. Conclusion 141
5.2. Recommendations 143
5.3. Future Work 144
References 146
Appendix A 151
Appendix B 152

List of tables

Table 2.1: Variable-step continuous implicit solvers 16
Table 2.2: Variable-step continuous explicit solvers 16
Table 2.3: Modelling, simulation and analysis of microgrids 24
Table 3.1: Source (Utility) parameters 30
Table 3.2: Transformer (T1) parameters 30
Table 3.3: Transmission line 16 parameters (TL16) 30
Table 3.4: Load 6 parameters (L6) 30
Table 3.5: Transmission line 25 parameters (TL25) 31
Table 3.6: Load 5 parameters (L5) 31
Table 3.7: Transmission line 33 parameters (TL33) 31
Table 3.8: Transmission line 35 parameters (TL35) 31
Table 3.9: Transmission line 34 parameters (TL34) 32
Table 3.9: Load 3 parameters (L3) 32
Table 3.10: Load 4 parameters (L4) 32
Table 3.11: Positive and Zero Sequence transmission line reactance 32
Table 3.12: Battery energy storage parameters (DER-Bt.S) 33
Table 3.13: Photovoltaic array 1 parameters (DER-PV1) 33
Table 3.14: Photovoltaic array 2 parameters (DER-PV2) 33
Table 3.15: Input parameters required based on simulation environment 37
Table 3.16: Load input parameters 39
Table 4.1: Mean, MAD and Variance of Load 6 76
Table 4.2: Mean, MAD and Variance of Load 5 76
Table 4.3: Mean, MAD and Variance of Load 4 76
Table 4.4: Mean, MAD and Variance of Load 3 76
Table 4.5: Mean, MAD and Variance of Load 6 94
Table 4.6: Mean, MAD and Variance of Load 5 94
Table 4.7: Mean, MAD and Variance of Load 4 94
Table 4.8: Mean, MAD and Variance of Load 3 94
Table 4.9: Mean, MAD and Variance of Load 5 118
Table 4.10: Mean, MAD and Variance of Load 4 119
Table 4.11: Mean, MAD and Variance of Load 3 119
Table 4.12: Mean, MAD and Variance of Load 5 134
Table 4.13: Mean, MAD and Variance of Load 4 135
Table 4.14: Mean, MAD and Variance of Load 3 135

List of figures

Fig 1.1: Legacy power system 2
Fig 1.2 Smart grid infrastructure 4
Fig 1.3 Microgrid system 5
Fig 2.1: Runge-Kutta Method 17
Fig 2.2: Trapezoidal Integration 18
Fig 3.1: CERTS microgrid in grid connected mode of operation 29
Fig 3.2: CERTS microgrid in island mode of operation 29
Fig 3.3: Basic system with no distributed generation 35
Fig 3.4: Single branch system 36
Fig 3.5: Transmission line represented by lumped resistance and inductance 36
Fig 3.6. Load represented as resistance and capacitance 40
Fig 3.7. Load represented as resistance and capacitance 40
Fig 3.8: Current mode control 43
Fig 3.9: Modified current mode control 45
Fig 3.10: Frequency mode control 46
Fig 3.11: Points of measurement for CERTS microgrid 51
Fig 4.1: Distributed Generation DC and AC Measurement Locations 55
Fig 4.2: Load Measurement Location 57
Fig 4.3: DG1 DC Side Point of Measurement 59
Fig 4.4: DC Link Voltage DG1 59
Fig 4.5: DC Link Current DG1 59
Fig 4.6: DG1 AC Side Point of Measurement 60
Fig 4.7: Voltage RMS at Point of Coupling 60
Fig 4.8: Voltage THD at Point of Coupling 60
Fig 4.9: Current RMS at Point of Coupling 61
Fig 4.10: Current THD at Point of Coupling 61
Fig 4.11: DG2 DC Side Point of Measurement 62
Fig 4.12: DC Link Voltage DG2 62
Fig 4.13: DC Link Current DG2 62
Fig 4.14: DG2 AC Side Point of Measurement 63
Fig 4.15: Voltage RMS at Point of Coupling 63
Fig 4.16: Voltage THD at Point of Coupling 63
Fig 4.17: Current RMS at Point of Coupling 64
Fig 4.18: Current THD at Point of Coupling 64
Fig 4.19: DG3 DC Side Point of Measurement 65
Fig 4.20: DC Link Voltage DG3 65
Fig 4.21: DC Link Current DG3 65
Fig 4.22: DG3 AC Side Point of Measurement 66
Fig 4.23: Voltage RMS at Point of Coupling 66
Fig 4.24: Voltage THD at Point of Coupling 66
Fig 4.25: Current RMS at Point of Coupling 67

Fig 4.26: Current THD at Point of Coupling 67
Fig 4.27: Load Measurement Point 68
Fig 4.28: Voltage RMS at Load 6 68
Fig 4.29: Voltage THD at Load 6 68
Fig 4.30: Current RMS at Load 6 69
Fig 4.31: Current THD at Load 6 69
Fig 4.32. Load 5 Measurement Point 70
Fig 4.33: Voltage RMS at Load 5 70
Fig 4.34: Voltage THD at Load 5 70
Fig 4.35: Current RMS at Load 5 71
Fig 4.36: Current THD at Load 5 71
Fig 4.37: Load 4 Measurement Point 72
Fig 4.38. Voltage RMS at Load 4 72
Fig 4.39. Voltage THD at Load 4 72
Fig 4.40: Current RMS at Load 4 73
Fig 4.41: Current RMS at Load 4 73
Fig 4.42: Load 3 Measurement Point 74
Fig 4.43: Voltage RMS at Load 3 74
Fig 4.44: Voltage THD at Load 3 74
Fig 4.45: Current RMS at Load 3 75
Fig 4.46: Current RMS at Load 3 75
Fig 4.47: DG1 DC Side Point of Measurement 77
Fig 4.48: DC Link Voltage DG1 78
Fig 4.49: DC Link Current DG1 78
Fig 4.50: DG1 AC Side Point of Measurement 78
Fig: 4.51: Voltage RMS at Point of Coupling 79
Fig: 4.52: Voltage THD at Point of Coupling 79
Fig: 4.53: Current RMS at Point of Coupling 79
Fig: 4.54. Current THD at Point of Coupling 79
Fig 4.55: DG2 DC Side Point of Measurement 80
Fig 4.56: DC Link Voltage DG2 81
Fig 4.57: DC Link Current DG2 81
Fig 4.58: DG2 AC Side Point of Measurement 81
Fig 4.59. Voltage RMS at Point of Coupling 82
Fig 4.60. Voltage THD at Point of Coupling 82
Fig 4.61. Current RMS at Point of Coupling 82
Fig 4.62. Current THD at Point of Coupling 82
Fig 4.63: DG3 DC Side Point of Measurement 83
Fig 4.64: DC Link Voltage DG3 84
Fig 4.65: DC Link Current DG3 84
Fig 4.66: DG3 AC Side Point of Measurement 84
Fig 4.67: Voltage RMS at Point of Coupling 85
Fig 4.68: Voltage THD at Point of Coupling 85

Fig 4.69: Current RMS at Point of Coupling 85
Fig 4.70: Current THD at Point of Coupling 85
Fig 4.71: Load 6 Measurement Point 86
Fig 4.72: Voltage RMS at Load 6 87
Fig 4.73: Voltage THD at Load 6 87
Fig 4.74: Current RMS at Load 6 87
Fig 4.75: Current THD at Load 6 87
Fig 4.76: Load 5 Measurement Point 88
Fig 4.77: Voltage RMS at Load 5 88
Fig 4.78: Voltage THD at Load 5 88
Fig 4.79. Current RMS at Load 5 89
Fig 4.80. Current THD at Load 5 89
Fig 4.81. Load 4 Measurement Point 90
Fig 4.82. Voltage RMS at Load 4 90
Fig 4.83. Voltage THD at Load 4 90
Fig 4.84. Current RMS at Load 4 91
Fig 4.85. Current THD at Load 4 91
Fig 4.86. Load 3 Measurement Point 92
Fig 4.87. Voltage RMS at Load 3 92
Fig 4.88 Voltage THD at Load 3 92
Fig 4.89. Current RMS at Load 3 93
Fig 4.90. Current THD at Load 3 93
Fig 4.91A: PSCAD Voltage RMS Load 6 95
Fig 4.91B: Simulink Voltage RMS Load 6 95
Fig 4.92A: PSCAD Voltage THD Load 6 95
Fig 4.92B: Simulink Voltage THD Load 6 95
Fig 4.93A: PSCAD Current RMS Load 6 96
Fig 4.93B: Simulink Current RMS Load 6 96
Fig 4.94A: PSCAD Current THD Load 6 96
Fig 4.94B: Simulink Current THD Load 6 96
Fig 4.95A: PSCAD Voltage RMS Load 5 97
Fig 4.95B: Simulink Voltage RMS Load 5 97
Fig 4.96A: PSCAD Voltage THD Load 5 97
Fig 4.96B: Simulink Voltage THD Load 5 97
Fig 4.97A: PSCAD Current RMS Load 5 97
Fig 4.97B: Simulink Current RMS Load 5 97
Fig 4.98A: PSCAD Current THD Load 5 98
Fig 4.98B: Simulink Current THD Load 5 98
Fig 4.99A: PSCAD Voltage RMS Load 4 98
Fig 4.99B: Simulink Voltage RMS Load 4 98
Fig 4.100A: PSCAD Voltage THD Load 4 99
Fig 4.100B: Simulink Voltage THD Load 4 99
Fig 4.101A: PSCAD Current RMS Load 4 99

Fig 4.101B: Simulink Current RMS Load 4 99
Fig 4.102A: PSCAD Current THD Load 4 99
Fig 4.102A: Simulink Current THD Load 4 99
Fig 4.103A: PSCAD Voltage RMS Load 3 100
Fig 4.103B: Simulink Voltage RMS Load 3 100
Fig 4.104A: PSCAD Voltage THD Load 3 100
Fig 4.104B: Simulink Voltage THD Load 3 100
Fig 4.105A: PSCAD Current RMS Load 3 101
Fig 4.105B: Simulink Current RMS Load 3 101
Fig 4.106A: PSCAD Current THD Load 3 101
Fig 4.106B: Simulink Current THD Load 3 101
Fig 4.107: CERTS Microgrid Schematic Islanded Mode of Operation 103
Fig 4.108: DG1 DC Side Point of Measurement 104
Fig 4.109: DC Link Voltage DG1 104
Fig 4.110: DC Link Current DG1 104
Fig 4.111: DG AC Side Point of Measurement 105
Fig 112: Voltage RMS at Point of Coupling 105
Fig 113: Voltage THD at Point of Coupling 105
Fig 114: Current RMS at Point of Coupling 106
Fig 4.115: Current THD at Point of Coupling 106
Fig 4.116: DG2 DC Side Point of Measurement 107
Fig 4.117: DC Link Voltage DG2 107
Fig 4.118: DC Link Current DG2 107
Fig 4.119: DG2 AC Side Point of Measurement 108
Fig 4.120: Voltage RMS at Point of Coupling 108
Fig 4.121: Voltage THD at Point of Coupling 108
Fig 4.122: Current RMS at Point of Coupling 109
Fig 4.123: Current THD at Point of Coupling 109
Fig 4.124: DG3 DC Side Point of Measurement 110
Fig 4.125: DC Link Voltage DG3 110
Fig 4.126: DC Link Current DG3 110
Fig 4.127: DG3 AC Side Point of Measurement 111
Fig 4.128: Voltage RMS at Point of Coupling 111
Fig 4.129: Voltage THD at Point of Coupling 111
Fig 4.130: Current RMS at Point of Coupling 112
Fig 4.131: Current THD at Point of Coupling 112
Fig 4.132: Load 5 Measurement Point 113
Fig 4.133: Voltage RMS at Load 5 113
Fig 4.134 Voltage THD at Load 5 113
Fig 4.135: Current RMS at Load 114
Fig 4.136: Current THD at Load 114
Fig 4.137: Load 4 Measurement Point 115
Fig. 4.138: Voltage RMS at Load 4 115

Fig 4.139: Voltage THD at Load 4 115
Fig 4.140: Current RMS at Load 4 116
Fig 4.141: Current THD at Load 4 116
Fig 4.142. Load 3 Measurement Point 117
Fig 4.143: Voltage RMS at Load 3 117
Fig 4.144: Voltage THD at Load3 117
Fig 4.145: Current RMS at Load 3 118
Fig 4.146: Current THD at Load 3 118
Fig 4.147: DG1 DC Side Point of Measurement 120
Fig 4.148: DC Link Voltage DG1 120
Fig 4.149: DC Link Current DG1 120
Fig 4.150: DG1 AC Side Point of Measurement 121
Fig 4.151: Voltage RMS at Point of Coupling 121
Fig 4.152: Voltage THD at Point of Coupling 121
Fig 4.153: Current RMS at Point of Coupling 122
Fig 4.154: Current THD at Point of Coupling 122
Fig 4.155: DG2 DC Side Point of Measurement 123
Fig 4.156: DC Link Voltage DG2 123
Fig 4.157: DC Link Current DG2 123
Fig 4.158: DG2 AC Side Point of Measurement 124
Fig 4.159: Voltage RMS at Point of Coupling 124
Fig 4.160: Voltage THD at Point of Coupling 124
Fig 4.161: Current RMS at Point of Coupling 125
Fig 4.162: Current THD at Point of Coupling 125
Fig 4.163: DG3 DC Side Point of Measurement 126
Fig 4.164: DC Link Voltage DG3 126
Fig 4.165: DC Link Current DG3 126
Fig 4.166: DG3 AC Side Point of Measurement 127
Fig 4.167: Voltage RMS at Point of Coupling 127
Fig 4.168: Voltage THD at Point of Coupling 127
Fig 4.169: Current RMS at Point of Coupling 128
Fig 4.170: Current THD at Point of Coupling 128
Fig 4.171: Load 5 Measurement Point 129
Fig 4.172: Voltage RMS at Load 5 129
Fig 4.173: Voltage THD at Load 5 129
Fig 4.174: Current RMS at Load 5 130
Fig 4.175: Current THD at Load 5 130
Fig 4.176: Load 4 Measurement Point 131
Fig 4.177: Voltage RMS at Load 4 131
Fig 4.178: Voltage THD at Load 4 131
Fig 4.179: Current RMS at Load 4 132
Fig 4.180: Current THD at Load 4 132
Fig 4.181: Load 3 Measurement Point 133

Fig 4.182: Voltage RMS at Load 3 133
Fig 4.183: Voltage THD at Load 3 133
Fig 4.184: Current RMS at Load 3 134
Fig 4.185: Current THD at Load 3 134
Fig 4.186A: PSCAD Voltage RMS Load 5 136
Fig 4.186B: Simulink Voltage RMS Load 5 136
Fig 4.187A: PSCAD Voltage THD Load 5 136
Fig 4.187B: Simulink Voltage THD Load 5 136
Fig 4.188A: PSCAD Current RMS Load 5 136
Fig 4.188B: Simulink Current RMS Load 5 136
Fig 4.189A: PSCAD Current THD Load 5 137
Fig 4.189B: Simulink Current THD Load 5 137
Fig 4.190A: PSCAD Voltage RMS Load 4 137
Fig 4.190B: Simulink Voltage RMS Load 4 137
Fig 4.191A: PSCAD Voltage THD Lo 4 138
Fig 4.191B: Simulink Voltage THD Lo 4 138
Fig 4.192A: PSCAD Current RMS Load 4 138
Fig 4.192B: Simulink Current RMS Load 4 138
Fig 4.193A: PSCAD Current THD Load 4 138
Fig 4.193A: Simulink Current THD Load 4 138
Fig 4.194A: PSCAD Voltage RMS Load 3 139
Fig 4.194B: Simulink Voltage RMS Load 3 139
Fig 4.195A: PSCAD Voltage THD Load 3 139
Fig 4.195B: Simulink Voltage THD Load 3 139
Fig 4.196A: PSCAD Current RMS Load 3 140
Fig 4.196B: Simulink Current THD Load 3 140
Fig 4.197A: PSCAD Current THD Load 3 140
Fig 4.197B: Simulink Current THD Load 3 140

Nomenclature

AC	Alternating Current
AEP	American Electric Power
BES	Battery Energy Storage
Bt.S	Battery Storage
CERTS	Consortium of Electric Reliability Technology Solution
CFL	Compact Fluorescent Lamp
DC	Direct Current
DER	Distributed Energy Resource
DG	Distributed Generation
EMTDC	Electromagnetic Transient Including DC
ES	Energy Storage
FFT	Fast Fourier Transform
HVDC	High Voltage Direct Current
I	Current
LED	Light Emitting Diode
L-G	Line to Ground Value
L-L	Line to Line Value
MAD	Mean Absolute Deviation
ODE	Ordinary Differential Equation
P	Active Power
PCC	Point of Common Coupling
PLL	Phase Locked Loop
PSCAD	Power System Computer Aided Design
PV	Photovoltaic
PWM	Pulse Width Modulation
Q	Reactive Power
RMS	Root Mean Square
RTDS	Real Time Digital Simulator
S	Apparent Power
THD	Total Harmonic Distortion
V	Voltage
V_n	Nominal Voltage
VSC	Voltage Source Converter

1. Introduction

1.1. Background

The advent of electricity resulted in the creation of the power system. Over the years, the power system has evolved to adapt to the changes that result from the demands of the consumers connected to the grid. These users vary from residential to commercial customers, hence these variations in the grid are a result of the changes in the loads connected to the grid. A prime example is the light bulb itself, which is a very basic load but has undergone a versatile transformation. The light bulb evolved from the resistive incandescent to the compact fluorescent (CFL) to the light emitting diode (LED) bulbs [1]. With the development of modern components such as electric vehicles, renewable energy, modern loads such as smart appliances, smart switches (i.e. increased number of loads that are being supplied by switch mode power supplies).

1.1.1 Legacy Grid

The legacy power system is a network constructed by the connection of electrical components capable of generating, transmitting and distributing electricity. In the legacy grid, the power is generated from a central power generation unit and is distributed to the consumer, which is known as a unidirectional power flow. The power system consists of three different zones. The first one being the generation zone, in which the power is generated at a central facility using one of the many different types of generation. The second is the transmission zone, where the voltage is stepped up and transmitted to the distribution system. Finally, in the distribution zone, the voltage is stepped down to a level which is safe to be used by the consumer. Figure 1.1 shows the typical legacy power system. Over the years, the grid has increased in magnitude and complexity, as the number of users increased. As a result, electricity was made readily available to the masses, which

enabled the innovation of new technology such as computers, photovoltaic, and electric cars.

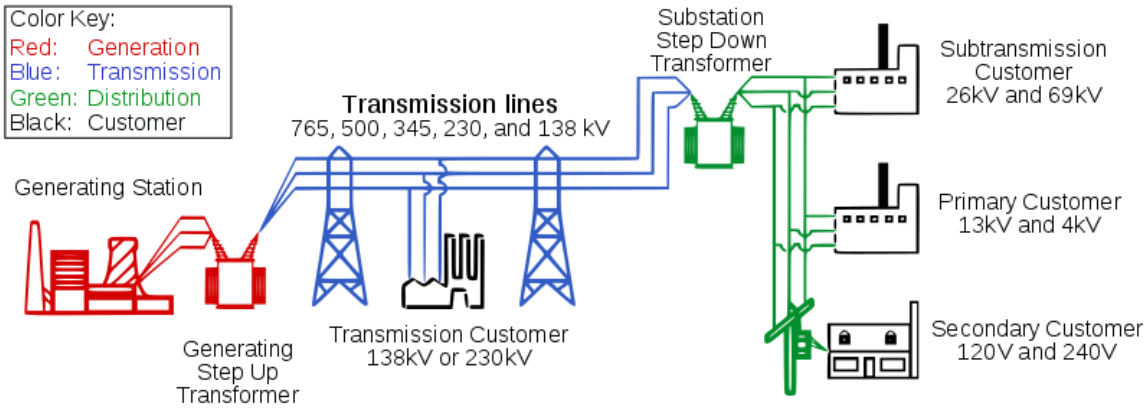

Fig 1.1: Legacy power system [2]

1.1.2 Smart Grid

In the legacy electric power system, the electricity produced is generated at a central facility and then transmitted to the end-user. The development of distributed energy resources has enabled the end-user to change roles from consumer to a prosumer. In a classical grid, the end-user would strictly consume electricity, whereas now consumers have the ability to generate electricity, thus earning them the title of prosumers. As the grid evolves, there arises a need for the grid to communicate data between different components within the grid. Not to mention, the development of technology such as electric vehicles has led to a steep increase in consumer demand [3]. As a result, a smart grid needs to be introduced, which is capable of providing the communication infrastructure, controls and distributed energy resource integration, along with the basic capabilities of the legacy power grid, as shown in figure 1.2 [3], [4].

A smart grid is an up-to-date and self-sufficient electricity supply system, which incorporates communication systems into the current electrical grid. This enables the

components in the grid to store and transfer data amongst each other. Computers, sensors and monitoring devices are utilized in order to improve the reliability, efficiency and safety of the system. A smart grid enables the monitoring and communication from the generation level to the consumer distribution level [5]. The smart grid is utilized in order to make the power system more efficient in terms of energy consumption, efficiency and reliability. As a result, the system is capable of monitoring, analyzing and controlling the power system. The smart grid is capable of healing itself; it allows consumers to be a part of the operation of the grid and it helps maintain the power quality of the electric power being supplied. The incorporation of the communication interface is vital in the smart grid as it allows for load handling, demand response and decentralization of power. The consumers can participate through demand side management and demand response programs to reduce the strain on the electric power network. Furthermore, the consumers can produce electricity using renewable energy resources such as wind and solar, in this case they are called prosumers (power producers and consumers). Given this change in the electric power grid, the widespread integration of renewable energy sources may lead to stability problems. There is a dire need for system impact studies in particular when considering microgrid operation and hence developing detailed and accurate models of microgrids becomes of paramount importance [6]–[8].

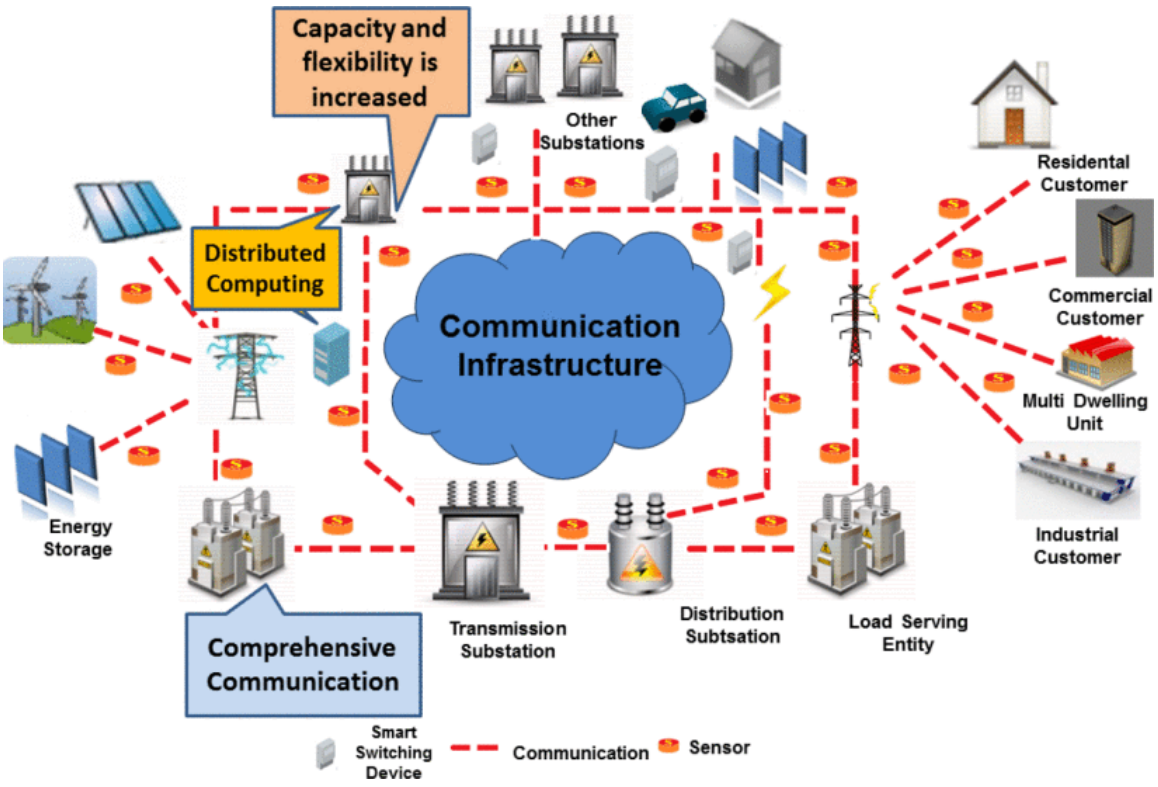

Fig 1.2 Smart grid infrastructure [4]

1.1.3 Microgrid System

A microgrid system is a network of electrical components such as distributed energy resources, energy storage systems and various types of loads, as shown in figure 1.3 [10]. The microgrid is capable of operating in two different modes of operation. The first one being the grid-connected mode and the second one being islanded mode of operation. During the grid-connected mode the distributed energy resources operate and generate electricity in parallel with the grid, where energy not being consumed is sent back to the grid. The microgrid operates in the islanded mode when the utility grid faces services interruptions such as power outages or power quality issues. Microgrids are designed in order to provide back-up power to crucial loads such as hospitals and airports. The

microgrid enables these loads to operate more efficiently along with improved reliability and power quality.

Fig 1.3 Microgrid system [10]

There are a variety of distributed generator (DG) types employed in microgrids across the world, some examples include photovoltaic arrays, energy storage, wind and fossil fuel powered generators. The output capacity of these DGs can range from small to rather large. The integration of such DGs effects the grid performance in both transient and steady state operation. This can be caused by numerous factors such as the inverters employed and the location of the point of common coupling of the DGs into the grid [11]–[15],[16]–[19]. Furthermore, a large-scale penetration of DGs in the grid can have an adverse impact on the operation of the grid. This can result in issues such as an increase in harmonics, voltage, frequency regulation, power quality degradation and a reversal in the direction of the power flow [20]–[27]. Moreover, as the penetration of DGs increases, there

arises a need to have well designed protection schemes. The objective of such protection schemes is to protect the DG itself in the event of a system interruption [28]–[30].

Based on the aforementioned discussion, a more practical study needs to be performed pertaining to microgrids. In order to do so, it is essential to construct a standardized microgrid such as the CERTS microgrid mentioned earlier. However, building such a system is a very costly endeavor, as the components and space required are very expensive to acquire and maintain. A suitable and cost-effective substitute to the practical approach is to model and simulate the CERTS microgrid using well known simulation platforms such as PSCAD, EMTP, MATLAB Matlab-Simscape and OpenDSS. From among the previously stated software the PSCAD and Matlab-Simscape are vastly employed in academia and industry.

Matlab-Simscape relies on the Simscape library[31], which enables the user to model and simulate different components and types of configurations relevant to the power systems. Simscape is part of Matlab and houses the Power System Library. In a similar manner to Matlab-Simscape, PSCAD enables the user to graphically represent the various components of a power system. PSCAD enables the user to monitor and control output data in a graphical environment. PSCAD models can be ported into real time simulators such as Real Time Digital Simulator (RTDS)[32], [33]. The key difference between the two simulation environments is that Matlab-Simscape is the solver type they utilize. In order to simulate a dynamic system over a defined time, it is necessary to compute the states of the model at successive time steps. These computations are based on the states described in the system state space model. A state space model is a set of first order

ordinary differential equations ODE that describes the dynamics and behavior of the system. This is the process to compute the states of the model being simulated.

A solver utilizes numerical methods (such as trapezoidal, Runge-Kutta, etc.) in order to evaluate the ordinary differential equations which represent the system. The proceeding time steps are determined based on the computation of the current state. These intervals are referred to as the solver's time steps.

A wide variety of numerical integration techniques have been developed for solving the ordinary differential equations (ODEs). A variety of fixed-step and variable step continuous solvers are developed in both simulation platforms, each of which utilizes a specific ODE solution methodology.

In general, the selection of an appropriate solver is based on matching the following criteria; system dynamics, solution stability, computation speed and solver robustness. Moreover, solvers can be classified based on the type of the time step they utilize into two types: fixed time step and variable time step [31].

A fixed step solver utilizes a consistent time step throughout the duration of the simulation. The step size can be predetermined or specified by the solver. A lower step size increases the accuracy of the results and the computation time to simulate the system.

On the other hand, variable step solvers, vary the step size during the simulation. In the event of rapid state changes, zero-crossing events and so on the time step is decreased in order to increase the accuracy of the system and to represent the signal accurately. In the event of slow state changes the time step can be increased in order to reduce the computation time.

Simulink offers the following solvers which offers fixability to tailor the accuracy of the simulation results. If a fixed time step is needed, Matlab-Simscape offers the following solvers ode3 and Runge-Kutta. For variable step size, wide variety of solvers are available as well, such as, ode15s and ode45.

By comparison, PSCAD utilizes EMTDC engine as its solver. It doesn't have the flexibility of choosing multiple solvers as in Matlab-Simscape. EMTDC (which stands for Electromagnetic Transients including DC) represents and solves the sets of ordinary differential equations ODEs (for both electromagnetic and electromechanical systems) in the time domain. Solutions are evaluated based on a fixed time step, and it allows for the representation of not only the power system components but also extends to the control systems, either with or without the implementation of electromagnetic or electromechanical systems [32], [33].

Henceforth, as both platforms utilize different engines, modelling the same component in either of them can result in some inconsistencies in the output quantities (voltage, current, and frequency). The key findings and differences have been highlighted in Appendix A. Thus, further work is necessary in order to fill such gaps between them as discussed in the following section.

1.2. Problem Statement and Motivation

Due to the widespread use of the microgrids, there is a growing need to model and simulate these microgrids. There are numerous software programs, which are employed in industry, but the two most common ones are MATLAB Matlab-Simscape and PSCAD. Both these simulating environments are great tools, which are capable of representing the microgrid systems, but which of these systems has the least computational time, which is

more efficient and finally which is more reliable. The answers to these questions enable faster computation time and a reduction in computation power needed.

There are numerous challenges, which may arise in the process of modelling and simulating the microgrid in PSCAD and Matlab-Simscape. One of the challenges is the control associated with the various types of distributed energy resources such as solar and battery energy storage systems. The main challenge, which arises is the maintenance of uniformity between the two simulating software, a prime example would be the photovoltaic array block in both PSCAD and Matlab-Simscape as different parameters are required in both simulation environments, one requires more details than the other. This same issue must be dealt with for all the other components utilized in the simulation.

In the literature and after studying research work, it is evident that there is a lack of studies, which provide a methodology for the modelling and simulation of micro-girds. There is also a lack in the previous work, which performs a comparative study of the two simulation environments, in order to determine which of the two is superior. However, there is a large volume of studies, which utilize microgrids in order to perform other studies such as power control, stability analysis, disturbance detection and frequency control to name a few.

The primary motivation for this research work is to introduce a methodology to model and simulate the CERTS microgrid testbed system in an efficient and reliable manner in both PSCAD and Matlab-Simscape. In order to do so, very close attention must be utilized in order to maintain uniformity in both PSCAD and Matlab-Simscape. Many of the factors which are involved in the modelling and simulation are very sensitive. A small

variation in any of these factors can result in large differences in the solution as the error propagates. Some of these factors include the solver type, step size and the simulation time. The solver type is a crucial factor as it is responsible for the numerical solution of the differential equations, this is especially true considering that both PSCAD and Matlab-Simscape represent the model as a set of differential equations. The CERTS microgrid testbed system is modelled in both simulating environments to evaluate the performance of the two simulation environments and to verify the effectiveness, robustness and accuracy of the solution. Steady state analysis is used in order to complete a comprehensive study of the CERTS microgrid testbed system. An evaluation scheme is developed to assess the performance of PSCAD and Matlab-Simscape under steady state conditions.

1.3. Research Objectives

The following list summarizes the objectives of this work:

- The purpose of this work is to introduce a methodology, which allows the modelling and simulation of the CERTS microgrid testbed system using two different simulation software namely PSCAD and Matlab-Simscape.
- This work aims to study the behavior of the CERTS microgrid testbed system when integrated with distributed renewable energy resources in the steady state.
- Lastly to study the performance of the two simulation environment in terms of the computation time, memory usage and total simulation time.

1.4. Contribution

The primary contribution of this thesis is to develop a methodology to model the CERTS microgrid. The objective is to uniformly model the CERTS microgrid in PSCAD

and Matlab-Simscape, which enables the evaluation of the performance of both simulation environments. Such a study is crucial in identifying the pros and cons of each simulation environment when modeling and simulating microgrids given the complexities which arise when integrating renewable distributed energy resources.

1.5. Thesis Organization

This thesis consists of six chapters. Chapter one provides an introduction to the problem being addressed. In this chapter the need to develop a comparative study for the simulation and modelling of the CERTS microgrid testbed system is outlined. Followed by the problem statement.

Chapter two discusses the literature review, which provides a comprehensive overview of the current work conducted in the research field on the simulation and modelling of microgrids and specifically the CERTS microgrid. The research gaps were identified, and the purpose of the proposed research is presented.

Chapter three introduces the proposed microgrid to be modelled and simulated. A detailed description of the CERTS microgrid is presented illustrating all of its components and specification related to each of the components. Details regarding the simulation parameters of both PSCAD and Matlab-Simscape are discussed. Details regarding the modelling and simulation of the CERTS microgrid are discussed such as solver type, simulation time, time step, distributed energy resource type and the control associated with each aspect of the microgrid.

Chapter four discusses the development of a methodology consisting of a certain set of tools utilized to evaluate the results and findings. The findings are analyzed and

illustrated. The results of the application of the CERTS microgrid on both PSCAD and Matlab-Simscape are tested, evaluations are presented. Along with the execution time and the computation demands of each PSCAD and Matlab-Simscape.

Chapter five presents the main conclusions drawn from the work. Recommendations regarding the proposed methodology presented in this thesis, outlining the performance of the two simulating environments.

2. Literature Review

2.1. Introduction

The literature review is intended to provide a study of the existing research with regards to the modelling and simulation of microgrids using a variety of simulation environments. The two specific simulation software investigated were PSCAD and MATLAB Matlab-Simscape. After reviewing the works published in the past from numerous sources the reader should be able to understand existing techniques and methodologies used in the modelling and simulation of microgrids in the various simulation environments. Each of the modelling and simulation studies are evaluated based on the simulation software employed. Whether the work utilized PSCAD, Matlab-Simscape or both and whether a comparative study of the performance of microgrids in both PSCAD and Matlab-Simscape was performed or not. In order to assess the performance, the measurement of numerous parameters will be recorded, along with the type of study performed in the work. Thereupon, the comparison between the two simulation environments is performed and the differences are presented.

2.2. Previous Work on Modelling and Simulation of Microgrids

In the literature, the previous work can be grouped based on two metrics, the first being the simulation environment, which may be PSCAD, Matlab-Simscape or a comparison study employing both. The second metric would the type of the analyses performed during the study, which may be steady state analysis, transient analysis or even both these analyses employed in one study.

2.2.1 PSCAD and MATLAB Matlab-Simscape

PSCAD is a simulation tool, which is premised in the time-domain, capable of performing transient simulations of a power system and its associated controls.

. There are two categories of solvers, which are fixed-step and variable-step. A fixed-step solver computes the states of the system from the beginning to the end of the simulation time specified using a specified time step, which remains consistent throughout the simulation. The step size can be generated automatically by Matlab-Simscape /PSCAD or it can be user defined. The tradeoff however arises between step size and solver accuracy, where reducing the step size increases the solver accuracy and vice versa. In a variable-step solver type, the step size varies throughout the simulation period specified. The variation is dependent on the rate at which the states of a model change and during zero-crossing events. The step size decreases when there exists a rapid change in the model and the step size increases when the change of state in the model is slow. This helps to increase the solver accuracy while concurrently ensuring the minimal solution time and decreasing the computation time. The step size and the computation time have a unique relationship, as the step size decreases the computation time increases. As the step size increases the computation time decreases, this is a resultant of the increase and decrease respectively of the samples.

PSCAD and Matlab-Simscape both use ordinary differential equations to represent the various components of a power system. A key difference is PSCAD utilizes a fixed time step size solver whereas Matlab-Simscape allows for both fixed and dynamic step sizes. Moreover, the solver type which is based on EMTDC in PSCAD cannot be changed, and the software utilizes this for all simulations. The solver type in Matlab-Simscape can however be changed between various solver types such as Runge-Kutta, trapezoidal integration and ordinary differential equations. Another important aspect to highlight is the usage of EMTDC by PSCAD in order to mathematically reduce the system of parallel and

series branches, to reduce the amount of nodes and branches. EMTDC which is based on EMTP [32],[33] decouples the various layers of the power system such as the transmission lines, loads, sources, transformers and distributed generation. This enables the calculation of each of the components equations to be performed in parallel. Whereas in Matlab-Simscape the calculation of the states is performed in a sequential manner as the entire system is treated as one. Matlab-Simscape is better suited for small scale systems as the sequential approach will increase the total computation time for large scale systems. The variable time step capability in Matlab-Simscape can help to decrease computation time but at the cost of varying resolutions during the simulation based on the changing time step size. PSCAD is more favorable for large scale systems due to the parallel computation capability. Both PSCAD and Simulink-Scape are great tools for the modelling and simulation of the various components of a power system, but the key differences mentioned in this section should be noted.

a. Continuous and Discrete Solver

Beyond the step-size of the solver there also lies the choice of either a Continuous or Discrete solver. A continuous solver utilizes numerical integration to determine the current state of the model at a given time step. This method is dependent on the previous time steps and the state derivatives. In the continuous domain the computation relies on the calculation of the values of the discrete states of each individual block of the model at each time step. The discrete solver is used in order to compute discrete models. This method computes the next simulation time step of a model. The computation is based on the model update for each of the block in the model. Each block must update its individual discrete state.

Table 2.1: Variable-step continuous implicit solvers

ODE Solver	Order of Accuracy	Mathematical Model
Ode15s	Variable, low to high	Numerical Differentiation Models
Ode23s	Low	Second-order, modified Rosenbrock formula
Ode23t	Low	Trapezoidal rule
Ode23tb	Low	TR-BDF2

Table 2.2: Variable-step continuous explicit solvers

ODE Solver	Order of Accuracy	Mathematical Model
Ode45	Medium	• Runge-Kutta • Dormand Prince
Ode23	Low	• Runge-Kutta
Ode113	Variable, low to high	• PECE Implementation of Adams-Bashforth-Moutlon

b. Approximation Methods

The two most commonly used methods are the Runge-Kutta and the Trapezoidal integration. Runge-Kutta is a family of iterative processes used to solve differential equations. In the Runge-Kutta method, the new value of the equation can be found using the old value of the equation added to the multiplication of the slope and step size. This process can be seen in figure 2.1 and in equations 2.1 and 2.2.

$$y_{i+1} = y_i + \emptyset h \tag{2.1}$$

Where

y_{i+1} is the new values of the function, y_i is the current value of the function, $\emptyset$ is the slope and h is the step size.

$$y_{i+1} = y_i + \int_{x_i}^{x_{i+1}} f(x, y)\, dx \tag{2.2}$$

Where

y_{i+1} is the new values of the function and y_i is the current value of the function. x_i is the initial position and x_{i+1} is the subsequent (final) position.

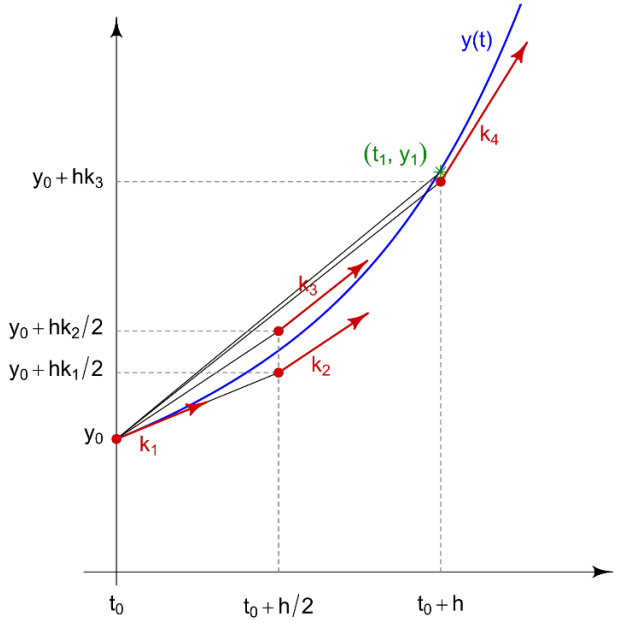

Fig 2.1: Runge-Kutta Method

The Trapezoidal Integration rule is a method utilized to solve a set of ordinary differential equations (ODE). This is done through calculating the area under the curve of the equation. The curve is sliced into n number of individual trapezoids, then the area of each trapezoid is calculated and the summation of the area of the n-set of trapezoids. This can be seen in equation 2.3-2.5 and in figure 2.2 below.

$$\int_a^b f(x)dx \cong \frac{\Delta x}{2}[f(x_0) + 2f(x_1) + 2f(x_2) + \cdots + 2f(x_{n-1}) + f(x_n)] \quad (2.3)$$

Where

Δ_x is the length of the trapezoid segment of the function and $[a\ b]$ is the initial and final condition being evaluated

$$\Delta_x = \frac{b-a}{n} \quad (2.4)$$

$$x_i = a + i\Delta x \quad (2.5)$$

Where

x_i is the i^{th} point to be evaluated and i is the segment number.

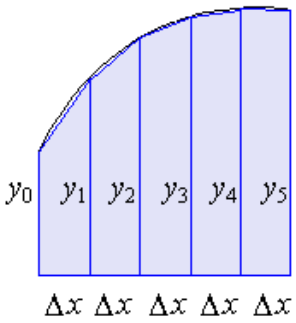

Fig 2.2: Trapezoidal Integration

2.3. Consortium for Electric Reliability Technology Solutions (CERTS)

The Consortium for Electric Reliability Technology Solutions (CERTS) is a microgrid developed by the American Electric Power (AEP) to overcome challenges faced when the penetration of distributed energy resources increases and the control related difficulties which arise as a result. The AEP is the largest electric utility in the Midwestern

United States. The CERTS microgrid was developed in the year 1998, it is a cluster of microgenerators and can operate in two different modes of operation. The CERTS microgrid was created as a benchmark system in order to provide a systematic approach to integrate distributed generation into the existing grid. The objective was the provide the methodology necessary to integrate various types of distributed generation into the grid along with their respective controls. As newer and greater capacity renewable generation would be introduced, the approach to integrate them into the existing grid would remain the same. The CERTS testbed system is seldom used by any work in the literature and at the same time it is a full-scale test bed system, which is being operated. This qualifies the CERTS microgrid as a prime candidate to be employed in the study conducted in this thesis.

Based on the study of the literature, it was evident that the modelling and simulation of the CERTS microgrid testbed system was not researched in detail. To add to the previous point, it is evident that studies that compare the performance of the two most commonly used simulation software for the same microgrid are rare. Upon further investigation, it became clear that numerous works utilized microgrids but for other purposes such as power control, stability analysis, disturbance detection, frequency control and load sharing [35]–[38]. It is also important to note that each of these works utilized either one of the two simulation software namely PSCAD or Matlab-Simscape and the amount of research conducted on the comparison of these software was small in scale. The previous work did not clearly justify the reasoning for the solver type, simulation time, analysis type and the system chosen to be modelled and simulated. Majority of the work in the literature focused on development of new algorithms or improvements to the microgrid operations itself. The study conducted by Faruque et al in [20] provided a detailed study of the comparison of

the CIGRE HVDC Benchmark System simulated in PSCAD and Matlab-Simscape, along with a detailed study of both transient and steady state circumstances. This paper outlined comparison of parameters of the CIGRE HVDC Benchmark System. The measurement points were clearly identified as well as the types of events introduced during transient studies.

The works performed by Yazdani et al in [39] emphasized their efforts to the development of an enhanced control strategy utilized to tie distributed generation to the utility. The objective of this work was to improve the performance of the microgrid during transient disturbances. The study was conducted using PSCAD, where a microgrid was simulated and the results were studied. The study primarily focused on the controls and the modelling of various components utilized to construct the microgrid was not discussed in detail. Along with this, the work had not utilized the CERTS microgrid, nor was Matlab-Simscape utilized or compared with PSCAD.

The study performed by Wang et al in [40] demonstrated a hybrid AC/DC microgrid, consisting of distributed generation units with AC and DC output. The objective of this work was to reduce the process of redundant conversions from AC to DC to AC or DC to AC to DC in a microgrid. A variety of distributed generators were employed as well as varying load conditions to provide ample testing of the proposed microgrid. The modelling and simulation of the microgrid system was discussed in detail and the final system was constructed utilizing Matlab-Simscape. This work did not employ the CERTS microgrid or utilize PSCAD and it also did not perform a comparison of the results.

The work conducted in [35] gave importance to developing a different method to control the switches to change between grid connected mode and islanded mode. The paper utilized fuzzy assessment tree based short time modified Hilbert transform as a detection and classifying technique. This work explored the utilization of signal processing techniques for distributed generation. This work did not employ the CERTS microgrid or utilize PSCAD and it also did not perform a comparison of the results.

Konig et al [36] explored model for battery energy storage for microgrid in order to improve the system stability and simulation dynamics. Various amounts of details of battery energy storage models were studied. The various models studied were developed in PSCAD and their performance was compared. The parameters utilized for the comparison were voltage stability, frequency stability and total harmonic distortion. This work did not employ the CERTS microgrid but rather used another benchmark test grid. Furthermore, this work did not perform a comparative study between PSCAD and Matlab-Simscape as the system was not developed in Matlab-Simscape.

The study conducted by Sudria-Andreq et al [41] in their work focused on the description of the control algorithm of a microgrid connected to the grid. The control methodologies studied were the active power and reactive power being controlled independently. The study evaluated the impact of centralized operation mode and distributed operation mode. The work utilized Matlab-Simscape to develop and model the microgrid chosen. This work did not perform a comparative study between PSCAD and Matlab-Simscape as the system was not developed in PSCAD and the CERTS microgrid was not employed either.

Ramezani et al [42] performed a study pertaining to the control of the inverters in a microgrid. In the study, non-traditional control techniques were explored, as in the tradition method, the voltage associated with the reactive power drops during the island mode of operation. This work emphasizes on the stability of the voltage during the island mode of operation. The microgrid was built in Matlab-Simscape and there was no emphasis placed on the modelling and simulation of the microgrid. This work did not utilize the CERTS microgrid and nor was the microgrid modelled in PSAD and a comparison between the two software was not performed.

Al Hosani et al in [43] demonstrate a hybrid AC/DC microgrid and their work proposes a new procedure to control the power flow, which enables the exchange of power between AC and DC microgrids. The traditional methods according to this work utilize proportion integral controller, which are challenging to tune and display slow response times. The proposed strategy is developed using the hill climbing algorithm [44]as the foundation. The average model of a microgrid is implemented in Matlab-Simscape and the proposed methodology is applied to the microgrid to evaluate the effectiveness. This work did not place an emphasis on the modelling of the microgrid but rather used an existing microgrid. Moreover, the system was only built in Matlab-Simscape and not in PSCAD, as a result a comparative study between the two software could not be performed. Lastly this work did not utilize the CERTS microgrid.

In [45], Zeineldin et al explore and study the hybrid microgrid. The work focuses on the stability of the system as various different AC and DC distributed generation sources are incorporated into the system. In this study, a synchronous diesel generator and inverters are utilized. This work is based on the CERTS microgrid, which is modelled using Matlab-

Simscape. The objective of the study is to realize the operational limits of the various microgrid connections and with an array of constraints being imposed on the system. This work did not focus on the modelling of the CERTS microgrid but rather emphasized the possibility of s hybrid connection within the grid. The system was only simulated in Matlab-Simscape and hence a comparison between PSCAD and Matlab-Simscape could not be made.

The study conducted by John et al [46] focused on introducing a decentralized droop control method, which enables accurate load sharing amongst the distributed generators as the system operated in the islanded mode of operation. In the proposed methodology the angle droop control is modified in order mitigate the dependence on the output inductance. This work did not perform a comparative study between PSCAD and Matlab-Simscape as the system was not developed in Matlab-Simscape and the CERTS microgrid was not employed either.

The work in [38], [47], [48] emphasized on numerous control strategies in order to achieve a variety of goals. New control methods are introduced such as the modified droop control based on virtual impedance and compensating voltage, which has the objective to balance the power sharing among the distributed generation units. Also, the modification of a control strategy to help improve power quality and proper load sharing in grid connected and island mode of operations was studied. The work in [47], proposes a control strategy to coordinate power sources and multilevel inverters in a medium voltage microgrid, while the objective still remaining improving power quality with the incorporation of unbalance or non-linear loads. All three of these works are concerned with the control related to the microgrid, rather than focusing about the modelling and

simulation of microgrids. Furthermore, each of the studies only employed one of either PSCAD or Matlab-Simscape and not both. As a result, a comparison between PSCAD and Matlab-Simscape was not evaluated in any of these studies. The CERTS microgrid was not utilized by any of these studies.

In the work implemented by Dinavahi et al in [49], the primary objective was to perform a comparative study between PSCAD and Matlab-Simscape while employing the CIGRE HVDC system and its controls. The work delivered a detailed report outlining the comparison between PSCAD and Matlab-Simscape while modeling the system identically in both simulation environments. The CIGRE HVDC benchmark is a rather simple system consisting of filtering devices, two sources interfaced together using an inverter and a rectifier. This study did not utilize the CERTS microgrid, but it did however employ both PSCAD and Matlab-Simscape. Table 2.3 summarizes the previous work published in the literature.

Table 2.3: Modelling, simulation and analysis of microgrids

Reference Number	**Simulation Environment**		**System Modelling and Simulation**	**Microgrid Utilized**	**Solver Type Specified**
	PSCAD	**Matlab-Simscape**			
[39]	✓	×	×	NS	×
[40]	×	✓	✓	NS	×
[35]	×	✓	×	Standard IEC Microgrid	×
[36]	✓	×	✓	NS	×
[41]	×	✓	×	NS	×
[42]	×	✓	×	NS	×
[37]	✓	×	×	NS	×
[43]	×	✓	×	NS	×
[45]	×	✓	×	CERTS	×
[46]	✓	×	×	NS	×

[47]	✓	×	×	NS	×
[38]	✓	×	×	NS	×
[48]	✓	×	×	NS	×
[50]	×	✓	×	NS	×
[51]	×	✓	×	Section of Canadian Benchmark System	×
[52]	×	✓	×	NS	×
[53]	✓	×	×	NS	×
[54]	×	✓	×	NS	×
[49]	✓	✓	✓	CIGRE HVDC Benchmark	✓
[55]	✓	✓	✓	NS	×
✓ indicates YES		× indicates NO		**NS** indicates Non-Standard	

2.4. Research Gaps

Based on the aforementioned literature, both PSCAD and Simulink are crucial in studying the performance of the microgrid, especially with the expectation of higher renewable energy penetration levels in the foreseeable future. However minimal work has been carried to investigate how the same system can be modelled in the two most utilized simulation environments in terms of maintaining consistency and uniformity in the modelling stages (transmission lines, loads, transformers etc.). It is essential to ensure accurate and consistent results can be obtained from the same system despite the simulation environment employed. Therefore, this work focuses on providing a systematic methodology to uniformly model the system in both simulation environments to ensure consistent results can be obtained while utilizing the same modelling parameters.

Moreover, the work that has been conducted in literature shows a lack of utilization of a standardized microgrid such as the CERTS microgrid. It is evident that a comparative study of a microgrid has not been conducted based on a standardized well-known system. It is of upmost importance that such a comparison is performed on a standard system to

form a proper benchmark. Although a comparative study has been conducted by Faruque et al [49] between PSCAD and Matlab-Simscape, however it was based on a rather simple High Voltage Direct Current (HVDC) two bus system, which is not inclusive of the workings of a microgrid as a microgrid is a more complex system which consists of a variety of components and control schematics. Due to the lack of studies concentrated towards modelling and simulation of microgrids, this work performs a comparative study based on the CERTS microgrid, which is a well modelled benchmark system.

The following list summarizes the research gap in the literature:

- The lack of work, which addresses the issue of the simulation and modelling of the CERTS microgrid itself taking into consideration the complexities when integrating distributed renewable energy resources.
- The lack of clear methods to model and simulate a microgrid in islanded and gird-connected modes with embedded DGs in operation.
- There is an evident lack of comparative studies comparing the performance of PSCAD and Matlab-Simscape while simulating the same system, as well as a lack of study in steady state analysis of the system.

2.5. Summary

In this chapter a comprehensive literature review was conducted of the work previously published on the topic of modelling and simulation of the CERTS microgrid using PSCAD and Matlab-Simscape. It was clear that there is a lack of studies, which provide a detailed methodology of the comparison of PSCAD and Matlab-Simscape while simulating the CERTS microgrid. Various different microgrids were modeled and

simulated in the literature but the limitation was of one simulation environment either PSCAD or Matlab-Simscape rather than a comparative study of the two. A good portion of the work conducted in the literature focused on improving specific aspects of the microgrid such as the control and not on the actual modelling of the microgrid. In addition, the solver type, simulation time, time step and grid-connected or islanded mode were not specified in the literature. All these parameters are crucial in maintaining consistency in the simulation of the system in both PSCAD and Matlab-Simscape, while ensuring the robustness of the system. As a result, this work will focus on the detailed study of the various parameters and objectives in order to ensure the CERTS microgrid testbed system is modelled and simulated consistently in both PSCAD and Matlab-Simscape in particular when considering the complexity due to integrating the distributed renewable energy resources.

Both PSCAD and Simulink utilize ordinary differential equations to represent the CERTS microgrid test-bed system. The difference pertaining to the step size selection and usage in each simulation platform has been discussed in detail. Along with the added capability of selecting from a variety of solver types in Matlab-Simscape as compared to PSCAD, which uses a single solver type. The computation approaches employed by both PSCAD and Matlab-Simscape have been presented in detail. PSCAD would be a better option to implement large scale systems, whereas Matlab-Simscape would be better suited towards a small-scale system.

3. CERTS Micro-Grid Testbed System

3.1. Introduction

The CERTS microgrid testbed system was developed by the Consortium of Electric Reliability Technology Solution (CERTS). The objective of the development of the system was to enable easy integration of small Distributed Generation sources (DG) into the utility connected network. Along with enabling the study of the impact that distributed generation has on the network, while ensuring that a uniform, unchanged and maintained system is available for any studies to be conducted.

3.2. CERTS Micro-Grid Testbed System

The CERTS Microgrid Testbed System is shown in Fig 3.1 and it is a micro-grid distribution system as discussed in [54] and [55]. The CERTS micro-grid test-bed system is capable of functioning in two different modes of operation, namely grid connected mode and islanded mode (non-grid connected mode). In the grid connected mode, the loads of the distribution system operate while consuming power from the utility, while in islanded mode the loads operate consuming power from the local Distributed Generation sources at the distribution end of the system. The islanded mode of operation is enabled when the grid is in an unhealthy state caused by faults or other such interruptions in service. The CERTS micro-grid test-bed system is connected to the grid utilizing a step-down transformer, this transformer is rated at 13.8kV on the primary side and 0.480kV on the secondary side. The CERTS Microgrid Testbed System consists of four loads (L3, L4, L5 and L6), and three distributed energy resources (DER-PV1, DER-PV2 and DER-Bt.S). The loads utilized are fixed loads, which are either capacitive or inductive in nature. The distributed energy resources are two photovoltaic sources and one battery energy storage device. The parameters of the CERTS microgrid testbed system are defined in Tables 3.1-3.14 as

follows. Moreover, the input parameters of the implemented PV arrays in both simulation platforms are illustrated in Appendix B.

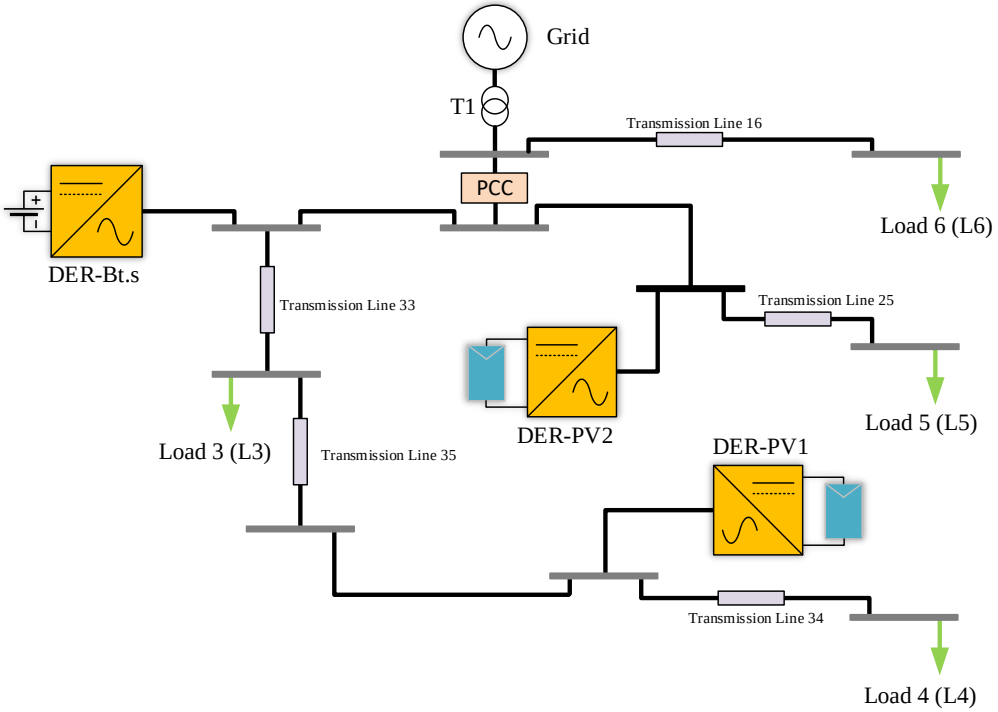

Fig 3.1: CERTS microgrid in grid connected mode of operation [58]

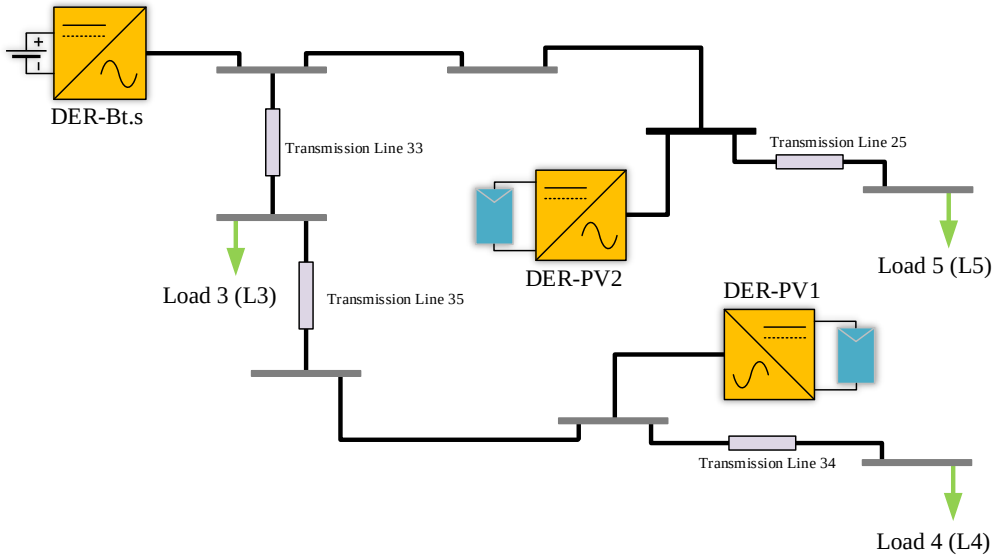

Fig 3.2: CERTS microgrid in island mode of operation

Table 3.1: Source (Utility) parameters

Source 1	
Base Apparent Power (3-Phase)	100 MVA
Base Voltage (L-L, RMS)	13.8 kV
Base Frequency	60.0 Hz
Voltage Input Time Constant	0.05 s
Infinite Bus	Yes

Table 3.2: Transformer (T1) parameters

Transformer (T1)	
3 Phase Transformer Rating	15.0 MVA
Base Operation Frequency	60.0 Hz
Winding #1 Type	Wye
Winding 21 Type	Delta
Delta lags or leads Y	Lags
Positive Sequence Leakage Reactance	0.08535 [p.u.]

Table 3.3: Transmission line 16 parameters (TL16)

Transmission Line – L16	
Impedance and Admittance Data Unit Type	Ohms
Nominal or Pie Coupled Model	Coupled Pi Model
Line Rated Frequency	60.0 Hz
Line Length	68.58 m

Table 3.4: Load 6 parameters (L6)

Load at Line 1 (L6)	
Rated Real Power per Phase	0.03 MW
Rated Reactive power (+inductive per phase)	-0.0067 MVAR
Rated Load Voltage (RMS, L_G)	0.277 kV
Fundamental Frequency	60 Hz

Table 3.5: Transmission line 25 parameters (TL25)

Transmission Line – L25	
Impedance and Admittance Data Unit Type	Ohms
Nominal or Pie Coupled Model	Coupled Pi Model
Line Rated Frequency	60.0 Hz
Line Length	68.58 m

Table 3.6: Load 5 parameters (L5)

Load at Line 25 (L5)	
Rated Real Power per Phase	0.05 MW
Rated Reactive power (+inductive per phase)	-0.0133 MVAR
Rated Load Voltage (RMS, L_G)	0.277 kV
Fundamental Frequency	60 Hz

Table 3.7: Transmission line 33 parameters (TL33)

Transmission Line – L33	
Impedance and Admittance Data Unit Type	Ohms
Nominal or Pie Coupled Model	Coupled Pi Model
Line Rated Frequency	60.0 Hz
Line Length	68.58 m

Table 3.8: Transmission line 35 parameters (TL35)

Transmission Line 3 – L35	
Impedance and Admittance Data Unit Type	Ohms
Nominal or Pie Coupled Model	Coupled Pi Model
Line Rated Frequency	60.0 Hz
Line Length	45.72 m

Table 3.9: Transmission line 34 parameters (TL34)

Transmission Line 3 – L34	
Impedance and Admittance Data Unit Type	Ohms
Nominal or Pie Coupled Model	Coupled Pi Model
Line Rated Frequency	60.0 Hz
Line Length	68.58 m

Table 3.9: Load 3 parameters (L3)

Load at Line 33 (L3)	
Rated Real Power per Phase	0.05 MW
Rated Reactive power (+inductive per phase)	0.0150 MVAR
Rated Load Voltage (RMS, L_G)	0.277 kV
Fundamental Frequency	60 Hz

Table 3.10: Load 4 parameters (L4)

Load at Line 34 (L4)	
Rated Real Power per Phase	0.05 MW
Rated Reactive power (+inductive per phase)	0.0150 MVAR
Rated Load Voltage (RMS, L_G)	0.277 kV
Fundamental Frequency	60 Hz

Table 3.11: Positive and Zero Sequence transmission line reactance [59]

Transmission Line Reactance (Ohms)	
Positive Sequence	
Resistance	6.1329×10^{-4} ohm/m
Inductive Reactance	1.0253×10^{-4} ohm/m
Capacitive Reactance	1×10^{21} ohm*m
Zero Sequence	
Resistance	0.0043 ohm/m
Inductive Reactance	1.8206×10^{-4} ohm/m
Capacitive Reactance	1×10^{21} ohm.m

Table 3.12: Battery energy storage parameters (DER-Bt.S)

Capacity	1.25 kV

Table 3.13: Photovoltaic array 1 parameters (DER-PV1)

Capacity	200W
Irradiance	1000 W/m^2
Temperature	28°C

Table 3.14: Photovoltaic array 2 parameters (DER-PV2)

Capacity	200 W
Irradiance	1000 W/m^2
Temperature	28 °C

3.3. Modelling of the CERTS Microgrid Testbed System

In order to ensure that an unbiased comparative study is performed, it is crucial to identically model the system in both PSCAD and Matlab-Simscape. The CERTS microgrid testbed system consists of a list of key components, such as source (utility), transformer, transmission lines, loads, photovoltaic arrays and battery energy storage. Both PSCAD and Matlab-Simscape have their own distinct method of modelling each of the components listed above. PSCAD and Matlab-Simscape each have a predetermined set of blocks that may be utilized in order to create the CERTS microgrid testbed system. These blocks were used in the initial development of the CERTS microgrid testbed system and are modified as differences were observed.

3.3.1 Discrepancies Between the Two Simulation Platforms

The CERTS microgrid testbed system was developed using the basic blocks provided by each of the simulating environments. The parameters listed in tables 3.1 through 3.14 are the inputs for each of the blocks utilized, such as transmission lines, transformer, loads and DGs. However, the results obtained from each simulation platform showed discrepancies and variations. Based on the readings at several measurement nodes, it was observed that the two system do not match. It was evident from the readings that the voltage and current readings were inconsistent with large variances. Hence, in order to facilitate the investigations and isolate the source of the issues, the CERTS testbed is reduced to a system with reduced complexity. That is being done to eliminate as many variables as possible that may contribute in the offset, e.g. DGs, controllers, PCC …etc. This reduced system is discussed in the following section.

3.3.2 Reduced CERTS System with no Distributed Generation

In order to pinpoint the cause of the offset in the results, a component by component breakdown is conducted to investigate the modelling in both in PSCAD and Matlab-Simscape along with reduction in the complexity of the system. The components were removed from the system in order to create a smaller system, while at the same time maintaining the same point of measurements throughout the system. The reduced CERTS microgrid testbed system consists of the source (utility), transmission lines, transformers and loads. All three distributed generators are removed along with their respective controls to simplify the system. This was done in order to verify each of the component blocks utilized during the simulation. The CERTS microgrid testbed system with no DG is shown in Fig 3.3.

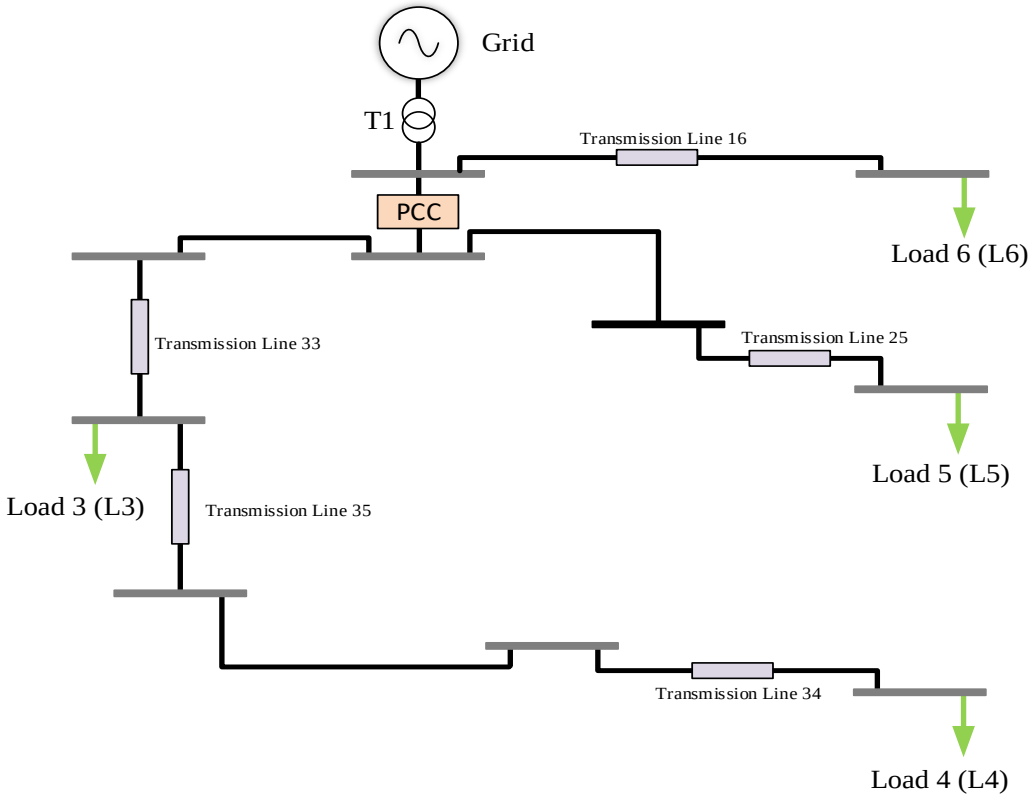

Fig 3.3: Basic system with no distributed generation

The first block, which was analyzed was the source and the parameters were adjusted in order to study the impact of the changes on the output. It can be seen that the source (utility) was generating the expected power in MVAR. For the transmission lines, the mathematical modelling utilized by PSCAD and Matlab-Simscape was analyzed and studied. The differences are shown in figures 3.4 and 3.5 below. It can be observed that the input parameters of each of the blocks differ within each platform. Similarly, in order to investigate the transmission lines a further simplified system without distributed generation was developed consisting of a single branch containing the source, a transmission line and a load. Two scenarios were investigated, one with the transmission line being represented by the preset block in each simulation environment and the second where the transmission line was represented by its equivalent RLC model. The results of both these models showed

extremely low to zero variance and it was evident that the transmission lines are not the component causing the offset in the system with distributed generation. Therefore, it is clear that, the loads are the components responsible for the offset and mismatch between the two platforms.

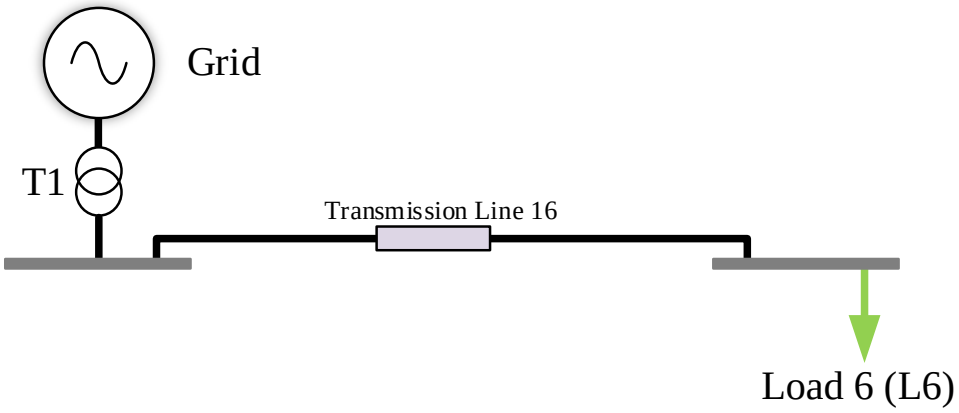

Fig 3.4: Single branch system

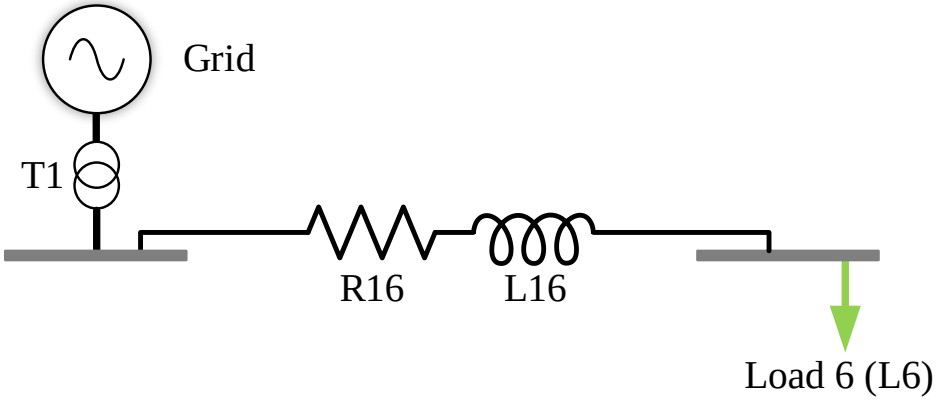

Fig 3.5: Transmission line represented by lumped resistance and inductance

3.3.3 Source of Inconsistency

Upon verification of all the components except the loads in the reduced system with no distributed generation, it is evident that the loads are the culprits behind the mismatch. There are four separate loads employed in this grid, each with varying power consumption, and capacitive or inductive nature.

The system without distributed generation is reduced to just once branch consisting of the source (utility), transformer, transmission line and a load. This reduction is illustrated in Fig 3.4. It can be seen in table 3.15 below that the input parameters differ in both PSCAD and Matlab-Simscape (they are not one to one transformation). It can be seen that, the Fixed Load block in PSCAD requires, the rated real power per phase, rated reactive power (positive or negative), rate load voltage (rms L-G) and finally, the fundamental frequency. Furthermore, PSCAD utilizes the constant impedance configuration, as per the associated documentation.

On the other hand, Matlab-Simscape requires nominal phase to phase voltage (V_n rms), nominal frequency, active power, inductive reactive power, capacitive reactive power, load type and finally a configuration setting (Y ground, Y floating, Y neutral or Delta). There are few parameters that are shared amongst the two platforms, such as the voltage, frequency and load type. These settings were kept constant in PSCAD and in Matlab-Simscape and the various configurations were utilized in an attempt to obtain match between PSCAD and Matlab-Simscape. In order to maintain uniformity, load modeling methodology is proposed based on their respective power and voltage ratings and described in the following section.

Table 3.15: Input parameters required based on simulation environment

Input Parameters	
PSCAD	**Matlab-Simscape**
Rater Real Power per Phase (MW)	Nominal Phase to Phase Voltage (Vrms)
Rated Reactive Power (MVAR)	Active Power (W)
Rated Load Voltage L-G (kV)	Inductive Reactive Power (Positive VAR)
	Capacitive Reactive Power (Negative VAR)
Fundamental Frequency (Hz)	Nominal Frequency (Hz)
	Configuration

3.3.4 Load Modelling Methodology

Based on the outputs and results of the two platforms, it was evident that a match could not be made regardless of the configuration. In order to create consistency and uniformity in both PSCAD and Matlab-Simscape, the loads were modelled based on their respective RL and RC equivalent models (i.e. based on whether the load was inductive or capacitive). It was evident from the output and results of the simulation that there was a match in all the readings. Based on the outputs and results of the two simulating platforms while implementing the proposed methodology, a match in the output by an error percentage of less than 1% as will be presented in Chapter 4.

Further investigation was carried out by implementing the proposed methodology (representing the loads based on their respective RL/RC equivalent) on the system with no distributed generation, which consists of the entire network with no distributed generation sources and their respective controls. The formulae necessary to convert the loads to their RL or RC equivalent models are defined below.

The reactance calculated in equation 3.2 is inductive in nature if the reactive power is a positive quantity and capacitive in nature when the reactive power is negative. Based on whether the reactance is capacitive or inductive equation 3.3 or equation 3.4 are invoked to calculate inductance and capacitance accordingly. The equivalent constant impedance parameters of each of the loads based on the active power, rated load voltage and rated reactive power are illustrated in Table 3.16 below. The values of R, L and C are obtained using equation 3.1 through equation 3.4.

$$R = \frac{E^2}{P} \tag{3.1}$$

Where

E is the L-G RMS voltage, P is the active power and R is the resistance.

$$X = \frac{E^2}{Q} \tag{3.2}$$

Where

E is the L-G RMS voltage, Q is the reactive power and X is the reactance.

$$L = \frac{X_L}{j\omega} \tag{3.3}$$

Where

X_L is the inductive reactance and ω is the frequency.

$$C = \frac{1}{j\omega X_c} \tag{3.4}$$

Where

X_C is the capacitive reactance and ω is the frequency.

Table 3.16: Load input parameters

Load Equivalent Impedance					
Load Name	**Voltage (KV)**	**Active Power P (MW)**	**Reactive Power Q (+Inductive)**	**Equivalent Resistance (Ω)**	**Equivalent C or L (F/H)**
Load 6	0.277	0.03	-0.0067	2.5576	2.3162e-4
Load 5	0.277	0.05	-0.0133	1.5346	4.5979e-4
Load 4	0.277	0.05	0.0150	1.5346	0.01356
Load 3	0.277	0.05	0.0150	1.5346	0.01356

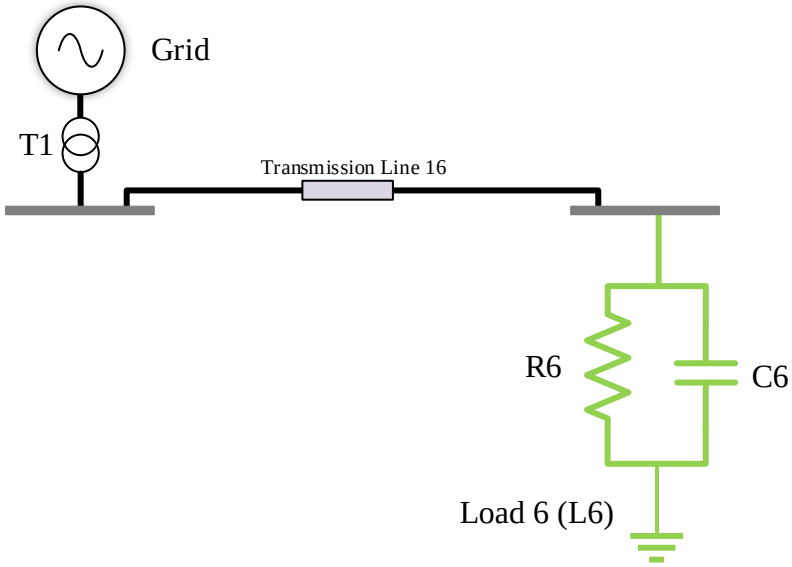

Fig 3.6. Load represented as resistance and capacitance

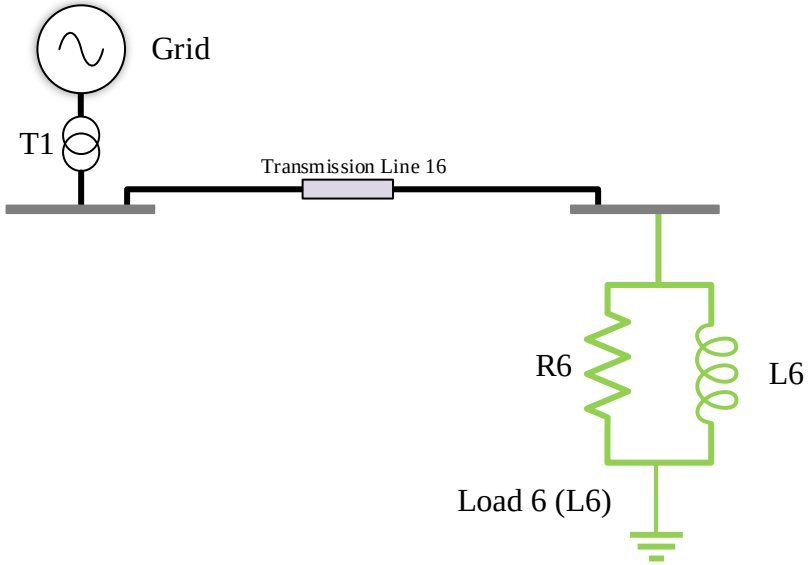

Fig 3.7. Load represented as resistance and capacitance

3.4. Voltage Source Converter Control Methodologies

The three Distributed Generation sources are connected to the network using Voltage Source Converters (VSC) to create the CERTS microgrid. This as a result enables the microgrid to operate in grid-connected mode and islanded mode. The point of common coupling allows the DGs to be integrated into the network. Voltage source converters are utilized in order to convert the DC generation to AC generation, in its essence the VSC is an inverter. The use of the voltage source converters helps converting the DC parameters to AC parameters. There are three voltage source converters employed, one for each of the three distributed energy resources. Each of these voltage source converters requires a gating signal in order to control the switching sequence of the switching devices. In order to generate the gating signal, Pulse Width Modulation (PWM) is utilized along with a high frequency repeating signal like a triangular wave. In order to turn the switches on, the gating signal is compared to a reference signal. In order to model and simulate the two different operation modes of the system, three different control methodologies are utilized. The battery energy storage utilizes a control methodology referred to as current-mode control and the PV arrays utilize a slightly modified version of the current-mode control called modified-current mode control mode with DC link voltage. The modification is done in order to ensure that the maximum power is derived from the photovoltaic array.

3.4.1 Current-Mode Control

In order to control any voltage source converter, the active power (P) and reactive power (Q) need to be controlled and tracked. The voltage source converters are three phase systems and thus require each of the three phases of the active power and reactive power to be controlled simultaneously. In order to simultaneously control all three phases, the

system needs to be transformed into a single-phase system. In order to represent the three-phase system as a single-phase system the park transformation [60] is employed, which enables the parameters from phases ABC to a rotating dq-frame as shown in Fig 3.10. The currents of the system are utilized and controlled in order to control the active power and reactive power as power is directly related to the current. In order to control the currents, they must be transformed from three phase to its equivalent representation in the dq0-frame [3]. The transformation process is based on the following equations outlined in [3].

$$\begin{bmatrix} V_d \\ V_1 \\ V_0 \end{bmatrix} = \frac{2}{3} \begin{bmatrix} \sin(\theta) & \sin\left(\theta - \frac{2\pi}{3}\right) & \sin\left(\theta + \frac{2\pi}{3}\right) \\ \cos(\theta) & \cos\left(\theta - \frac{2\pi}{3}\right) & \cos\left(\theta + \frac{2\pi}{3}\right) \\ \frac{1}{2} & \frac{1}{2} & \frac{1}{2} \end{bmatrix} \begin{bmatrix} V_a \\ V_b \\ V_c \end{bmatrix} \tag{3.5}$$

$$P_s(t) = \frac{3}{2}\left(v_{sd}(t)i_d(t) + v_{sq}(t)i_q(t)\right) \tag{3.6}$$

$$Q_s(t) = \frac{3}{2}\left(-v_{sd}(t)i_q(t) + v_{sq}(t)i_d(t)\right) \tag{3.7}$$

The dq-frame components of the AC-side voltages and currents are represented using v_{sd}(t), v_{sq}(t), i_d(t) and i_q(t). The phase locked loop (PLL) enables the v_{sq}(t) to be kept constant at zero in the steady state condition, this as a result simplifies equation (3.6) and (3.7). The currents i_{dref}(t) and i_{qref}(t) need to be calculated using the reference active and reactive powers using equations (3.8) and (3.9). Figure 3.8 Shows the complete diagram of the process undertaken in order to implement the current-mode control method.

$$i_{dref}(t) = \frac{2}{3v_{sd}}\left(P_{sref}(t)\right) \tag{3.8}$$

$$i_{1ref}(t) = \frac{2}{3v_{sd}}\left(Q_{sref}(t)\right) \tag{3.9}$$

The process is initiated by first calculating the reference currents utilizing equations (3.8) and (3.9). Following the generation of the reference currents, the reference currents are then fed into the compensator along with the AC side currents and AC side voltages. The output of the compensator is then converted back to three phase from the dq0 frame and is fed into the PWM Generator, which generates the gating signals needed for the firing of the voltage source converter. The following figures illustrate the modelling of the control strategy for the battery energy storage (DER-Bt.S) in both PSCAD and Matlab-Simscape.

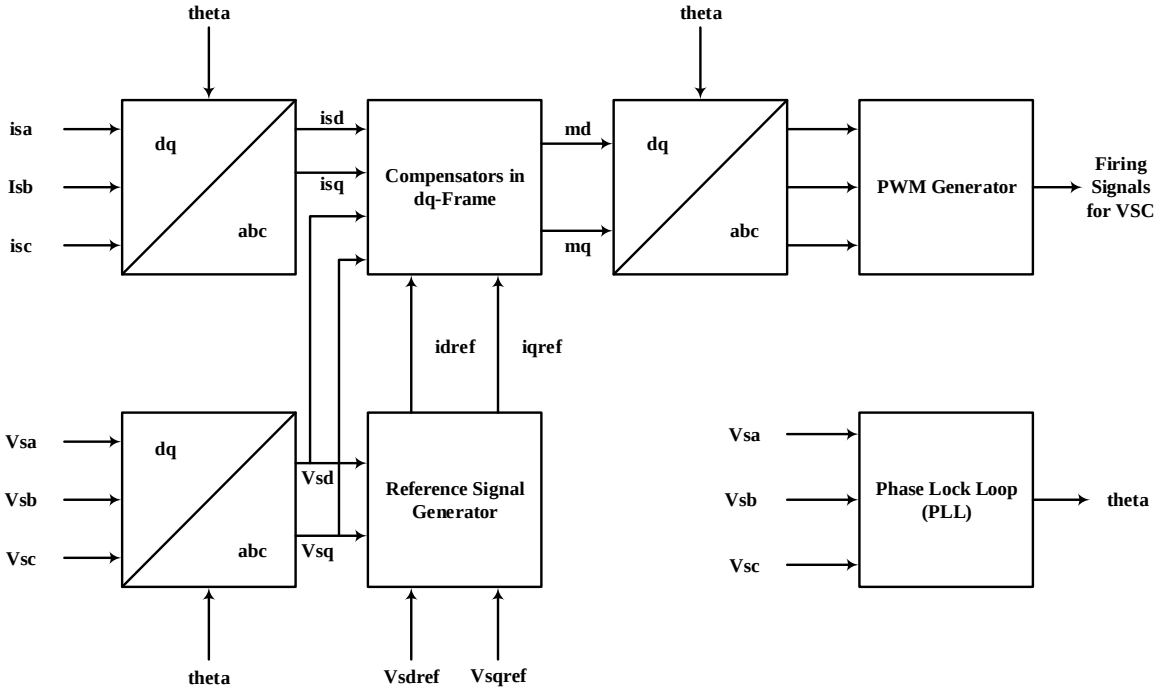

Fig 3.8: Current mode control

3.4.2 Modified Current-Mode Control with DC Link Voltage

The modified current-mode control with DC link voltage is discussed in [61], which presents the theory as a variant of the current-model control methodology. The primary

objective of the modified current-mode control with DC link voltage is to ensure that the power factor of the photovoltaic system is regulated. The DC link voltage-control scheme enables the control of the amount of power generated by the photovoltaic system. The DC link voltage-control scheme also ensures that the photovoltaic system behaves in a stable manner and safe operation of the voltage source converter. Fig 3.9. Shows the complete diagram of the process undertaken to implement the modified current-mode with DC link voltage control method.

The process is initiated by first obtaining the reference currents from the Q_{sref} and V_{dcref}. Following the generation of the reference currents, the reference currents are then fed into the compensator along with the AC side currents and AC side voltages. The output of the compensator is then converted back to three-phase from the dq0 frame and fed into the PWM Generator, which generates the gating signals need for the firing of the voltage source converter. The following figure (Fig 3.9) illustrates the modelling of the control strategy for the photovoltaic source-2 (DER-PV2) in both PSCAD and Matlab-Simscape.

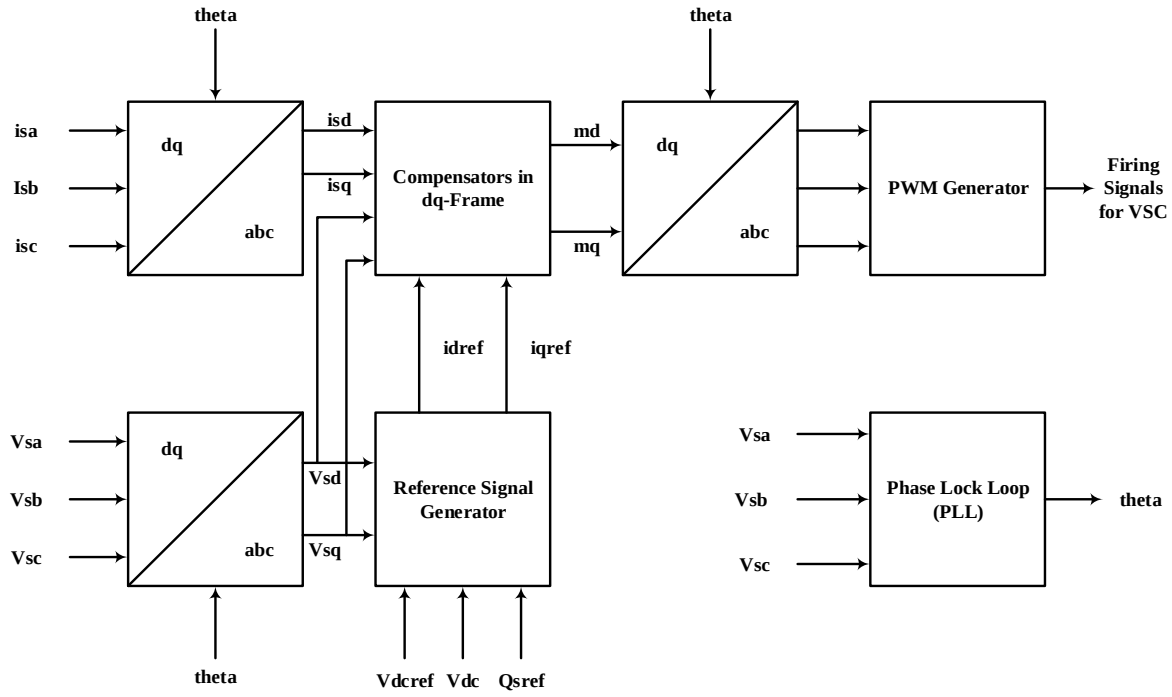

Fig 3.9: Modified current mode control

3.4.3 Frequency Mode Control

During the island mode of operation, the system operates in stand-alone mode, completely disconnected from the grid and it is self-sufficient. In order for any power system to be functional, the frequency is a crucial parameter (typically 60Hz), during grid connected mode the frequency is provided by the utility grid, while in islanded mode the frequency needs to be generated in order to be used in the system. The frequency and voltage are both controlled by the voltage source converter in the islanded mode and this done by utilizing the frequency mode control methodology. The photovoltaic source-1 is controlled using both the current-mode control and the frequency mode control as it is modelled to operate in both islanded mode and grid-connected mode. For this distributed energy source, it is important to create a control scheme, which is capable of utilizing the utility grid frequency in grid-connected mode and switch it to a generated frequency in the islanded mode of operation in the event of a service disruption or other such issues. Fig

3.10 Shows the complete diagram of the process undertaken in order to implement the frequency mode control method.

The process is initiated by first obtaining the reference currents from the V_{sdref} and V_{sqref}. V_{sdref} and V_{sqref} are calculated using (3.5), which calculates the dq0 frame equivalent values of the three-phase voltage and current values. Following the generation of the reference currents, the reference currents are then fed into the compensator along with the AC side currents and AC side voltages. The output of the compensator is then converted back to three-phase from the dq0 frame and fed into the PWM Generator, which generates the gating signals need for the firing of the voltage source converter. The following figure (Fig 3.10) illustrates the modelling of the control strategy for the photovoltaic source-1 (DER-PV1) in both PSCAD and Matlab-Simscape.

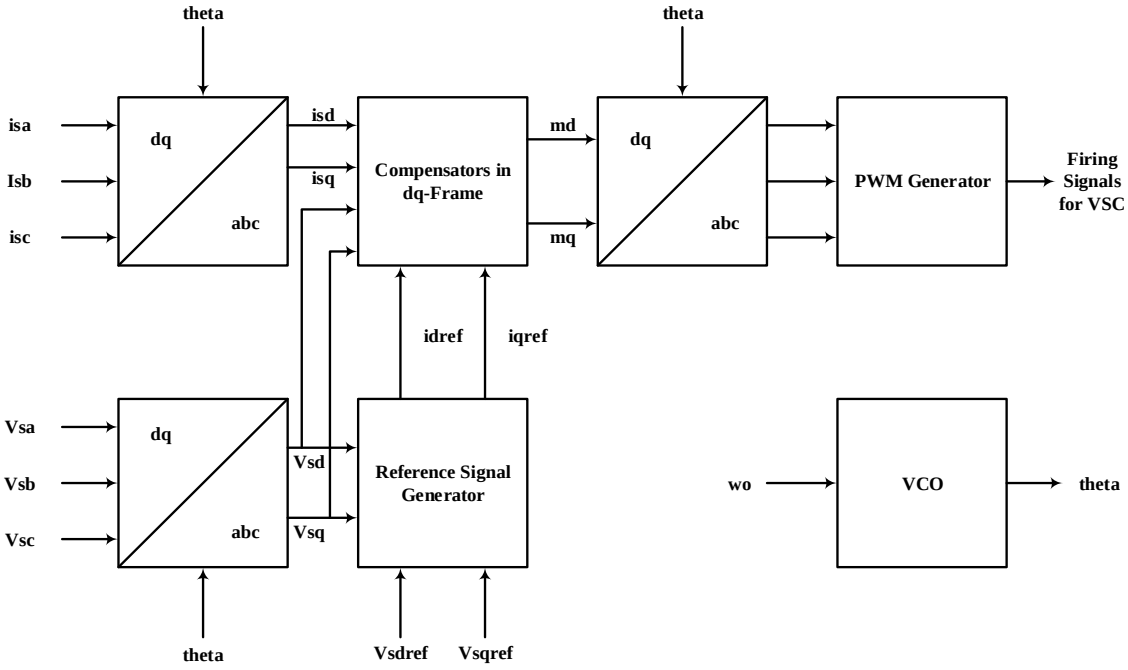

Fig 3.10: Frequency mode control

3.5. Data Acquisition and the Recorded Parameters

To keep uniformity in the analysis of the data collected during testing, the location of the points of measurement and their respective measured parameters were kept uniform. Doing so allowed an unbiased and consistent comparison of the CERTS microgrid testbed system in both PSCAD and Matlab-Simscape. The parameters measured and logged were the voltages and currents at various points in the CERTS microgrid testbed system as can be seen in Fig 3.11. The simulation parameters utilized during these simulations were a total run duration of one second, a step size of ten microseconds, a plot step of ten microseconds along with trapezoidal integration and EMTDC methods. The time step size is selected based on the Nyquist Criteria which states that the sampling frequency must be twice the highest frequency of the system in order to attain accurate results and representation of the signal. The highest frequency in this system is 15.3 kHz of the carrier frequency in the VSC controls. Based on the Nyquist criteria the sample time should be based on the frequency 30.6kHz which would require a time step size of 32.68μs. The 10μs utilized in this work is able to clearly and accurately represent the data, as a 10μs is compatible with a frequency of 100kHz. This step size of 10μs is sufficient to serve the objective of the steady state analysis, but this will not be sufficient for a transient study of the system and will need to be adjusted accordingly.

There are several indices that were utilized in this thesis, such as Total Harmonic Distortion (THD), Mean Absolute Deviation (MAD). The MAD is a measure of the variability in a dataset, as the MAD is essentially a measure of the average distance between any data point to the mean of the data set. The MAD is obtained by computing equation (3.10). The mean of any data set is essentially the average of the entire data set, obtained

by acquiring the sum of all data points and dividing by the total number of data points in the data set as shown by equation (3.11).

$$MAD = \frac{\sum|x_i - \bar{x}|}{n} \tag{3.10}$$

Where

x_i is the i^{th} value,$\bar{x}$ is the mean of all values and n is the number of samples in the dataset.

$$mean = \frac{\sum x_i}{n} \tag{3.11}$$

Where

x_i is the i^{th} value and n is the number of samples in the dataset.

The Total Harmonic Distortion (THD) on the other hand is a concept, which is a little more complex than the mean and MAD. The THD is the measure of the harmonics present in any parameter measured in a system, such as the voltage and current. The THD is the summation of all harmonic components of the current and voltage and can be calculated using equation (3.12) below [57]. In order to derive the harmonics of each of the voltage and current measurements recorded the Fast Fourier Transform [62] needs to be invoked (FFT).

$$THD = \frac{\sqrt{\sum_{j=2}^{\infty} V_j}}{V_1} * 100 \tag{3.12}$$

Where

j is the harmonic order, V_j is the RMS voltage of j^{th} harmonic and $V_1$is the fundamental RMS voltage.

The Fast Fourier Transform (FFT) is a signal processing tool, which enables the analysis of a signal spectrum. The FFT algorithm is capable of computing the discrete Fourier transform DFT for a time series. The FFT algorithm has enabled the calculation of the harmonics at numerous levels for each of the signals under analysis. There are two forms of the FFT algorithm, one is the decimation in time (DIT) while the other is the decimation in frequency (DIF). In PSCAD the FFT block, the decimation in time DIT is employed in order to calculate the distortion in each of the voltage and current signals. The formulation of the DIT used by FFT to calculate the DFT of the input signal as defined in equations (3.13) to (3.16) below [63], [64].

$$B_r = \sum_{k=0}^{\left(\frac{N}{2}\right)-1} Yk \exp\left(-4\pi jrk/_N\right) \tag{3.13}$$

$$Y_k = X_{2k}$$

$$Z_k = X_{2k+1}$$

$$k = 0,1,2,\dots,\frac{N}{2}-1$$

Where

B_r is the discrete Fourier Transform of the even-numbered values, Y_k is the set of points consisting of the even-numbered points of the timeseries and N is the total number of data points in the timeseries.

$$C_r = \sum_{k=0}^{\left(\frac{N}{2}-1\right)} Zk \exp\left(-4\pi jrk/_N\right) \tag{3.14}$$

$$r = 0,1,2,\dots,\frac{N}{2}-1$$

$$r = 0,1,2 \ldots, N-1$$

Where

C_r is the discrete Fourier Transform of the odd-numbered values, Z_k is the set of points consisting of the odd-numbered points of the timeseries and N is the total number of data points in the timeseries.

$$A_r = \sum_{k=0}^{\left(\frac{N}{2}\right)-1} \left\{ Y_k \exp\left(\frac{-4\pi jrk}{N}\right) + Z_k \exp\left(\frac{-2\pi jr}{N}[2k+1]\right) \right. \tag{3.15}$$

$$r = 0,1,2 \ldots, N-1$$

$$A_r = \sum_{k=0}^{\left(\frac{N}{2}-1\right)} Yk \ \exp\left(-\frac{4\pi jrk}{N}\right) + \exp\left(\frac{-2\pi jr}{N}\right) \sum_{k=0}^{\left(\frac{N}{2}-1\right)} Z_k \ \exp\left(\frac{-4\pi jrk}{N}\right) \tag{3.16}$$

Where

A_r is the discrete Fourier Transform of the even-numbered and odd-numbered values combined and Y_k is the set of points consisting of the even-numbered points of the timeseries. Z_k is the set of points consisting of the odd-numbered points of the timeseries and N is the total number of data points in the timeseries.

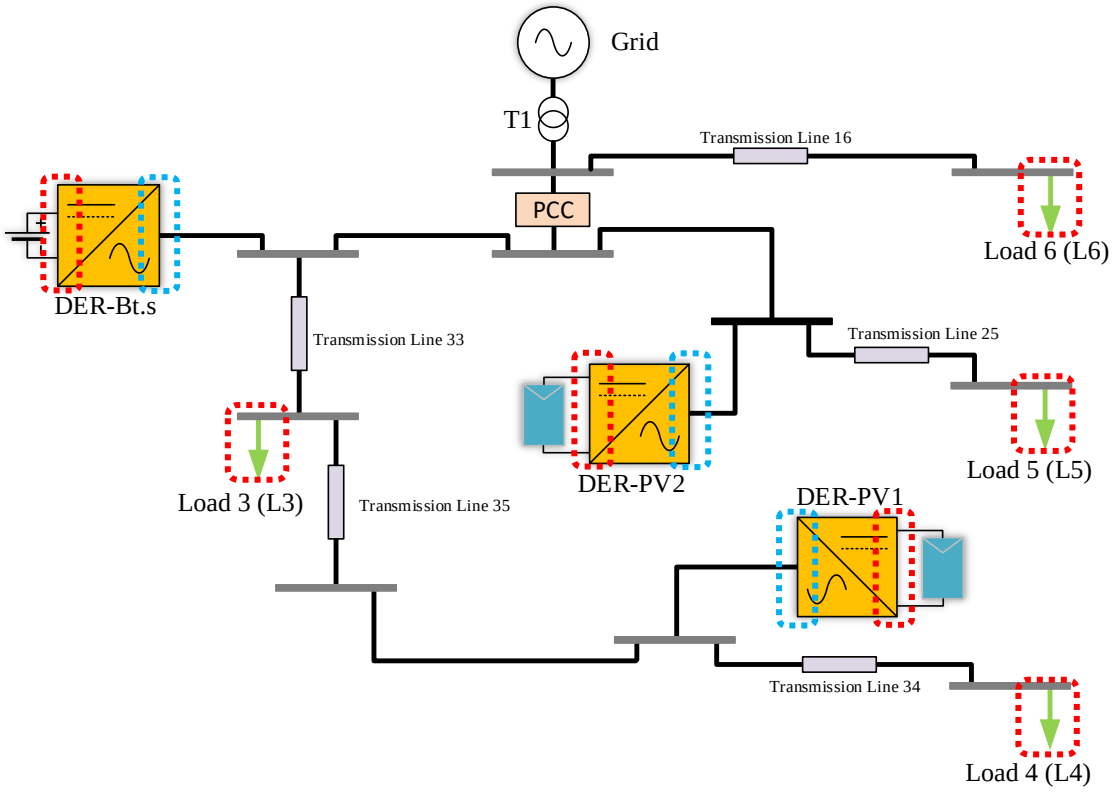

Fig 3.11: Points of measurement for CERTS microgrid

3.6. Summary

In this chapter the modelling and simulation of the CERTS microgrid testbed system was performed. The CERTS microgrid testbed system was discussed in detail, while outlining the parameters needed to model each of the components utilized in the system. Followed by a detailed description of the control methodologies utilized to control the voltage source converters utilized to integrate the various distributed generation units into the microgrid. Three different control techniques were described and illustrated, namely Current-Mode Control, Modified Current Mode Control with DC Link Voltage and Frequency Mode Control. The voltage source converters are employed in order to transform DC generation to AC generation. The systems modelling techniques were described in detail and the impact of each component on the comparison being performed

was outlined. The procedures followed in order to mitigate the offsets in results between both PSCAD and Matlab-Simcape were described in detail. Followed by the detailed description of the methodology utilized in order to unify the modelling in the two simulation environments. The step size selection criteria were described in detail, the objective of this work is to perform a steady state analysis of the system. In the case of transient analysis, the time step must be chosen accordingly as a much smaller time step size would be beneficial to accurately represent the data. It must also be mentioned that a transient study will require more computation time than the steady state study performed in this work. Finally, the points of measurement in the CERTS microgrid testbed were illustrated and the analytical analysis techniques utilized to study the data were described in detail.

4. Results and Evaluation

4.1. Introduction

In this chapter, the performance of the CERTS microgrid testbed is evaluated in Power System Computer Aided Design (PSCAD) and MATLAB Matlab-Simscape. This study assesses the effects of the distributed generators (DGs) and renewable energy sources on the point of common coupling (PCC). The CERTS microgrid testbed system is modelled and is simulated in two different simulation environments with the objective of performing a comparative evaluation of the system in mind. In order to ensure that a comprehensive study is conducted, the CERTS microgrid testbed system is operated in both grid-connected mode and island mode. The parameters logged were the root mean square (RMS) voltage and current. Along with the total harmonic distortion (THD) of both the voltage and the current.

Following the completion of the modelling of the CERTS microgrid testbed system, several runs were conducted of the simulation to gather a large dataset and to account for any variances during different runs. The simulation parameters utilized during these simulations were a total run duration of one second, a step size of ten microseconds, a plot step of ten microseconds along with trapezoidal integration and EMTDC methods. The RMS block in Matlab-Simscape shows an initialization at 120V, which did not have an impact on the steady study performed in this work. However, in the transient study the initialization of the simulation in Matlab-Simscape should be considered in detail. Lastly a variety of analysis techniques are utilized in order to compare the performance of the CERTS microgrid testbed system in the grid-connected and islanded modes of operation.

The performance of both environments is validated by comparing the measured data collected at the same measurement points described in Fig 4.12. A variance of only 1% is considered acceptable based on the work previously introduced in [49], which is based on a similar study between the same two simulation platform but targeting a very different system. The study provided in the thesis is focused on the steady-state performance of the CERTS microgrid. The time at which the system is considered in steady state is at the point when the system reaches an equilibrium point without visible oscillation. In order to unify the description throughout the discussion, the time at which the system is considered in steady-state is adjusted to t=0.1s. similar assumption has been already considered in the discussion in [49].

4.2. Test System Description

The CERTS microgrid testbed system was utilized in this study which consists of an ideal source acting as the grid, a step-down transformer, five transmission lines, four loads and three distributed generation units. In order to perform a comprehensive study of the system it is essential to study the power generated by these distributed generation units and their impact on the point integration into the CERTS microgrid testbed system. In order to perform this study, it was necessary to monitor and analyze the voltage, current and power generated on the Primary side of all inverters. Prior to the conversion from DC to AC with the aid of inverters, as well as the secondary side of the inverts. This can be seen in figure 4.1. The red indicates the DC side and the blue indicates the secondary side. This is necessary in order to confirm that the required values of each of the voltage, current and power are being produced and supplied to the grid. It is essential that these values be

consistent in both PSCAD and Matlab-Simscape, as the objective of the study is to perform a comparative analysis of the same system in both PSCAD and Matlab-Simscape.

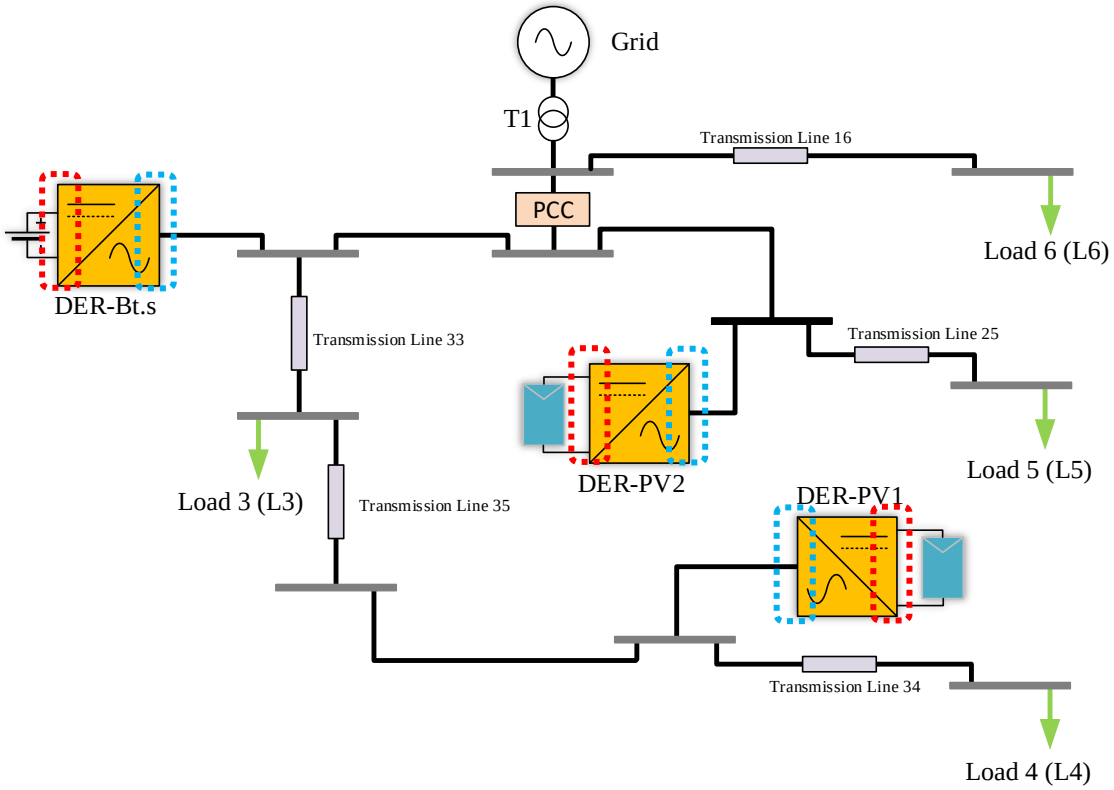

Fig 4.1: Distributed Generation DC and AC Measurement Locations

Along with these measurement locations, it is of upmost importance to ensure that the voltage, power and current at load 3, load 4, load5 and load 6 match in both the systems. This is necessary in order to verify that the system has been modelled correctly and is similar in both simulation environments. The location of each of these loads can be seen in Figure 4.2 below. In order to further diversify the study, the system is analyzed and is studied in both the Grid Connected Mode of Operation and in the Island mode of Operation. In the Grid Connected Mode of Operation, the entire system is part of the simulation and the feedback values required by the control loops to calculate md, mq, Vd and Vq are attained directly from the grid, whereas in the Island Mode of Operation certain

components of the grid are disconnected. The disconnected components include the Grid, Transformer 1(T1), Transmission Line 16 and finally Load 6. The remainder of the system remains intact being powered only by the Distributed Generation Sources. In this case the reference values required to calculate md, mq, Vd and Vq are calculated using the values attained from the battery in the absence of the grid. The battery is preferred over the photovoltaic sources due to its ability to absorb large amount of power, a more predictable power curve as the photovoltaic units power generation varies based on numerous factors such as temperature, irradiance and the number of hours for which the sun shines throughout the day as all these factors vary day by and season by season.

It is important to note that, in all simulation runs demonstrated within this chapter, the system always starts from reset with initial values equal to zero. Although such a scenario is very unlikely with the current state of the utility grid which is already up and running. The CERTS microgrid system is specifically designed to not only investigate the system performance and impact on the utility grid in terms of harmonics, voltage and frequency. It is also important to investigate the system dynamics where it will be connected and disconnected from the utility grid known as the point of common coupling (PCC), including system starting from reset (zero initial conditions). That being said, the model provided by Matlab-Simscape and PSCAD as accurate to a degree enough to provide useful insights on the system performance, but it actually cannot completely model the grid. Therefore, in all power system simulation platforms, the chosen system starts from zero-initial conditions as it is the neutral unbiased point of operation. However, if the system dynamic is the concern (which is not in this work), the proper transient is to be

applied the grid model in the simulation after giving it the proper time to reach steady state operation from reset.

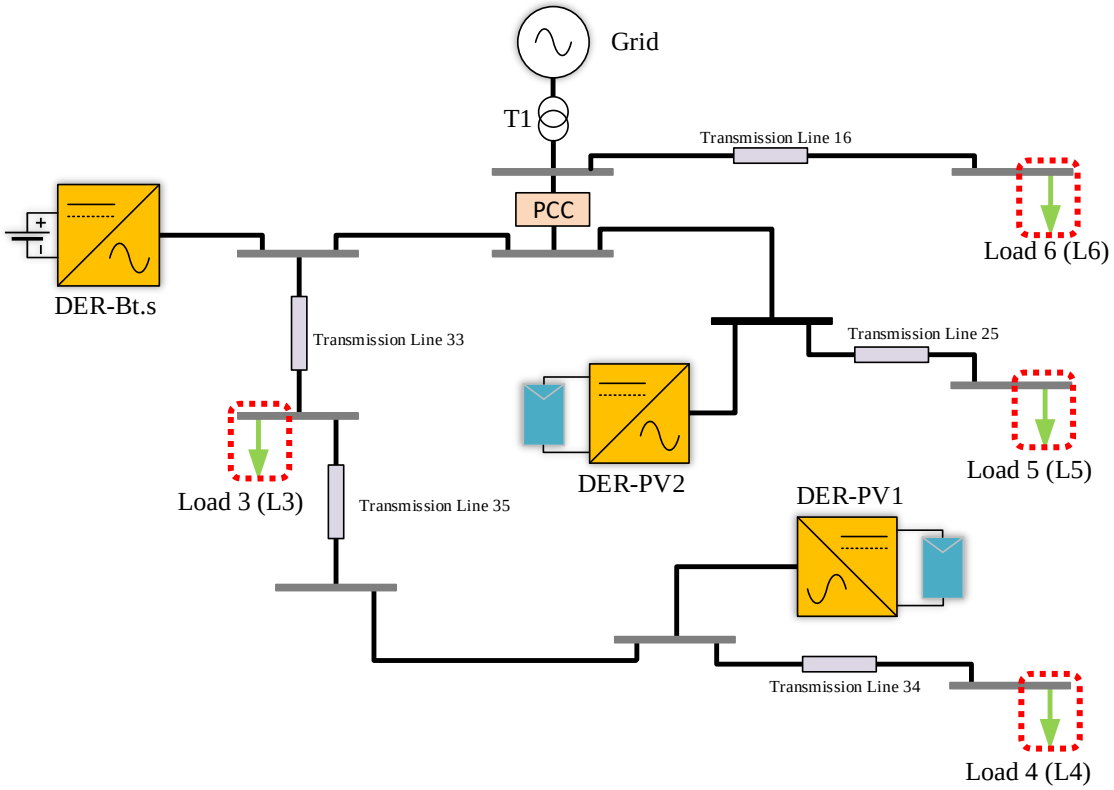

Fig 4.2: Load Measurement Location

4.3. Grid Connected Mode

This chapter is oriented to study the impact of the distributed generation units at various points of coupling with the CERTS microgrid testbed system in the Grid Connected mode of operation. In the grid connected mode of operation all the distributed generation sources operate in parallel with the grid in order to supply energy to all the loads and meet the demands of these loads. There are four loads located all over the grid, namely L3, L4, L5 and L6. Along with three distributed energy sources, specifically DER-Bat, DER-PV1 and DER-PV2. This system is modelled and is simulated in both PSCAD and Matlab-Simscape. It is crucial to study and analyze the output at various measuring points verify

and compare performance of the system in both simulation environments. Along with the verification of the modelling parameters and techniques in both PSCAD and Simulink. Section 4.3.1 illustrates the results of the PSCAD simulation in the grid connected mode of operation, whereas 4.3.2 depicts the results of the Matlab-Simscape simulation in the grid connected mode operation.

4.3.1 PSCAD Simulation Grid Connected Mode

In this chapter the results obtained from PSCAD are illustrated and discussed. The points of measurement utilized were discussed in section 4.2 and are illustrated here using the single line diagram of the CERTS microgrid testbed system. The data collected through ten iterations is represented graphically and numerically, as can be seen in this section.

First the DC side voltage and DC side current generated by the distributed generation units are discussed. Followed by the AC side voltage and AC side current of inverters utilized to couple the distributed generators to the grid. Finally, the voltage and current of each of load is illustrated. In order to conduct thorough work, it was necessary to investigate the Root Mean Square and Total Harmonic Distortion of all AC values being analyzed.

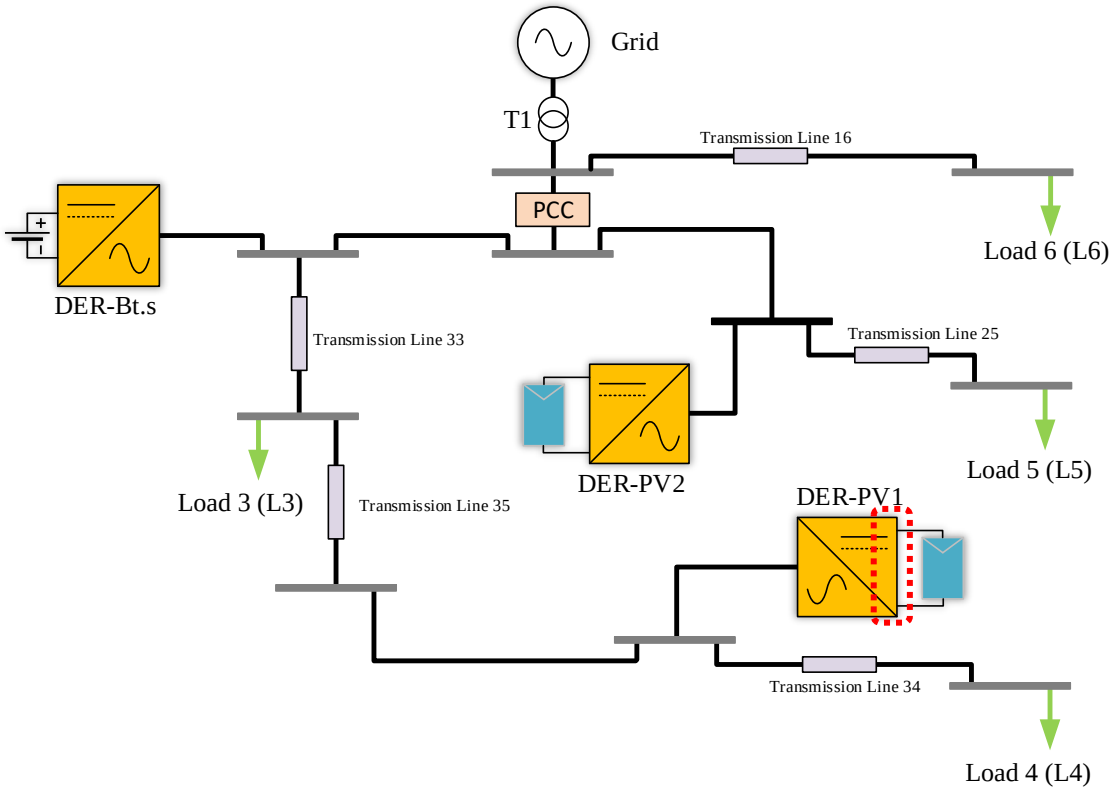

Fig 4.3: DG1 DC Side Point of Measurement

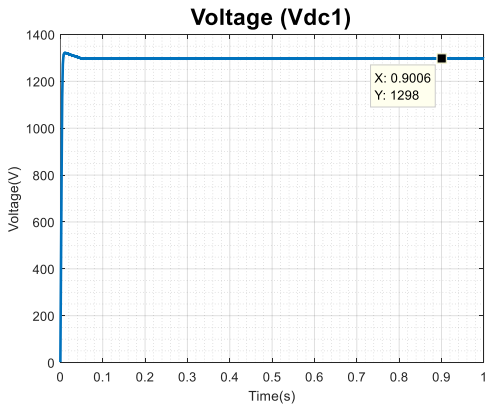

Fig 4.4: DC Link Voltage DG1

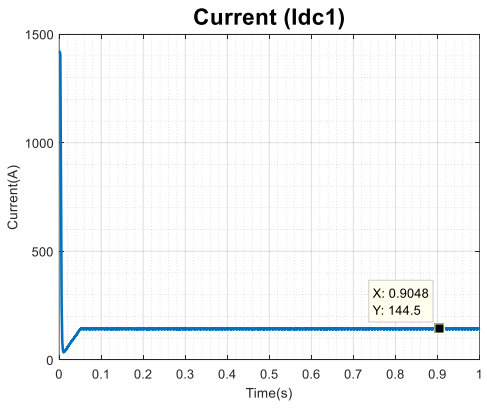

Fig 4.5: DC Link Current DG1

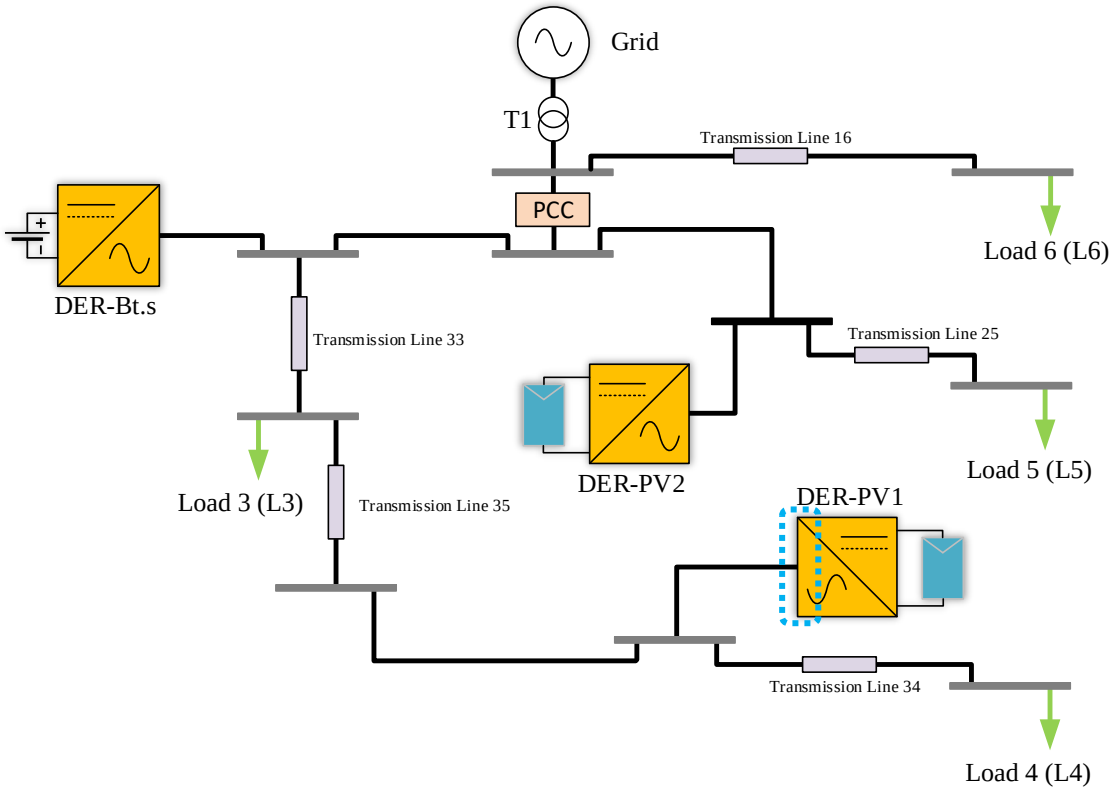

Fig 4.6: DG1 AC Side Point of Measurement

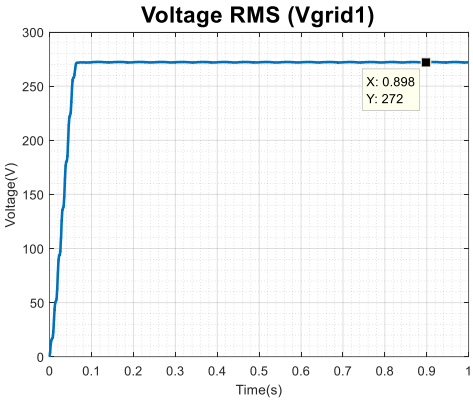

Fig 4.7: Voltage RMS at Point of Coupling

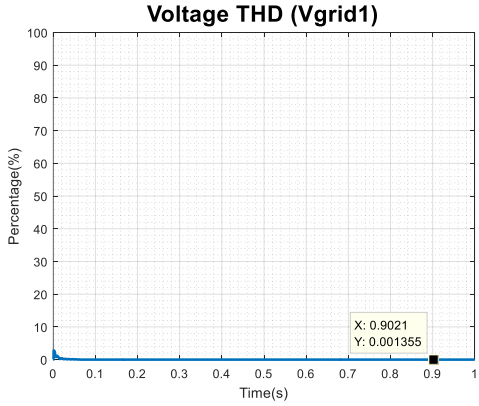

Fig 4.8: Voltage THD at Point of Coupling

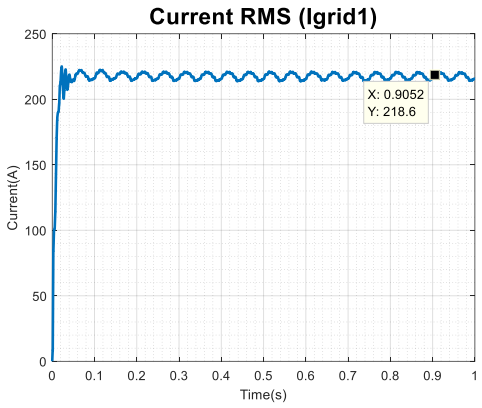

Fig 4.9: Current RMS at Point of Coupling

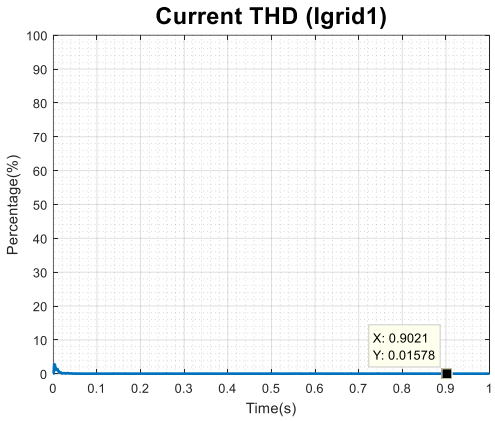

Fig 4.10: Current THD at Point of Coupling

Figure 4.3 highlights the DC side of the inverter, which is the point under study. Figures 4.4 and Figure 4.5 illustrate the output of the PSCAD results for the DC side of the inverter integrated with the first distributed generation unit (PV1), which is a photovoltaic source namely DER-PV1. Figure 4.6 highlights the AC side of the inverter, which is the point under study, whereas Figures 4.7 through 4.10 indicate the output of the PSCAD results on the AC side of the inverter for the first distributed generation unit (PV1). It is evident through the analysis of the figures generated that the system reaches a stable point of operation free of any transients in the neighborhood of 0.1 seconds and the total duration of the run is 1.0 second. It is clear that on the DC side of the inverter PV1 generates approximately 1,297V and 140.2A. The RMS voltage measured at the secondary side of the inverter at which point PV1 is incorporated into PV1 is approximately 272V, along with a Total Harmonic Distortion value of 0.0012%, whereas the RMS current measured at the same point is approximately 218.4A accompanied by a Total Harmonic Distortion value of approximately 0.0220%. The THD for both the voltage and current was very low and at an ideally acceptable level.

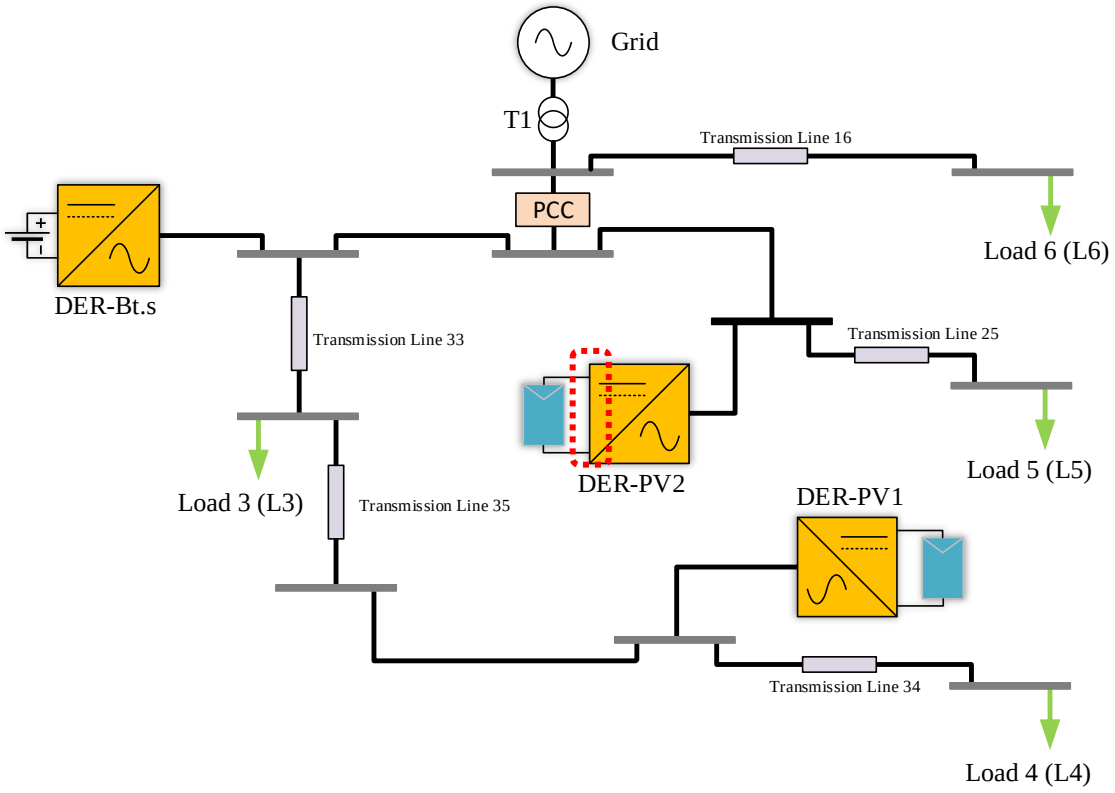

Fig 4.11: DG2 DC Side Point of Measurement

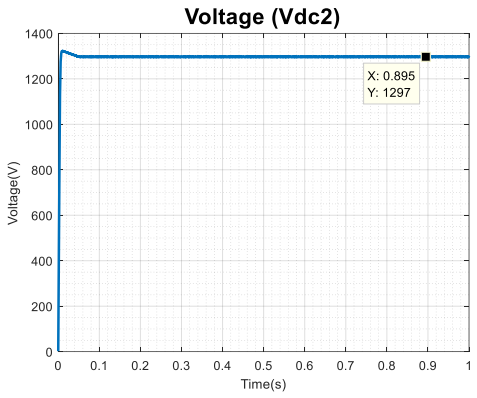

Fig 4.12: DC Link Voltage DG2

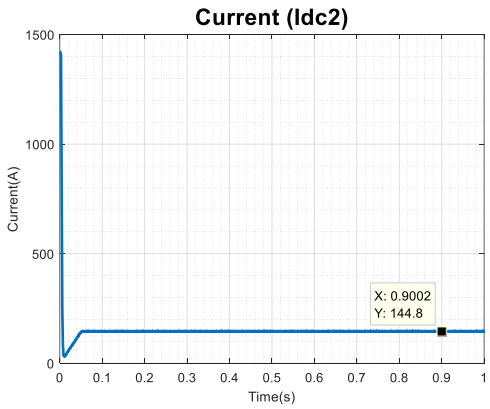

Fig 4.13: DC Link Current DG2

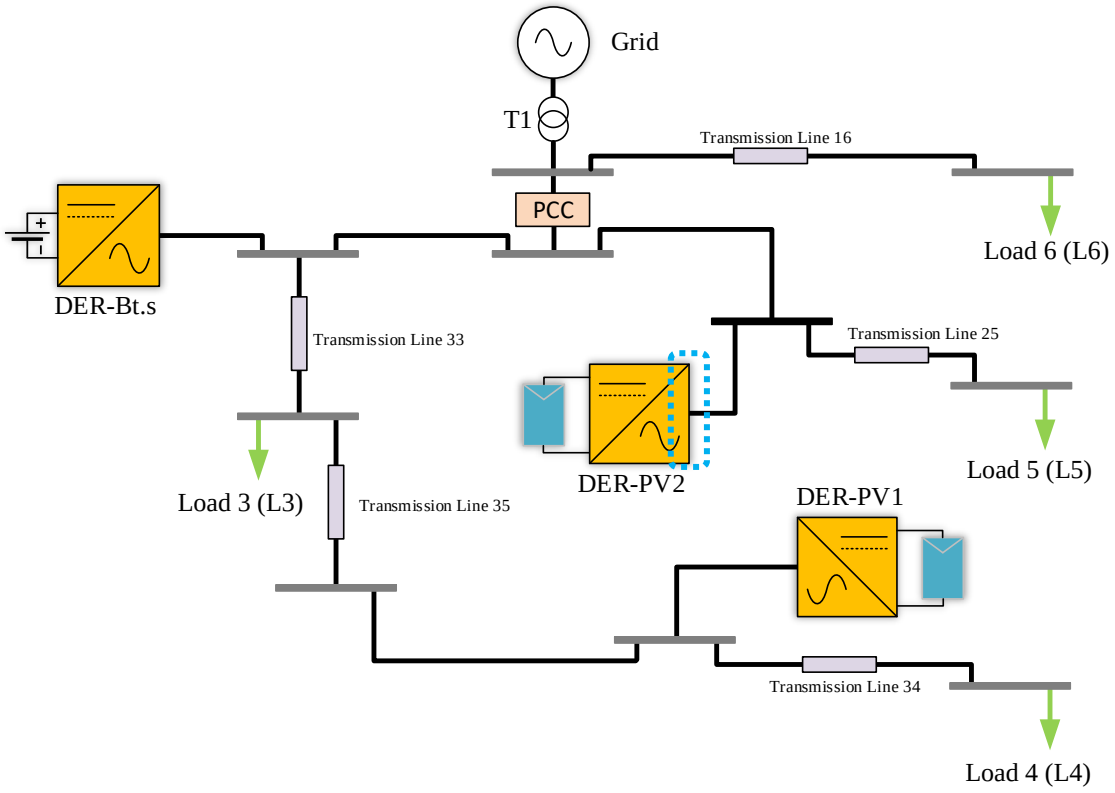

Fig 4.14: DG2 AC Side Point of Measurement

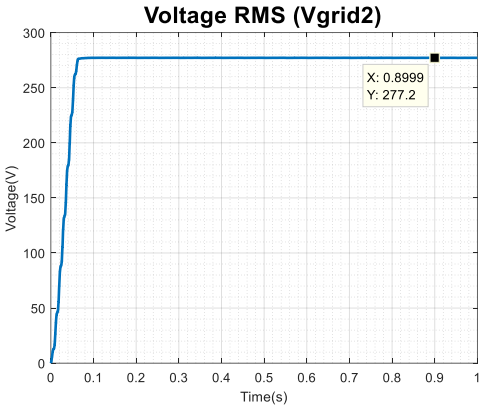

Fig 4.15: Voltage RMS at Point of Coupling

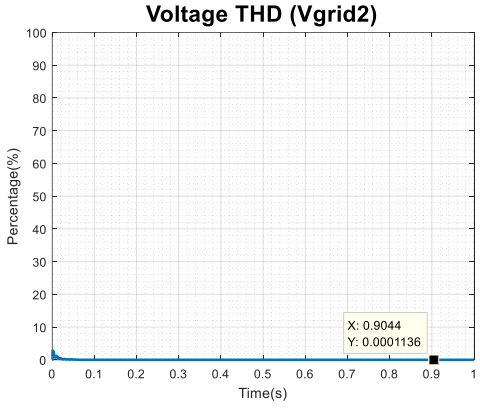

Fig 4.16: Voltage THD at Point of Coupling

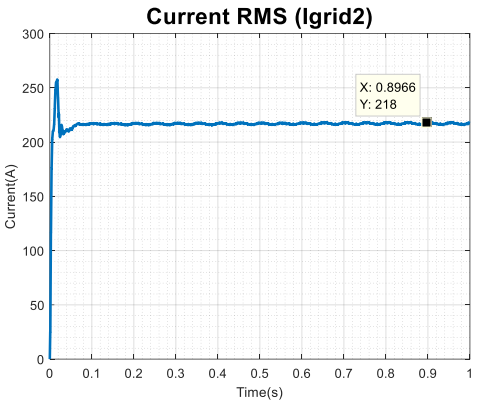

Fig 4.17: Current RMS at Point of Coupling

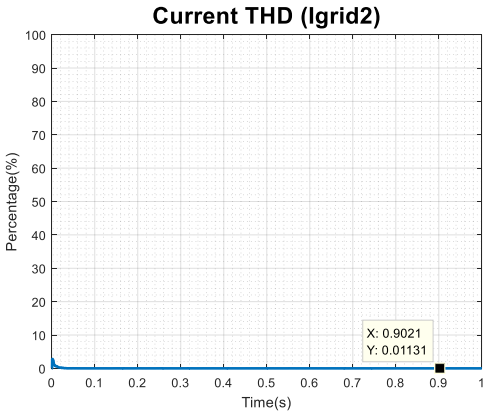

Fig 4.18: Current THD at Point of Coupling

Figure 4.11 highlights the DC side of the inverter, which is the point under study. Figures 4.12 and Figure 4.13 illustrate the output of the PSCAD results for the DC side of the inverter integrated with the second distributed generation unit (PV2), which is a photovoltaic source namely DER-PV2. Figure 4.14 highlights the AC side of the inverter, which is the point under study, whereas Figures 4.15 through 4.18 indicate the output of the PSCAD results on the AC side of the inverter for the second distributed generation unit (PV2). It is evident through analysis of the figures generated that the system reaches a stable point of operation free of any transients in the neighborhood of 0.1 seconds and the total duration of the run is 1.0 second. It is clear that on the DC side of the inverter PV2 generates approximately 1297V and 146.9A. The RMS voltage measured at the secondary side of the inverter at which point PV2 is incorporated into PV2 is approximately 277.1V, along with a Total Harmonic Distortion value of $9.2820\,x10^{-5}\%$, whereas the RMS current measured at the same point is approximately 217.9A, accompanied by a Total Harmonic Distortion value of approximately 0.0076%. The THD for both the voltage and current was very low and at an ideally acceptable level.

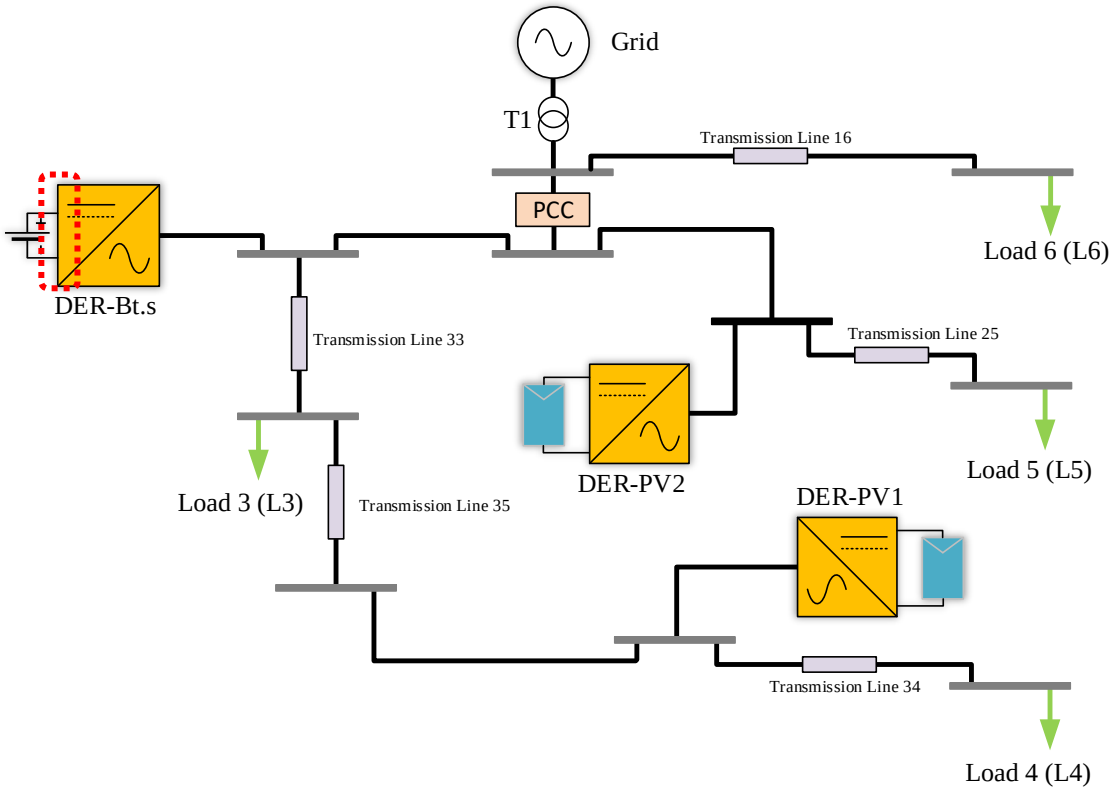

Fig 4.19: DG3 DC Side Point of Measurement

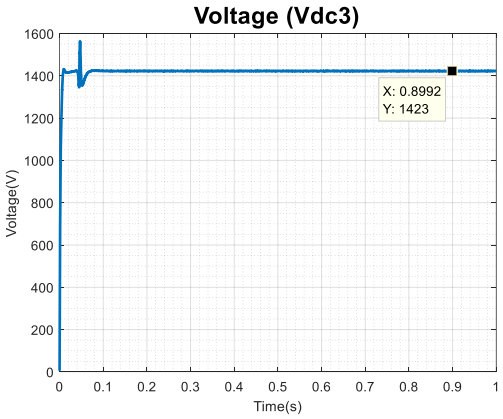

Fig 4.20: DC Link Voltage DG3

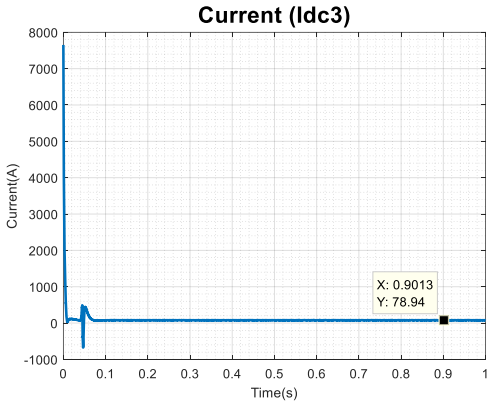

Fig 4.21: DC Link Current DG3

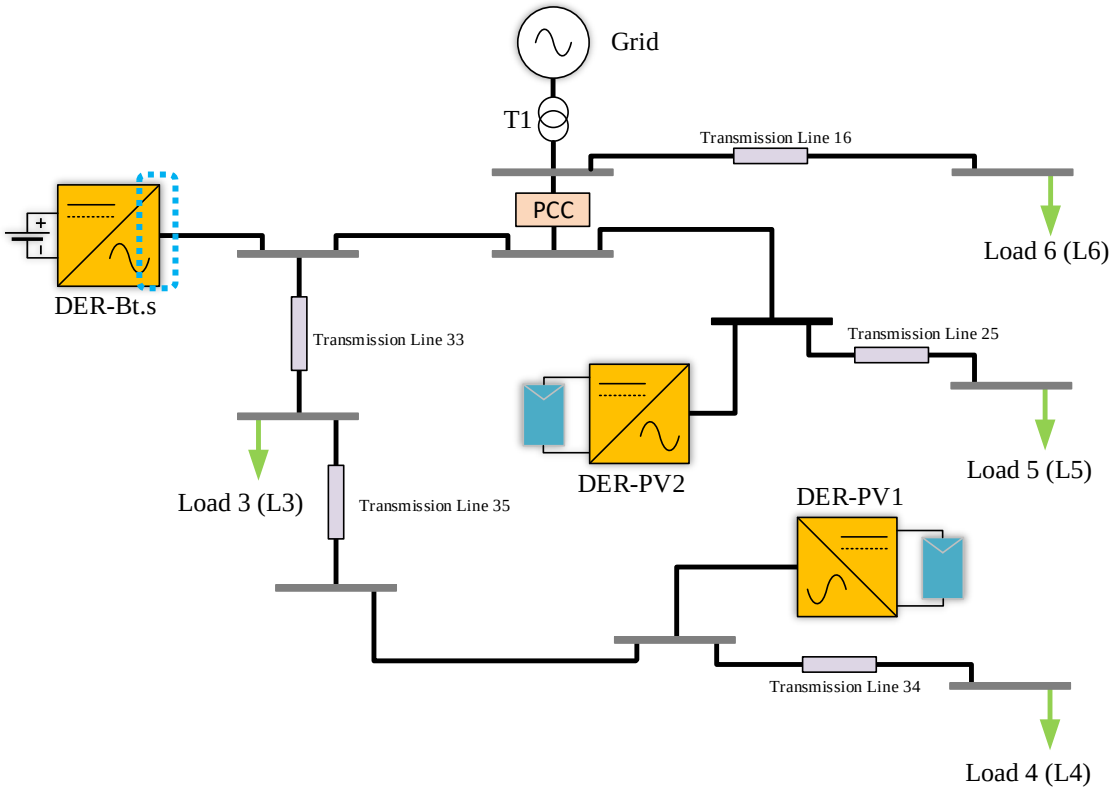

Fig 4.22: DG3 AC Side Point of Measurement

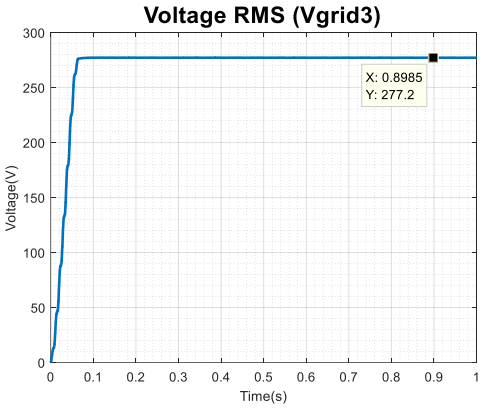

Fig 4.23: Voltage RMS at Point of Coupling

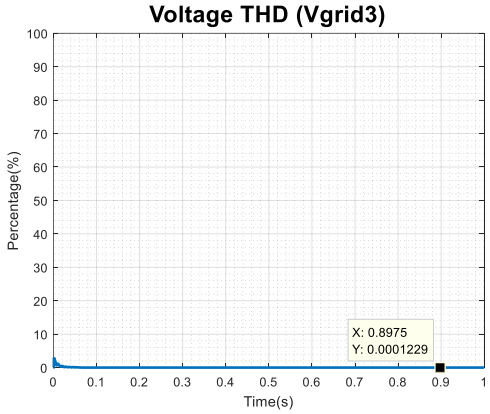

Fig 4.24: Voltage THD at Point of Coupling

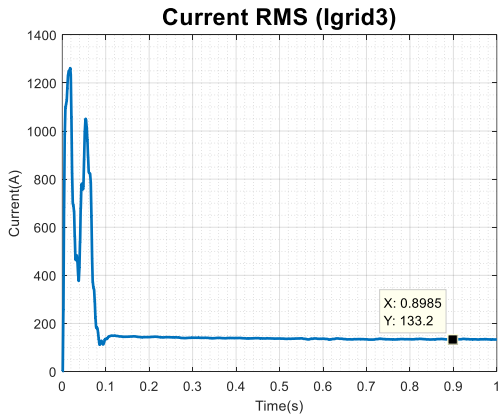

Fig 4.25: Current RMS at Point of Coupling

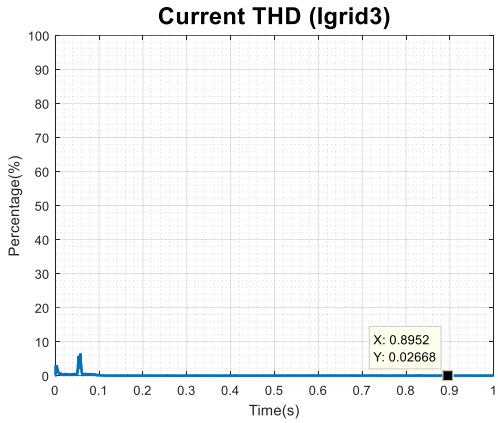

Fig 4.26: Current THD at Point of Coupling

Figure 4.19 highlights the DC side of the inverter, which is the point under study. Figures 4.20 and Figure 4.21 illustrate the output of the PSCAD results for the DC side of the inverter integrated with the third distributed generation unit (BES), which is a battery energy storage source namely DER-Bt.S. Figure 4.22 highlights the AC side of the inverter, which is the point under study. Whereas Figures 4.23 through 4.26 indicate the output of the PSCAD results on the AC side of the inverter for the third distributed generation unit (BES). It is evident through the analysis of the figures generated that the system reaches a stable point of operation free of any transients in the neighborhood of 0.1 seconds and the total duration of the run is 1.0 second. It is clear that on the DC side of the inverter BES generates approximately 1,423V and 78.62A. The RMS voltage measured at the secondary side of the inverter at which point BES is incorporated into BES is approximately 277.1V, along with a Total Harmonic Distortion value of 0.0001%, whereas the RMS current measured at the same point is approximately 133.3A, accompanied by a Total Harmonic Distortion value of approximately 0.0280%. The THD for both the voltage and current was very low and at an ideally acceptable level.

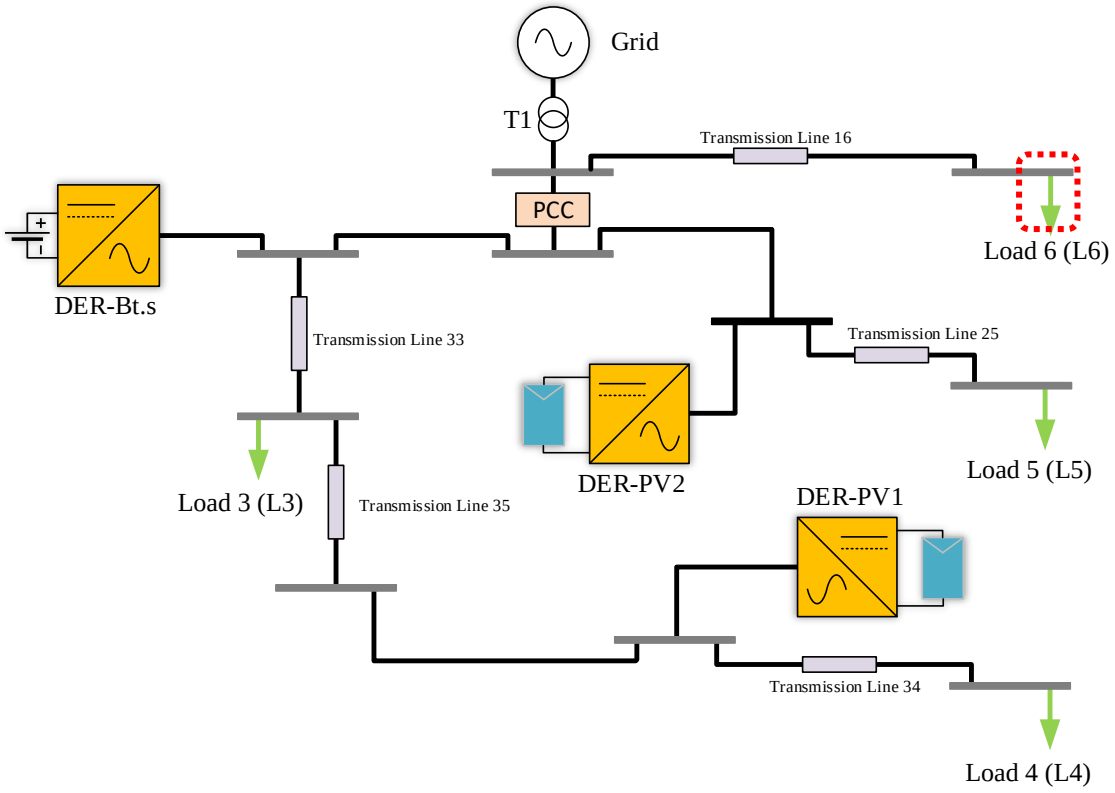

Fig 4.27: Load Measurement Point

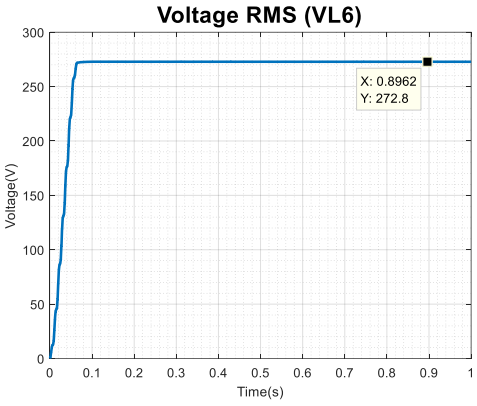

Fig 4.28: Voltage RMS at Load 6

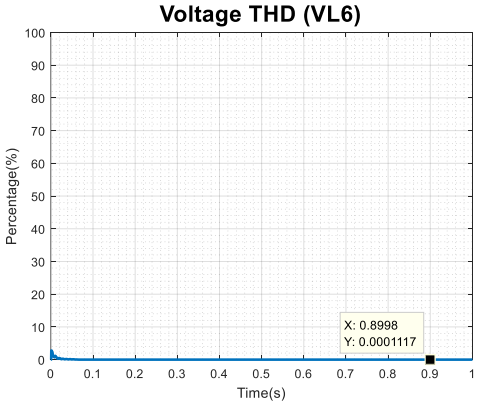

Fig 4.29: Voltage THD at Load 6

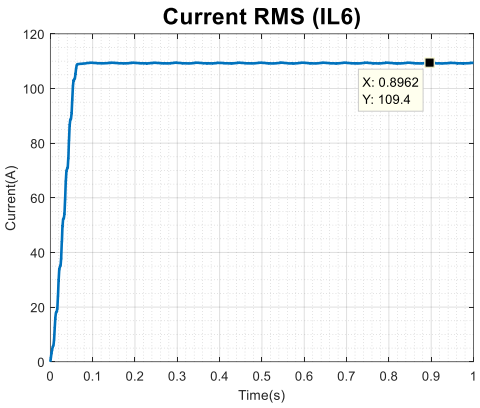

Fig 4.30: Current RMS at Load 6

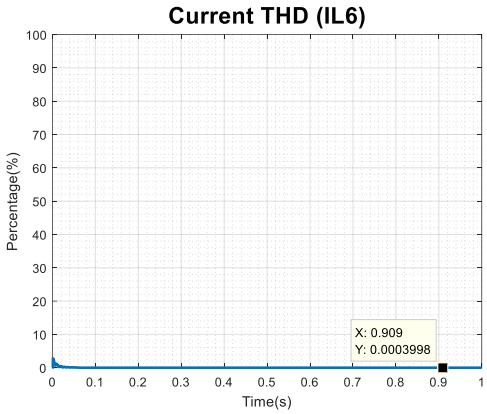

Fig 4.31: Current THD at Load 6

Figure 4.27 highlights Load 6, which is the node under study. Figures 4.28 through figures 4.31 illustrate the output of the PSCAD results for the load side of Line16, which is the first branch of the CERTS microgrid testbed system. Between Load 6 and the Grid there is a transmission line which results in transmission losses. It is essential to study the measurements at Load 6 to verify that the load demand is being satisfied. It is evident through analysis of the figures that the system stabilizes at 0.1 seconds and the total duration of the run is 1.0 second. It is clear that the RMS voltage is 272.8V and the THD of the voltage is 0.0449%. The measurements indicate that the RMS current is approximately 109.9A and the THD is approximately 0.0421%. The THD for both the voltage and current is very low and at an ideally acceptable level.

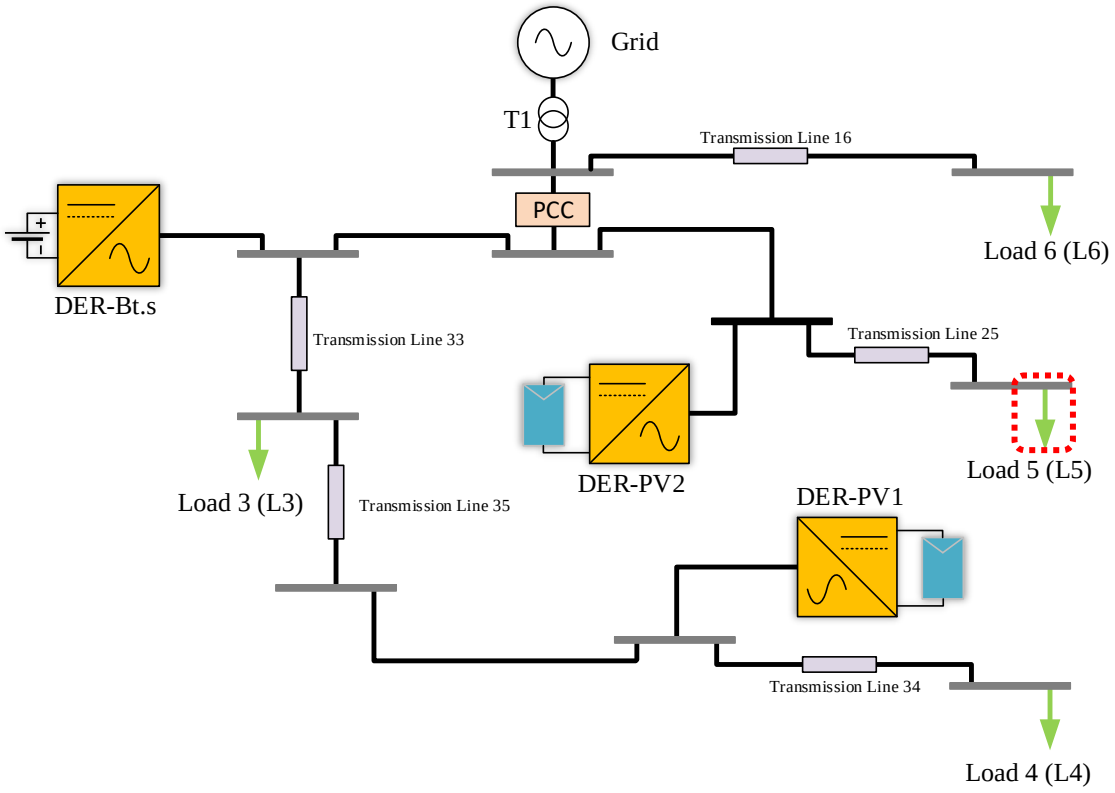

Fig 4.32. Load 5 Measurement Point

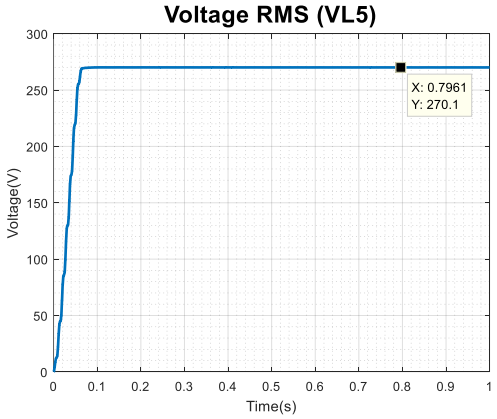

Fig 4.33: Voltage RMS at Load 5

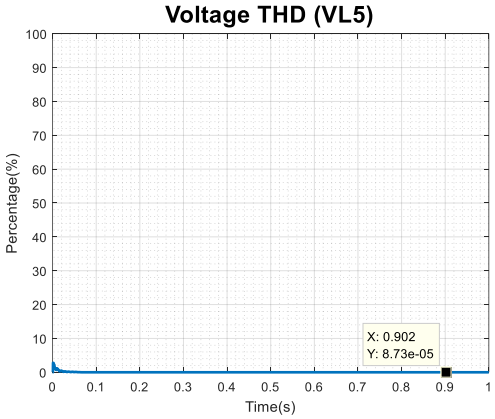

Fig 4.34: Voltage THD at Load 5

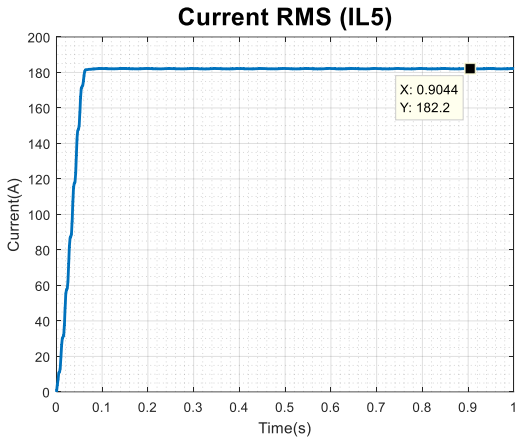

Fig 4.35: Current RMS at Load 5

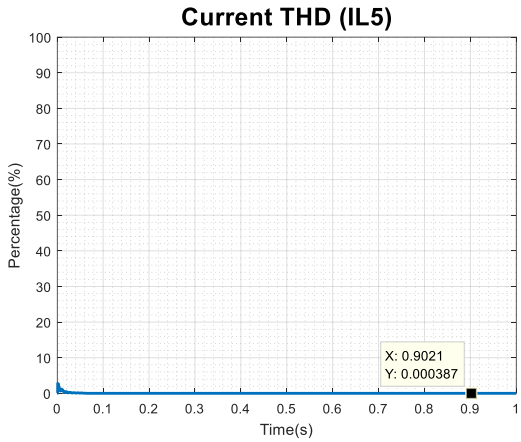

Fig 4.36: Current THD at Load 5

Figure 4.32 shows Load 5, which is connected at the node under study. Figures 4.33 through figures 4.36 illustrate the output of the PSCAD results for the load side of Line25, which is the second branch of the CERTS microgrid testbed system. Between Load 5 and the Grid there is a transmission line, which results in transmission losses, along with the point of coupling of PV2 It is essential to study the measurements at Load 5 to verify that the load demand is being satisfied. The addition of a DG has an impact on the output parameters, and it is essential to study the impact of the amalgamation. It is evident through analysis of the figures that the system stabilizes at 0.1 seconds and the total duration of the run is 1.0 second. It is clear that the RMS voltage is 269.9V and the THD of the voltage is 0.0111%. The measurements indicate that the RMS current is approximately 182.7A and the THD is approximately 0.0504%. The THD for both the voltage and current is very low and at an ideally acceptable level.

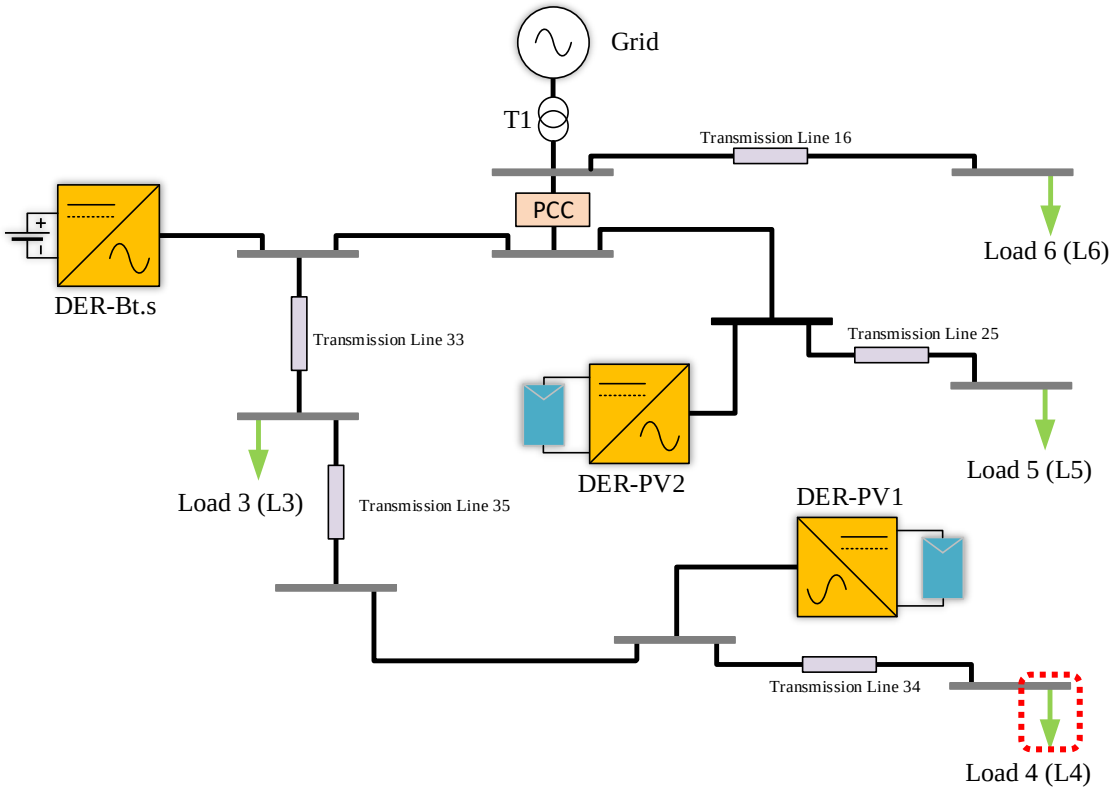

Fig 4.37: Load 4 Measurement Point

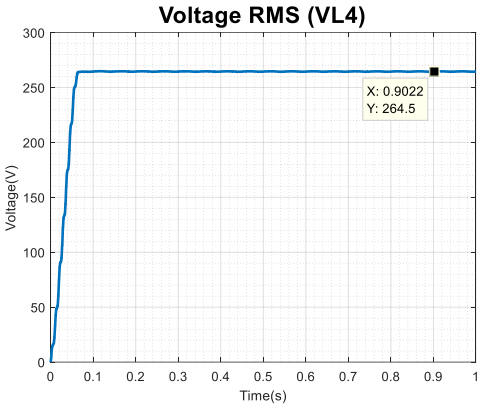

Fig 4.38. Voltage RMS at Load 4

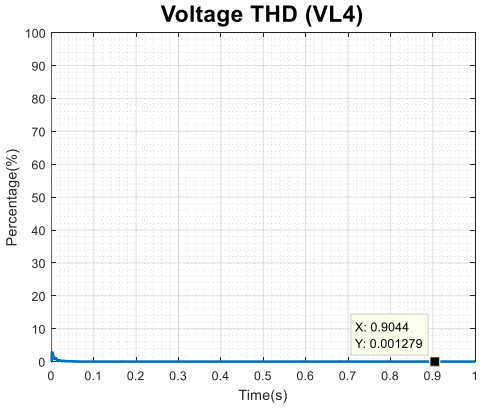

Fig 4.39. Voltage THD at Load 4

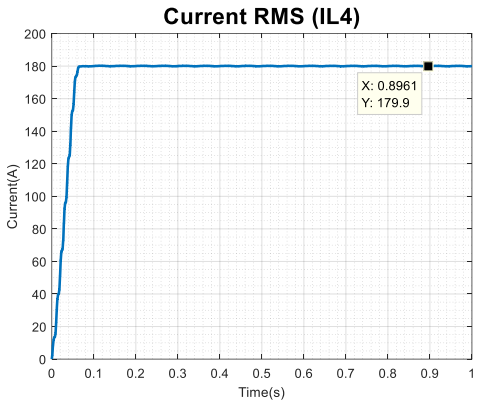

Fig 4.40: Current RMS at Load 4

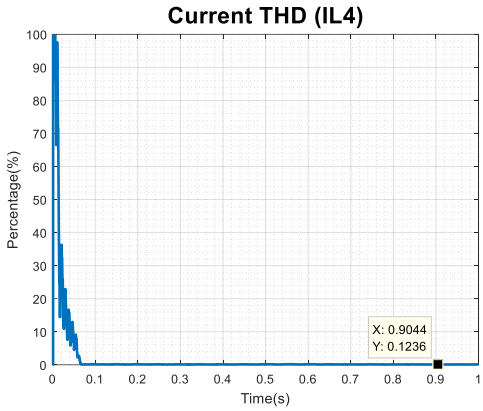

Fig 4.41: Current RMS at Load 4

Figure 4.37 shows Load 4, which is connected at the node under study. Figures 4.38 through figures 4.41 illustrate the output of the PSCAD results for the load side of Line44, which is the third branch of the CERTS microgrid testbed system. Between Load 4 and the Grid there are three sets of transmission lines which result in transmission losses, along with the point of coupling of PV1 and BES. It is essential to study the measurements at Load 4 to verify that the load demand is being satisfied. The addition of two DGs has an impact on the output parameters and it is essential to study the impact of the amalgamation. Load 4 is the furthest from the source and as such encounters the most variation and the highest offset. It is evident through analysis of the figures that the system stabilizes at 0.1 seconds and the total duration of the run is 1.0 second. It is clear that the RMS voltage is 264.5V and the THD of the voltage is 0.0013%. The measurements indicate that the RMS current is approximately 179.9A and the THD is approximately 0.1271%. The THD for both the voltage and current is very low and at an ideally acceptable level.

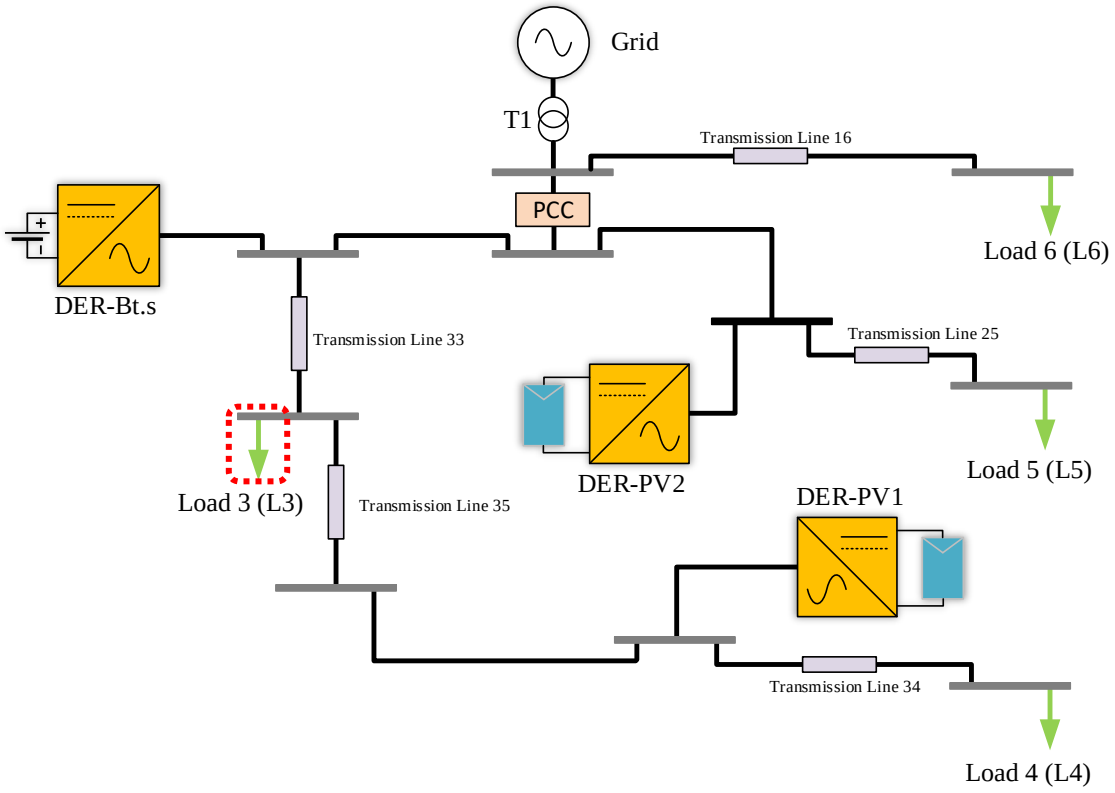

Fig 4.42: Load 3 Measurement Point

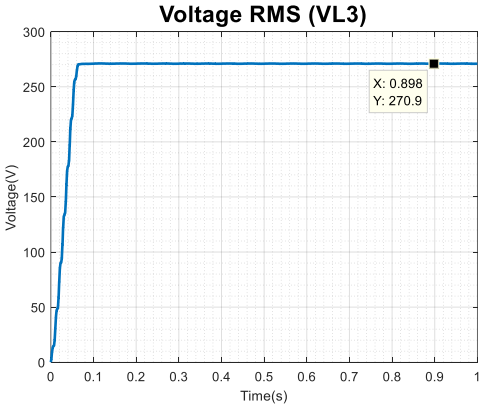

Fig 4.43: Voltage RMS at Load 3

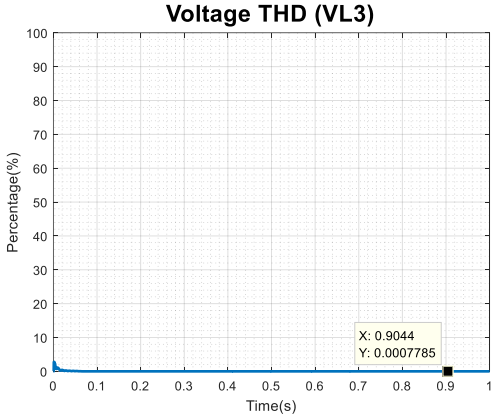

Fig 4.44: Voltage THD at Load 3

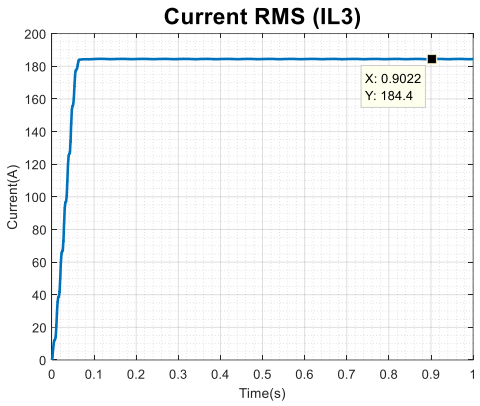

Fig 4.45: Current RMS at Load 3

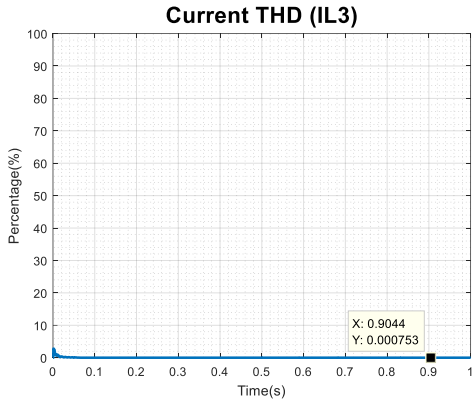

Fig 4.46: Current RMS at Load 3

Figure 4.42 shows Load 3, which is connected at the node under study. Figures 4.43 through figures 4.46 illustrate the output of the PSCAD results for the load side of Line34, which is the third branch of the CERTS microgrid testbed system. Between Load 3 and the Grid there is one transmission line, which result in transmission losses, along with the point of coupling of BES. It is essential to study the measurements at Load 3 to verify that the load demand is being satisfied. The addition of two DGs has an impact on the output parameters and it is essential to study the impact of the amalgamation. Load 4 is the furthest from the source and as such encounters the most variation and the highest offset. It is evident through analysis of the figures that the system stabilizes at 0.1 seconds and the total duration of the run is 1.0 second. It is clear that the RMS voltage is 270.9V and the THD of the voltage is 0.0082%. The measurements indicate that the RMS current is approximately 184.4A and the THD is approximately 0.0079%. The THD for both the voltage and current is very low and at an ideally acceptable level.

Table 4.1: Mean, MAD and Variance of Load 6

Load 6 PSCAD								
	Run1	**Run2**	**Run3**	**Run4**	**Run5**	**Avg of Means**	**MAD**	**Variance**
VRMS	263.89	263.89	263.89	263.943	263.89	263.9002	0.01712	0.00057245
VTHD	0.0263	0.0263	0.0263	0.0264	0.0263	0.02632	3.2E-05	2E-09
IRMS	105.753	105.753	105.753	105.774	105.753	105.75682	0.006912	9.3312E-05
ITHD	0.0254	0.0254	0.0254	0.0254	0.0254	0.0254	0	0

Table 4.2: Mean, MAD and Variance of Load 5

Load 5 PSCAD								
	Run1	**Run2**	**Run3**	**Run4**	**Run5**	**Avg of Means**	**MAD**	**Variance**
VRMS	261.207	261.207	261.207	261.26	261.207	261.21768	0.016928	0.000559682
VTHD	0.0264	0.0264	0.0264	0.0264	0.0264	0.0264	0	0
IRMS	176.272	176.272	176.272	176.308	176.272	176.2791	0.01152	0.0002592
ITHD	0.0254	0.0254	0.0254	0.0254	0.0254	0.0254	0	0

Table 4.3: Mean, MAD and Variance of Load 4

Load 4 PSCAD								
	Run1	**Run2**	**Run3**	**Run4**	**Run5**	**Avg of Means**	**MAD**	**Variance**
VRMS	256.138	256.138	256.138	256.19	256.138	256.14836	0.016736	0.000547058
VTHD	0.0264	0.0264	0.0264	0.0264	0.0264	0.0264	0	0
IRMS	178.653	174.461	174.461	174.497	174.461	175.3064	1.3388	3.50099312
ITHD	0.0252	2.5386	2.5386	2.5417	2.5386	2.03654	0.804536	1.264216988

Table 4.4: Mean, MAD and Variance of Load 3

Load 3 PSCAD								
	Run1	**Run2**	**Run3**	**Run4**	**Run5**	**Avg of Means**	**MAD**	**Variance**
VRMS	262.292	262.292	262.292	262.346	262.292	262.30306	0.017056	0.000568178
VTHD	0.0261	0.0261	0.0261	0.0261	0.0261	0.0261	0	0
IRMS	178.653	178.653	178.653	178.69	178.653	178.66072	0.011712	0.000267912
	0.0252	0.0252	0.252	0.0253	0.0252	0.07058	0.072568	0.010285382

4.3.2 Matlab-Simscape Simulation Grid Connected Mode

In this chapter, the results obtained from Matlab-Simscape are illustrated and discussed. The points of measurement utilized were discussed in section 4.2 and are illustrated here using the single line diagram of the CERTS microgrid testbed system. The data collected through ten iterations is represented graphically and numerically, as can be seen in this section.

First the DC side voltage and DC side current generated by the distributed generation units are discussed. Followed by the AC side voltage and AC side current of inverters utilized to couple the distributed generators to the grid. Finally, the voltage and current of each of load is illustrated. In order to conduct thorough work, it was necessary to investigate the Root Mean Square and Total Harmonic Distortion of all AC values being analyzed.

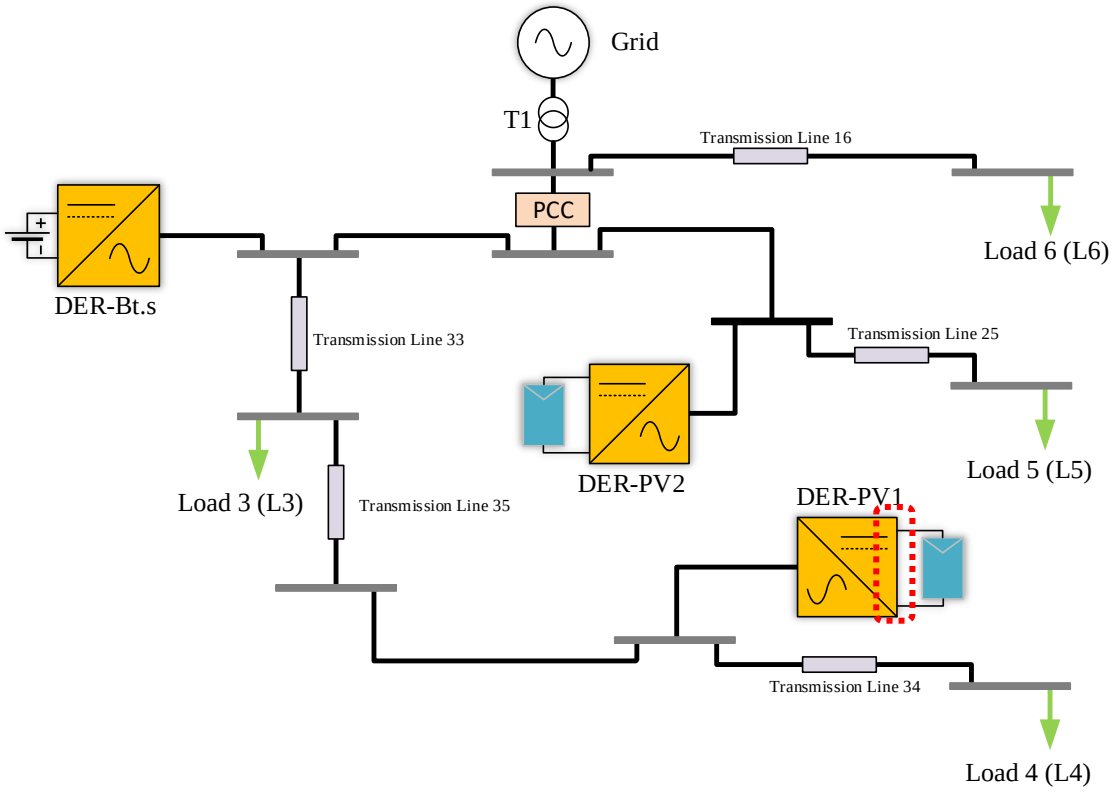

Fig 4.47: DG1 DC Side Point of Measurement

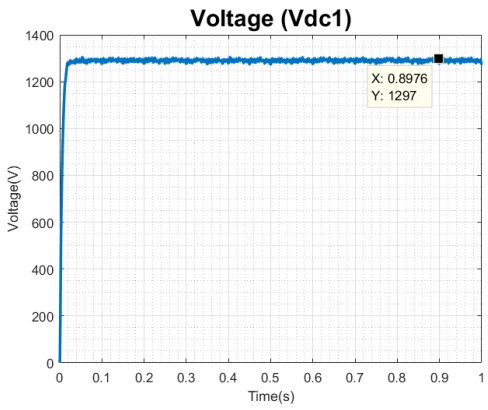

Fig 4.48: DC Link Voltage DG1

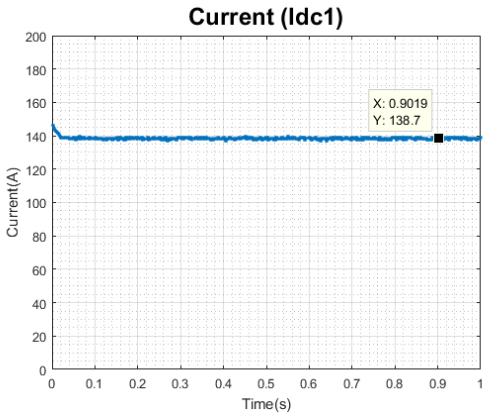

Fig 4.49: DC Link Current DG1

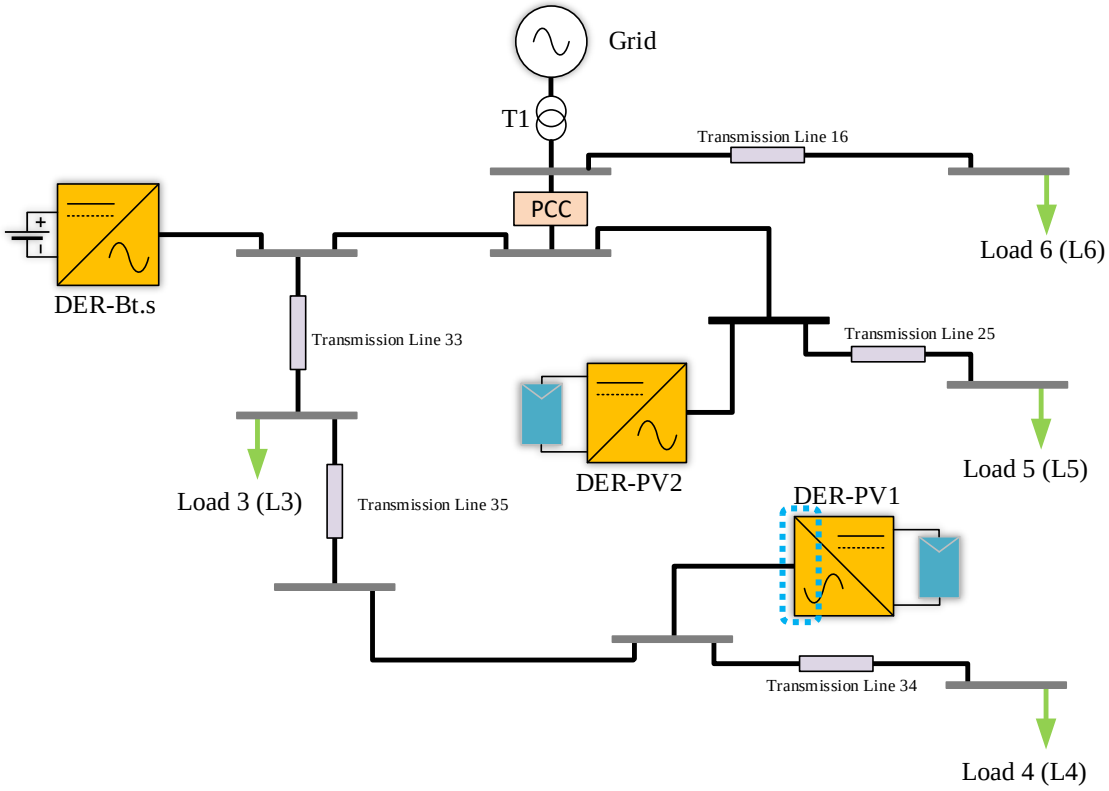

Fig 4.50: DG1 AC Side Point of Measurement

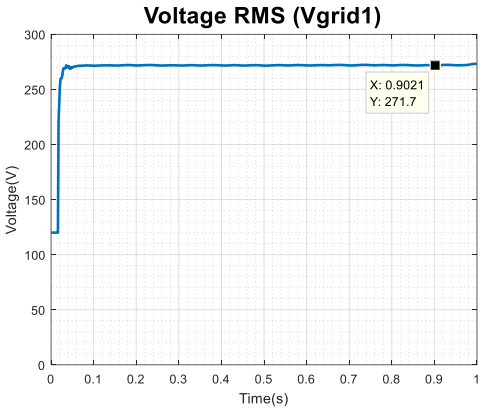

Fig: 4.51: Voltage RMS at Point of Coupling

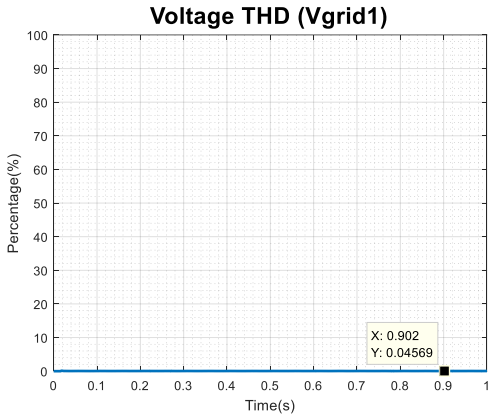

Fig: 4.52: Voltage THD at Point of Coupling

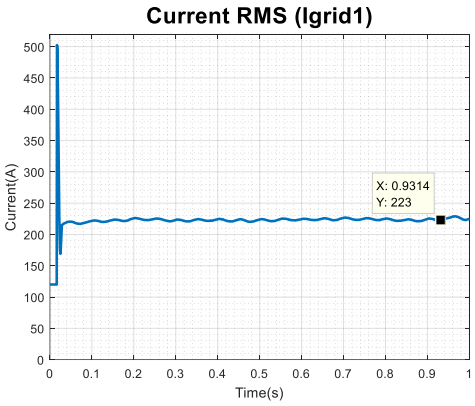

Fig: 4.53: Current RMS at Point of Coupling

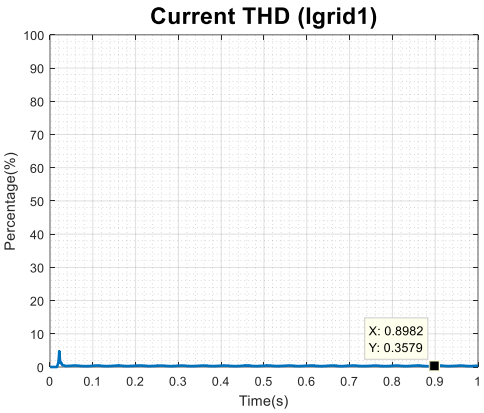

Fig: 4.54. Current THD at Point of Coupling

Figure 4.3 depicts the DC side of the inverter, which is the point under study. Figures 4.4 and Figure 4.5 illustrate the output of the PSCAD results for the DC side of the inverter integrated with the first distributed generation unit (PV1), which is a photovoltaic source namely DER-PV1. Figure 4.6 highlights the AC side of the inverter, which is the point under study, whereas Figures 4.7 through 4.10 indicate the output of the PSCAD results on the AC side of the inverter for the first distributed generation unit (PV1). It is evident through analysis of the figures generated that the system reaches a stable point of operation free of any transients in the neighborhood of 0.1 seconds and the total duration of the run is 1.0 second. It is clear that on the DC side of the inverter PV1 generates

approximately 1297V and 138.7A. The RMS voltage measured at the secondary side of the inverter at which point PV1 is incorporated into PV1 is approximately 271.7V, along with a Total Harmonic Distortion value of 0.0457%, whereas the RMS current measured at the same point is approximately 223A, accompanied by a Total Harmonic Distortion value of approximately 0.3579%. The THD for both the voltage and current was very low and at an ideally acceptable level.

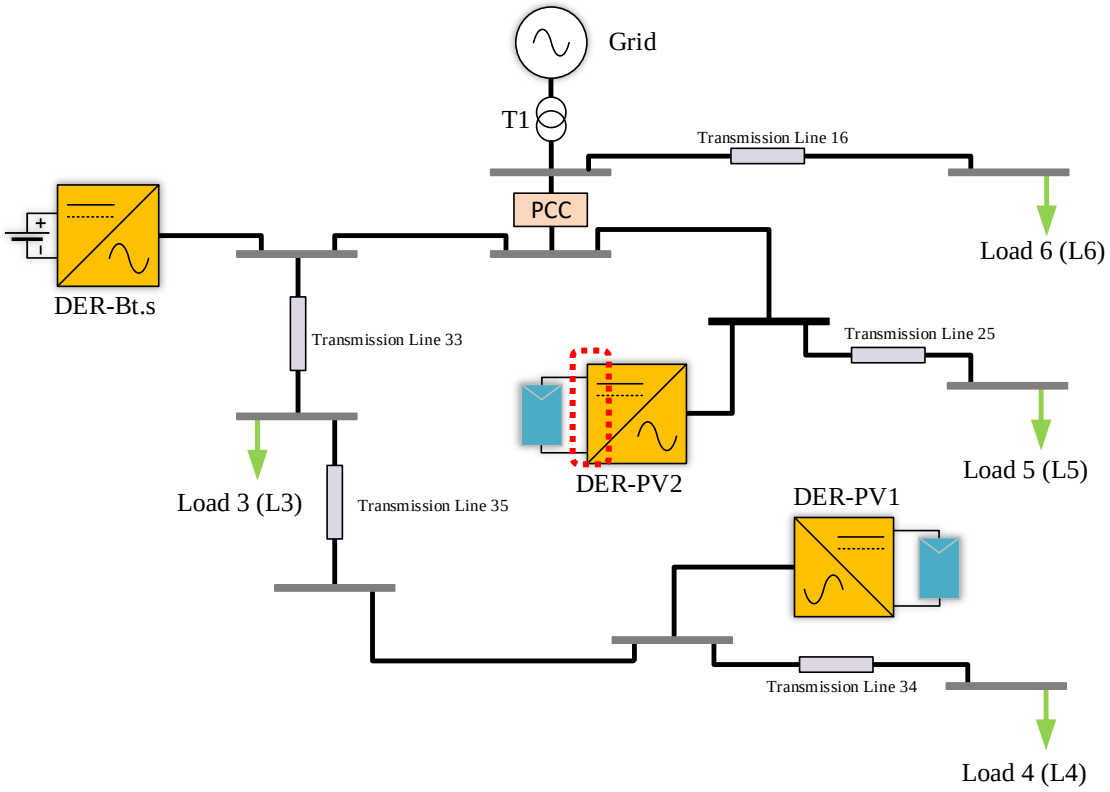

Fig 4.55: DG2 DC Side Point of Measurement

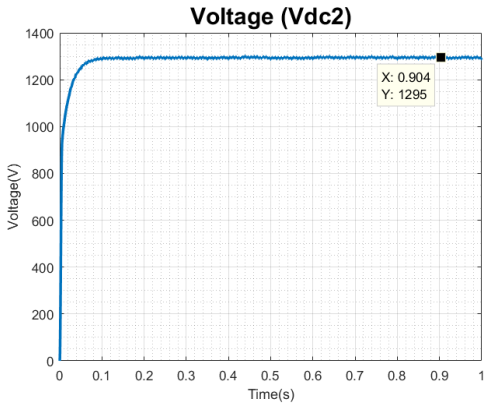

Fig 4.56: DC Link Voltage DG2

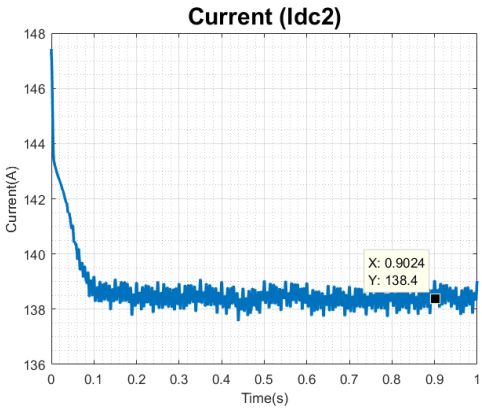

Fig 4.57: DC Link Current DG2

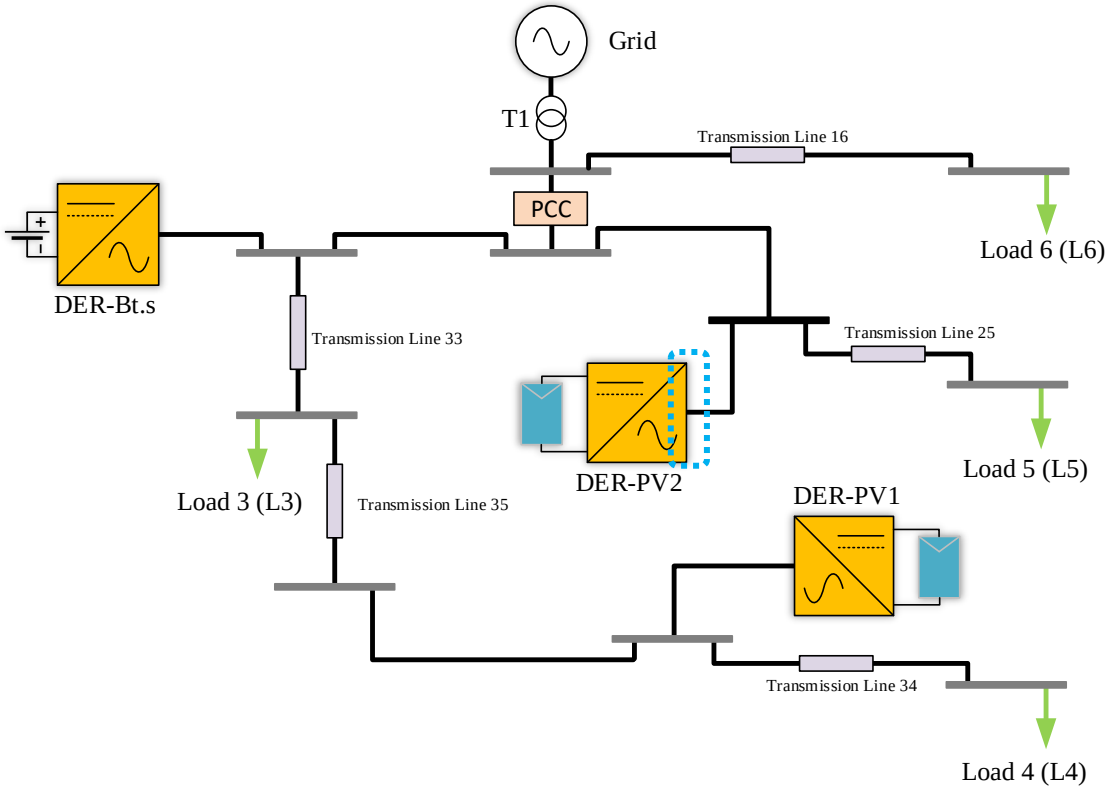

Fig 4.58: DG2 AC Side Point of Measurement

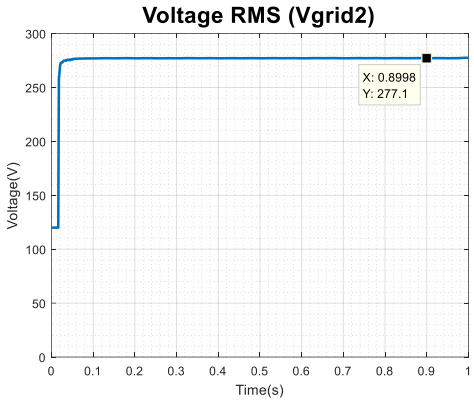

Fig 4.59. Voltage RMS at Point of Coupling

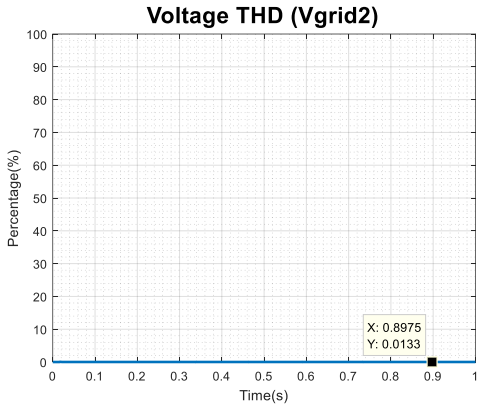

Fig 4.60. Voltage THD at Point of Coupling

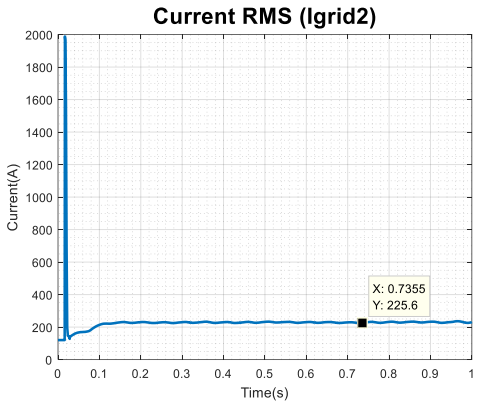

Fig 4.61. Current RMS at Point of Coupling

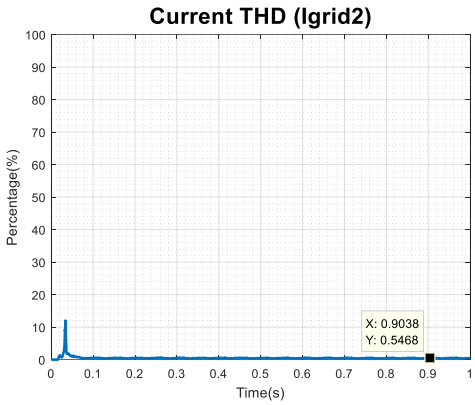

Fig 4.62. Current THD at Point of Coupling

Figure 4.55 highlights the DC side of the inverter which is the point under study. Figures 4.56 and Figure 4.57 illustrate the output of the PSCAD results for the DC side of the inverter integrated with the second distributed generation unit (PV2), which is a photovoltaic source namely DER-PV2. Figure 4.58 highlights the AC side of the inverter, which is the point under study. Whereas Figures 4.59 through 4.62 indicate the output of the PSCAD results on the AC side of the inverter for the second distributed generation unit

(PV2). It is evident through analysis of the figures generated that the system reaches a stable point of operation free of any transients in the neighborhood of 0.1 seconds and the total duration of the run is 1.0 second. It is clear that on the DC side of the inverter PV2 generates approximately 1295V and 138.4A. The RMS voltage measured at the secondary side of the inverter at which point PV2 is incorporated into PV2 is approximately 277.1V, along with a Total Harmonic Distortion value of 0.0133%, whereas the RMS current measured at the same point is approximately 225.6A, accompanied by a Total Harmonic Distortion value of approximately 0.5468%. The THD for both the voltage and current was very low and at an ideally acceptable level.

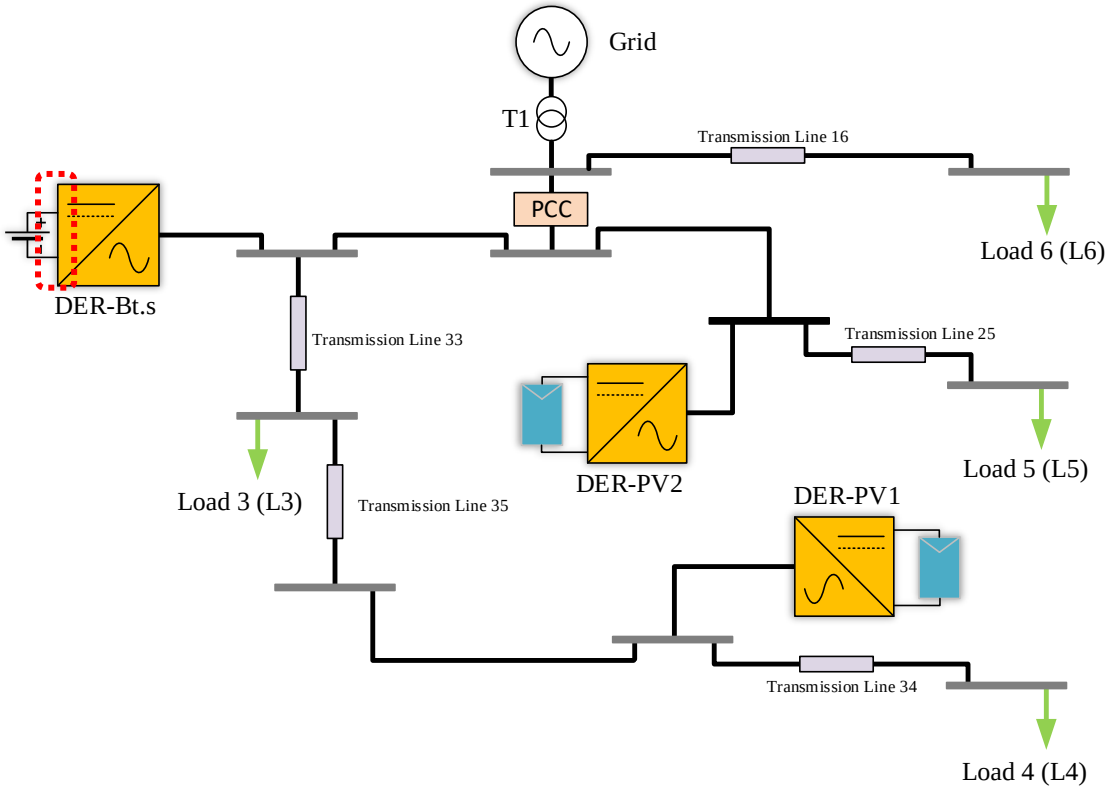

Fig 4.63: DG3 DC Side Point of Measurement

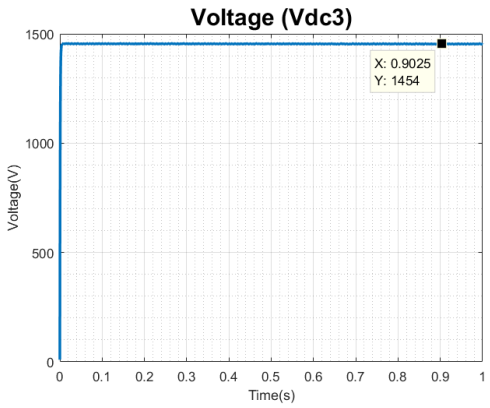

Fig 4.64: DC Link Voltage DG3

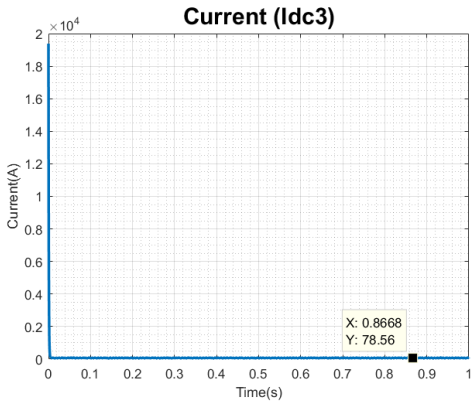

Fig 4.65: DC Link Current DG3

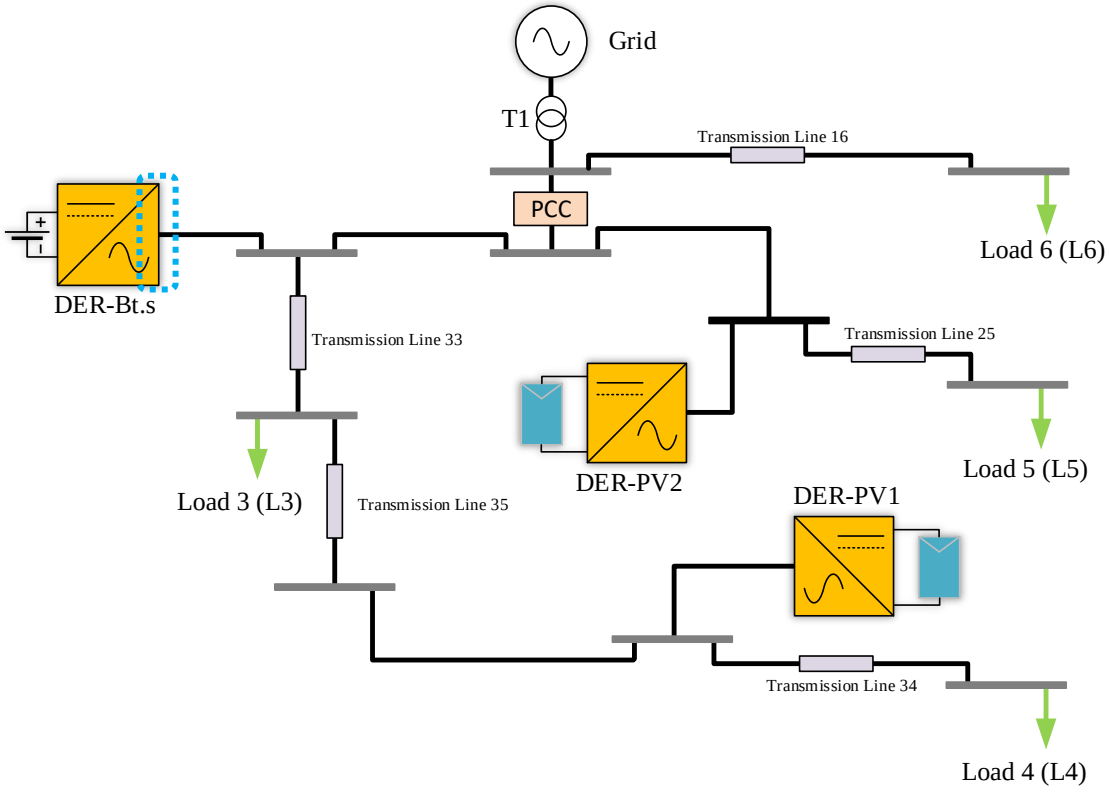

Fig 4.66: DG3 AC Side Point of Measurement

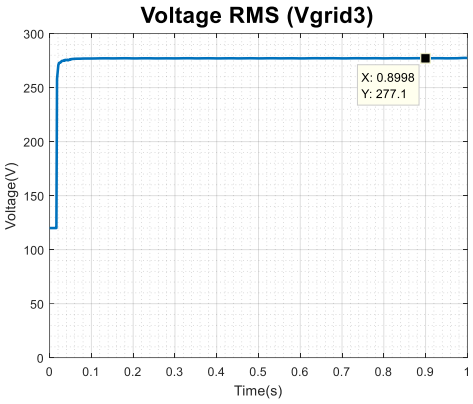

Fig 4.67: Voltage RMS at Point of Coupling

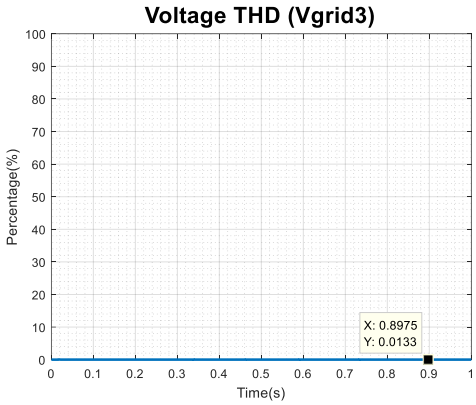

Fig 4.68: Voltage THD at Point of Coupling

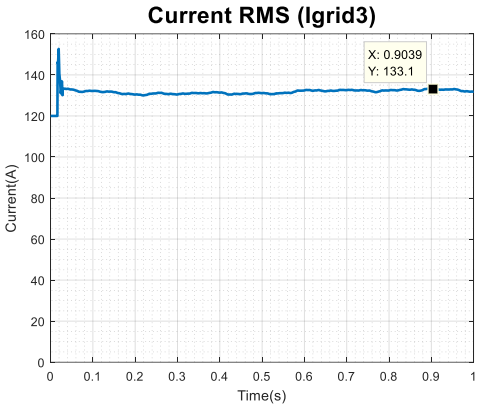

Fig 4.69: Current RMS at Point of Coupling

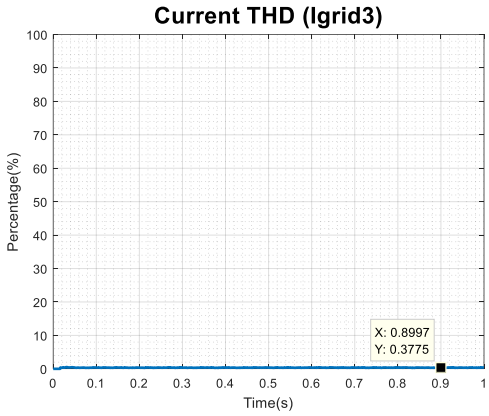

Fig 4.70: Current THD at Point of Coupling

Figure 4.63 highlights the DC side of the inverter, which is the point under study. Figures 4.64 and Figure 4.65 illustrate the output of the PSCAD results for the DC side of the inverter integrated with the third distributed generation unit (BES), which is a battery energy storage source namely DER-Bt.S. Figure 4.66 highlights the AC side of the inverter which is the point under study, whereas Figures 4.67 through 4.70 indicate the output of

the PSCAD results on the AC side of the inverter for the third distributed generation unit (BES). It is evident through analysis of the figures generated that the system reaches a stable point of operation free of any transients in the neighborhood of 0.1 seconds and the total duration of the run is 1.0 second. It is clear that on the DC side of the inverter BES generates approximately 1454V and 78.56A. The RMS voltage measured at the secondary side of the inverter at which point BES is incorporated into BES is approximately 277.1V, along with a Total Harmonic Distortion value of 0.0133 %, whereas the RMS current measured at the same point is approximately 133.1A, accompanied by a Total Harmonic Distortion value of approximately 0.3775%. The THD for both the voltage and current was very low and at an ideally acceptable level.

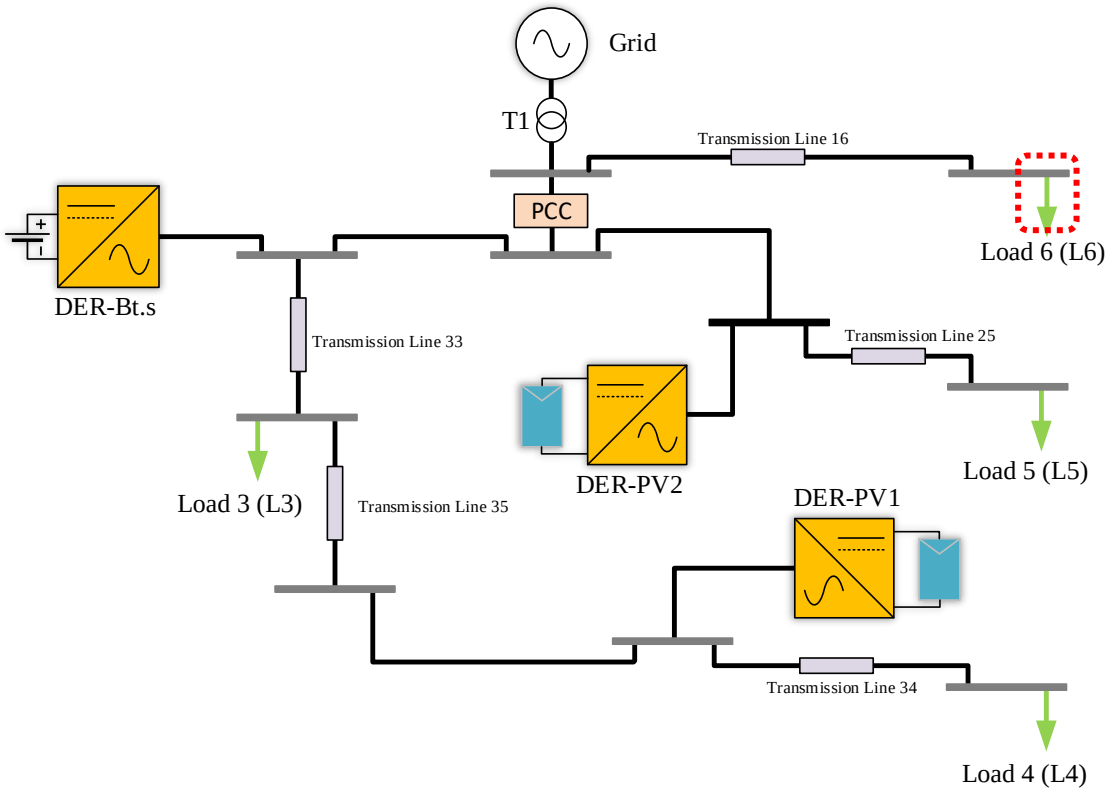

Fig 4.71: Load 6 Measurement Point

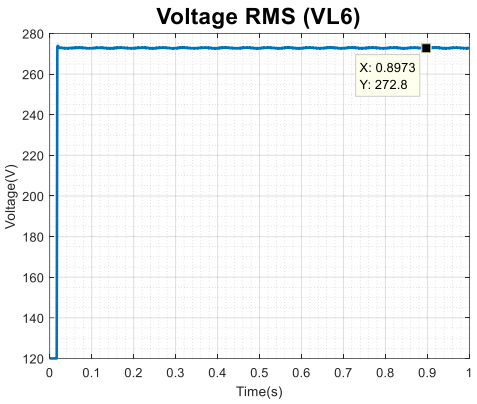

Fig 4.72: Voltage RMS at Load 6

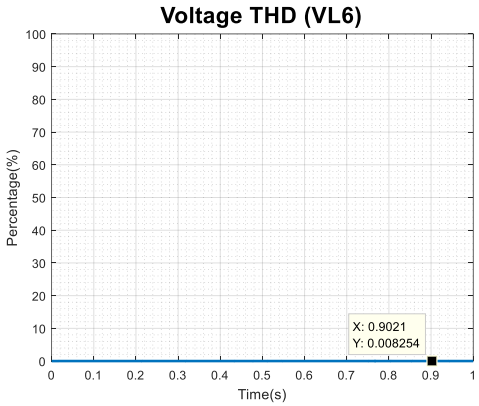

Fig 4.73: Voltage THD at Load 6

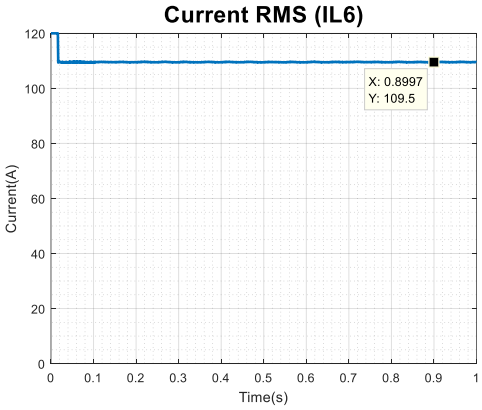

Fig 4.74: Current RMS at Load 6

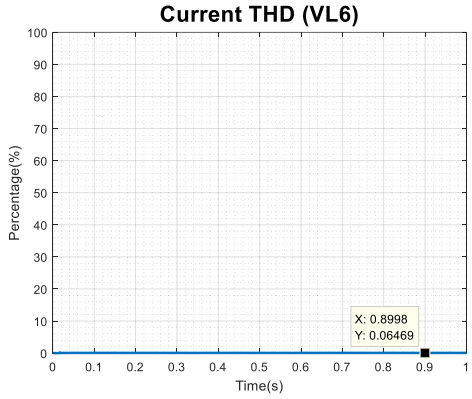

Fig 4.75: Current THD at Load 6

Figure 4.71 highlights Load 6, which the node under study. Figures 4.72 through figures 4.75 illustrate the output of the PSCAD results for the load side of Line16, which is the first branch of the CERTS microgrid testbed system. Between Load 6 and the Grid there is a transmission line, which results in transmission losses. It is essential to study the measurements at Load 6 to verify that the load demand is being satisfied. It is evident through analysis of the figures that the system stabilizes at 0.1 seconds and the total duration of the run is 1.0 second. It is clear that the RMS voltage is 272.8V and the THD of the voltage is 0.0083%. The measurements indicate that the RMS current is

approximately 109.9A and the THD is approximately 0.0647%. The THD for both the voltage and current is very low and at an ideally acceptable level

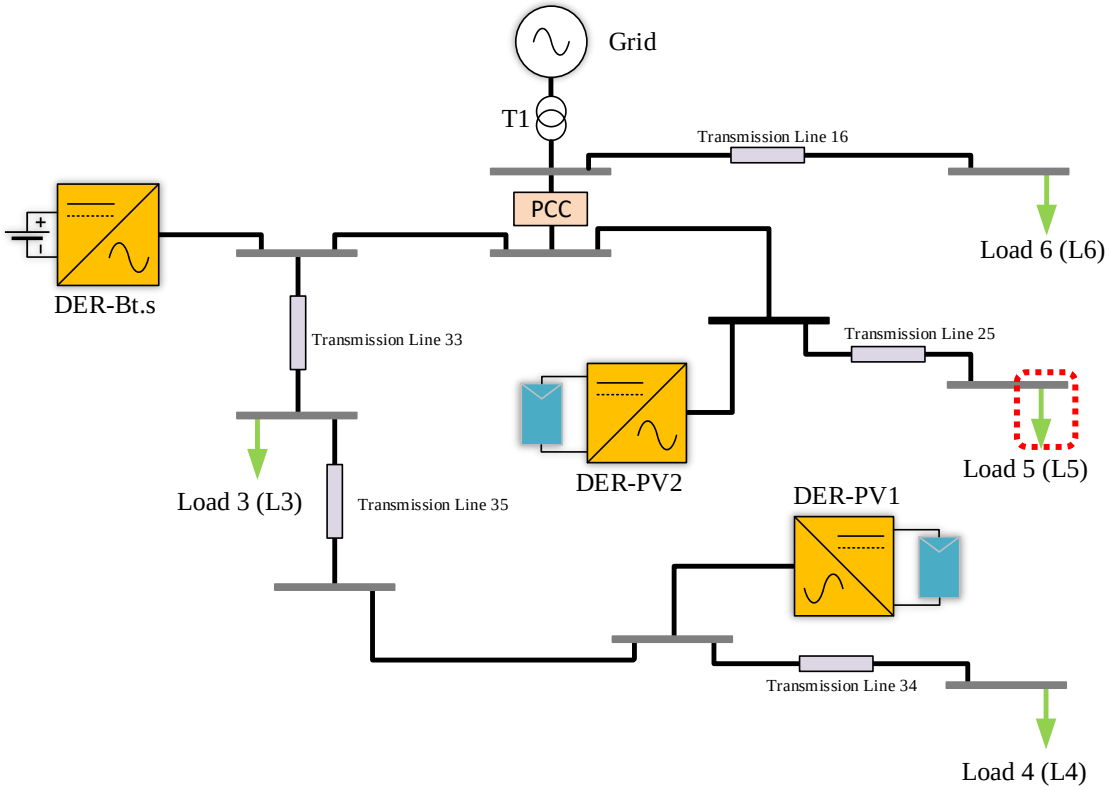

Fig 4.76: Load 5 Measurement Point

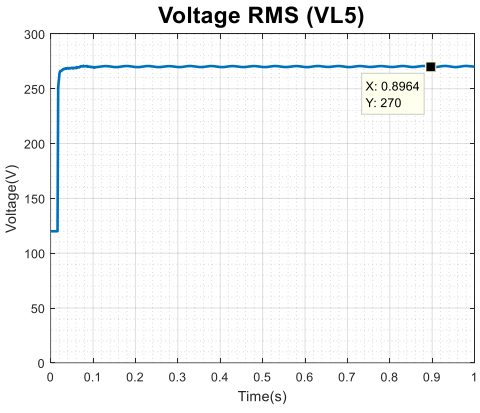

Fig 4.77: Voltage RMS at Load 5

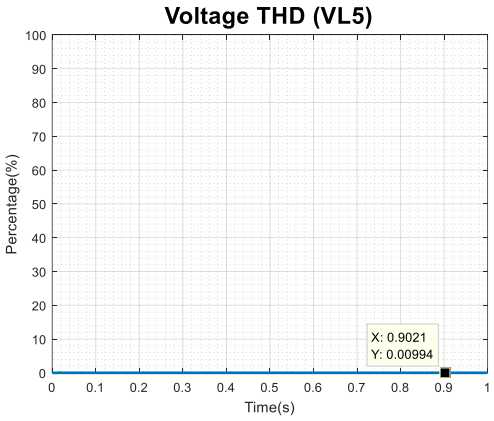

Fig 4.78: Voltage THD at Load 5

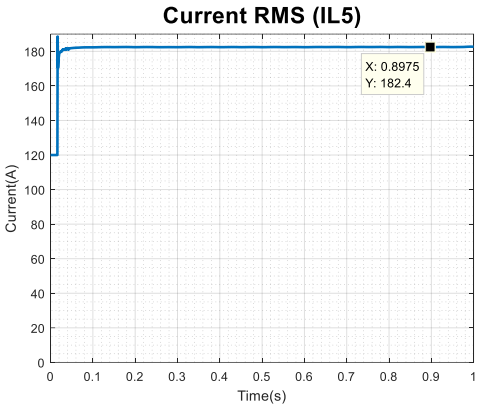

Fig 4.79. Current RMS at Load 5

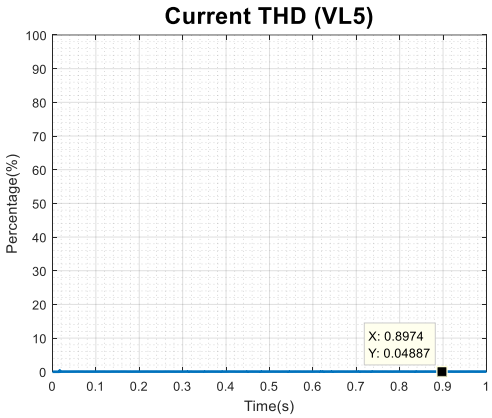

Fig 4.80. Current THD at Load 5

Figure 4.76 highlights Load 5, which is connected at the node under study. Figures 4.37 through figures 4.80 illustrate the output of the PSCAD results for the load side of Line25 which is the second branch of the CERTS microgrid testbed system. Between Load 5 and the Grid there is a transmission line which results in transmission losses, along with the point of coupling of PV2 It is essential to study the measurements at Load 5 to verify that the load demand is being satisfied. The addition of a DG has an impact on the output parameters, and it is essential to study the impact of the amalgamation. It is evident through analysis of the figures that the system stabilizes at 0.1 seconds and the total duration of the run is 1.0 second. It is clear that the RMS voltage is 270V and the THD of the voltage is 0.0094%. The measurements indicate that the RMS current is approximately 182.4A and the THD is approximately 0.0489%. The THD for both the voltage and current is very low and at an ideally acceptable level.

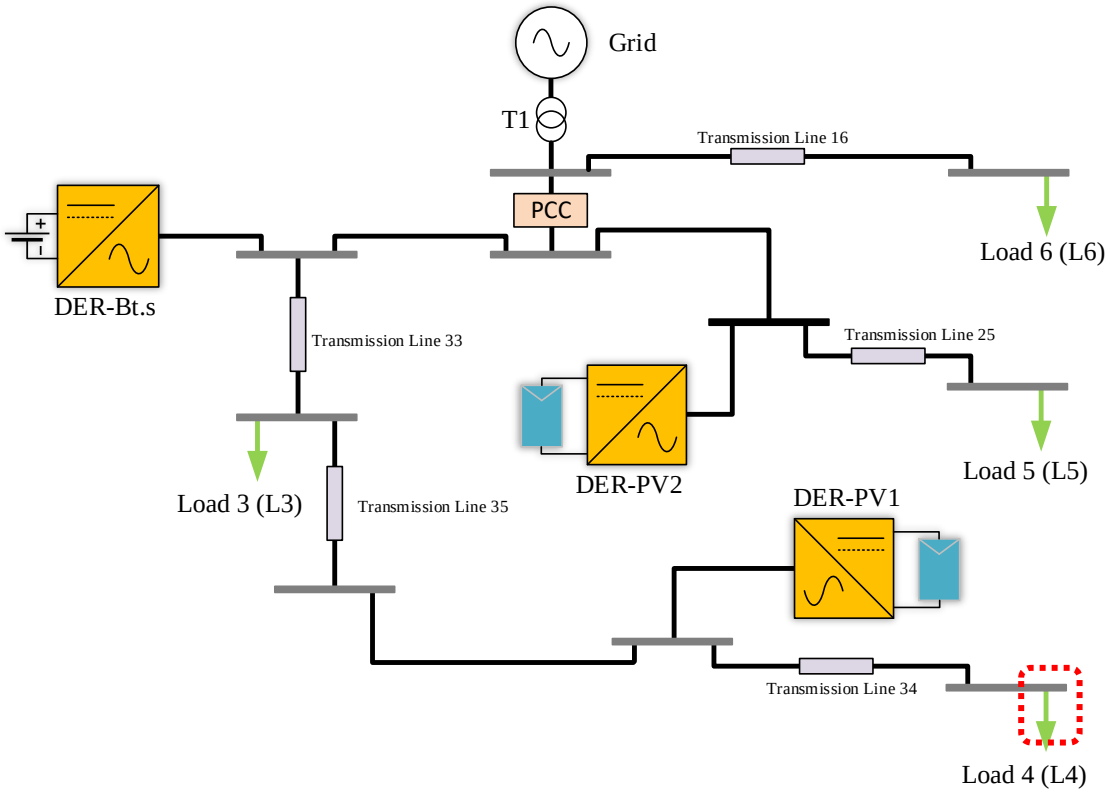

Fig 4.81. Load 4 Measurement Point

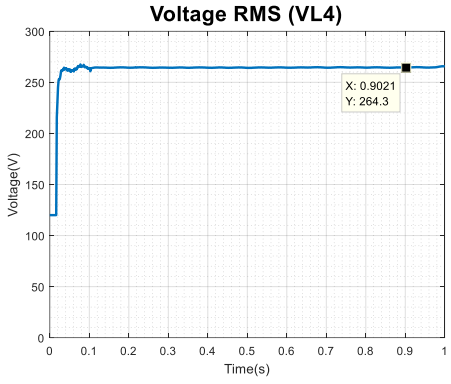

Fig 4.82. Voltage RMS at Load 4

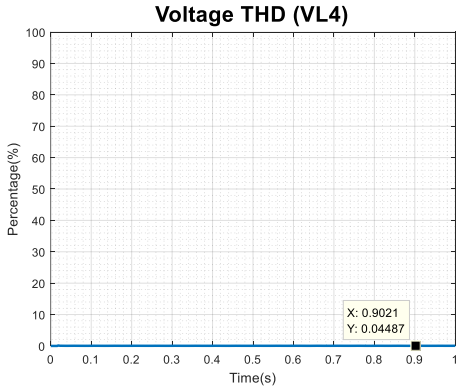

Fig 4.83. Voltage THD at Load 4

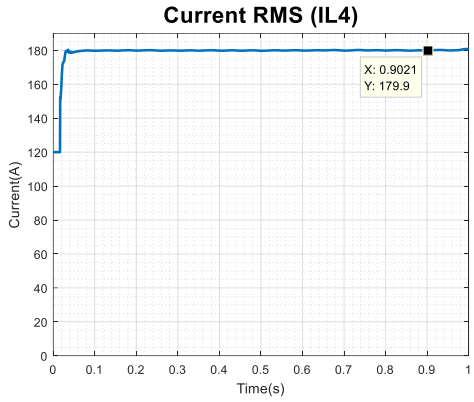

Fig 4.84. Current RMS at Load 4

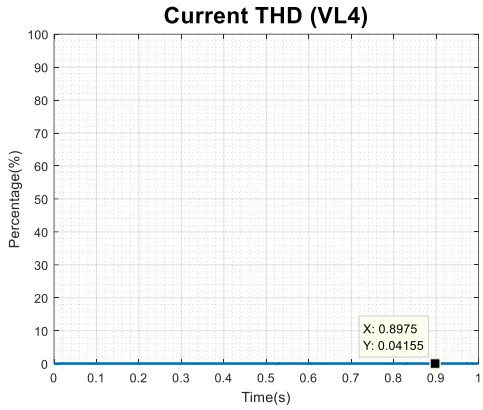

Fig 4.85. Current THD at Load 4

Figure 4.81 highlights Load 4, which is connected at the node under study. Figures 4.82 through figures 4.85 illustrate the output of the PSCAD results for the load side of Line44 which is the third branch of the CERTS microgrid testbed system. Between Load 4 and the Grid there are three sets of transmission lines which result in transmission losses, along with the point of coupling of PV1 and BES. It is essential to study the measurements at Load 4 to verify that the load demand is being satisfied. The addition of two DGs has an impact on the output parameters and it is essential to study the impact of the amalgamation. Load 4 is the furthest from the source and as such encounters the most variation and the highest offset. It is evident through analysis of the figures that the system stabilizes at 0.1 seconds and the total duration of the run is 1.0 second. It is clear that the RMS voltage is 264.3V and the THD of the voltage is 0.0449%. The measurements indicate that the RMS current is approximately 179.9A and the THD is approximately 0.0415%. The THD for

both the voltage and current is very low and at an ideally acceptable level.

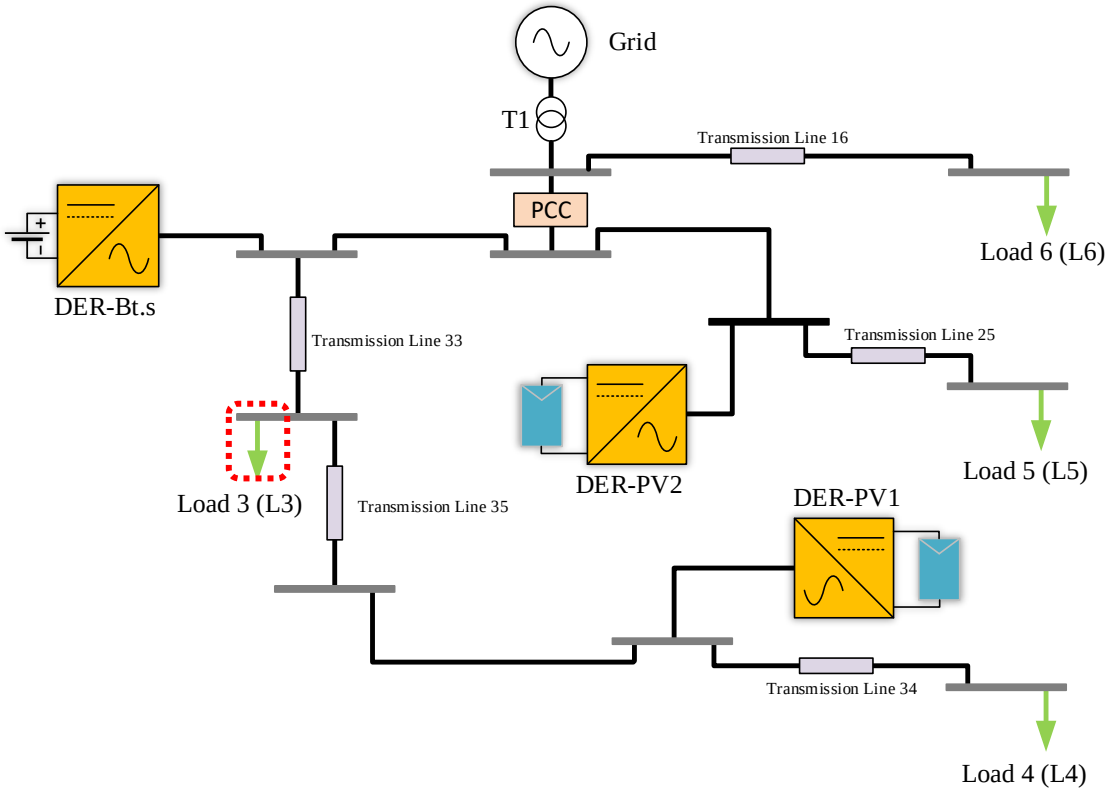

Fig 4.86. Load 3 Measurement Point

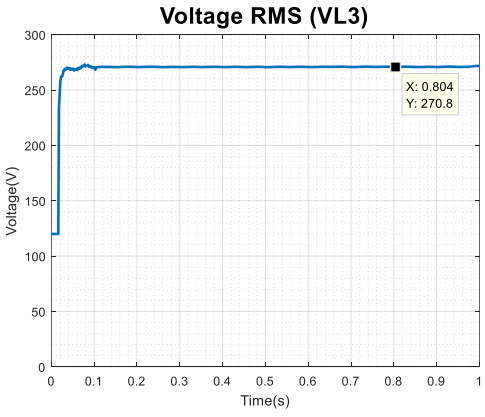

Fig 4.87. Voltage RMS at Load 3

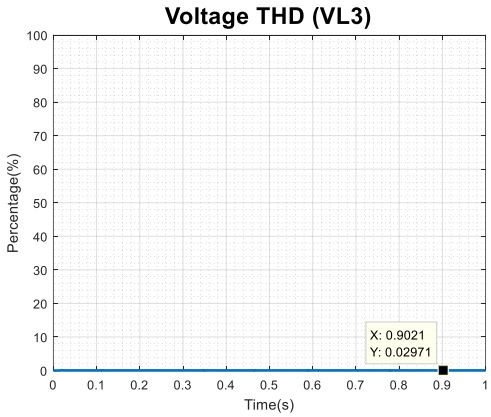

Fig 4.88 Voltage THD at Load 3

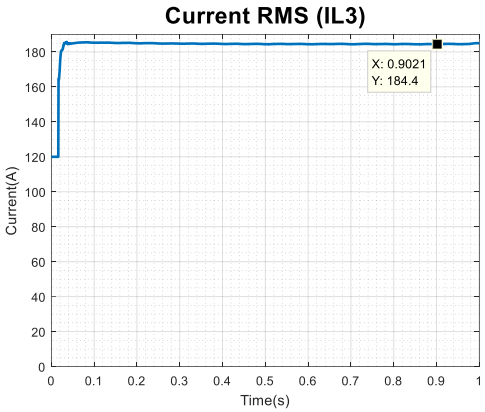

Fig 4.89. Current RMS at Load 3

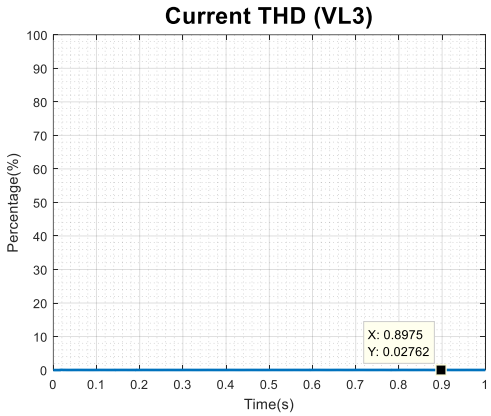

Fig 4.90. Current THD at Load 3

Figure 4.86 highlights Load 3, which is connected at the node under study. Figures 4.87 through figures 4.90 illustrate the output of the PSCAD results for the load side of Line34, which is the third branch of the CERTS microgrid testbed system. Between Load 3 and the Grid there is one transmission line, which result in transmission losses, along with the point of coupling of BES. It is essential to study the measurements at Load 3 to verify that the load demand is being satisfied. The addition of two DGs has an impact on the output parameters and it is essential to study the impact of the amalgamation. Load 4 is the furthest from the source and as such encounters the most variation and the highest offset. It is evident through analysis of the figures that the system stabilizes at 0.1 seconds and the total duration of the run is 1.0 second. It is clear that the RMS voltage is 270.8V and the THD of the voltage is 0.0297%. The measurements indicate that the RMS current is approximately 184.4A and the THD is approximately 0.0276%. The THD for both the voltage and current is very low and at an ideally acceptable level.

Table 4.5: Mean, MAD and Variance of Load 6

Load 6 Simulink								
	Run1	**Run2**	**Run3**	**Run4**	**Run5**	**Avg of Means**	**MAD**	**Variance**
VRMS	270.748	270.748	270.748	270.748	270.748	270.7478	0	0
VTHD	0.0084	0.0084	0.0084	0.0084	0.0084	0.0084	0	0
IRMS	109.687	109.687	109.687	109.687	109.687	109.6874	0	0
ITHD	0.0598	0.0598	0.0598	0.0598	0.0598	0.0598	0	0

Table 4.6: Mean, MAD and Variance of Load 5

Load 5 Simulink								
	Run1	**Run2**	**Run3**	**Run4**	**Run5**	**Avg of Means**	**MAD**	**Variance**
VRMS	267.967	267.967	267.967	267.967	267.967	267.9667	0	0
VTHD	0.0106	0.0106	0.0106	0.0106	0.0106	0.0106	0	0
IRMS	181.513	181.513	181.513	181.513	181.513	181.5125	0	0
ITHD	0.0504	0.0504	0.0504	0.0504	0.0504	0.0504	0	0

Table 4.7: Mean, MAD and Variance of Load 4

Load 4 Simulink								
	Run1	**Run2**	**Run3**	**Run4**	**Run5**	**Avg of Means**	**MAD**	**Variance**
VRMS	168.163	168.163	168.163	168.163	168.163	168.1628	0	
VTHD	0.0448	0.0448	0.0448	0.0448	0.0448	0.0448	0	0
IRMS	178.958	178.958	178.958	178.958	178.958	178.9575	0	0
ITHD	0.0428	0.0428	0.0428	0.0428	0.0428	0.0428	0	0

Table 4.8: Mean, MAD and Variance of Load 3

Load 3 Simulink								
	Run1	**Run2**	**Run3**	**Run4**	**Run5**	**Avg of Means**	**MAD**	**Variance**
VRMS	268.52	268.52	268.52	268.52	268.52	268.5199	0	0
VTHD	0.0298	0.0298	0.0298	0.0298	0.0298	0.0298	0	0
IRMS	183.694	183.694	183.694	183.694	183.694	183.6944	0	0
ITHD	0.0284	0.0284	0.0284	0.0284	0.0284	0.0284	0	0

4.3.3 PSCAD and Simulink in Grid Connected Mode Comparative Study

In order to analyze and compare the performance of both PSCAD and Matlab-Simscape, simulating the CERTS microgrid testbed system in the grid connected mode of operation is necessary. In sections 4.3.1 and 4.3.2 the results of the simulation in individual software was illustrated. In this chapter, the results are compared and explored side by side

in order to determine whether the output of each of the systems is similar and within the acceptable margin of error. In order to do so there needs to be a comparison made at the voltage and current readings at each of the four loads. The root mean square (RMS) and total harmonic distortion (THD) are calculated and demonstrated at each of the loads. This is done in order to demonstrate which of the software provide a more robust solution to the system. The CERTS microgrid testbed system was modelled identically in both PSCAD and Matlab-Simscape while following the same parameters for each of the components utilized.

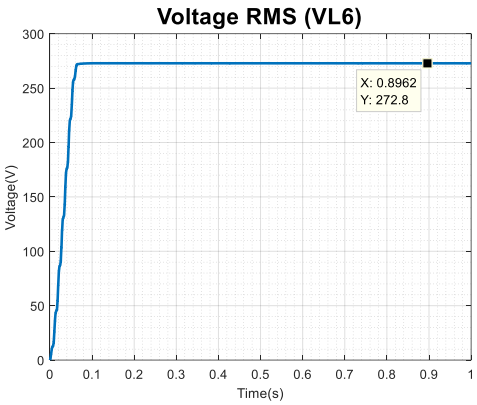

Fig 4.91A: PSCAD Voltage RMS Load 6

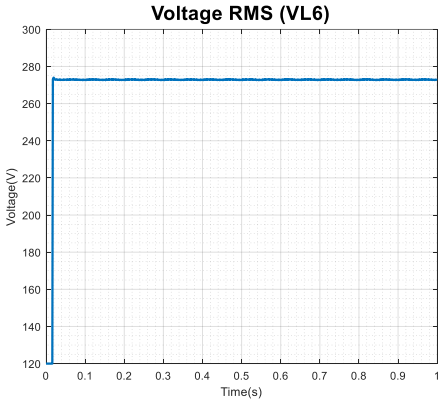

Fig 4.91B: Simulink Voltage RMS Load 6

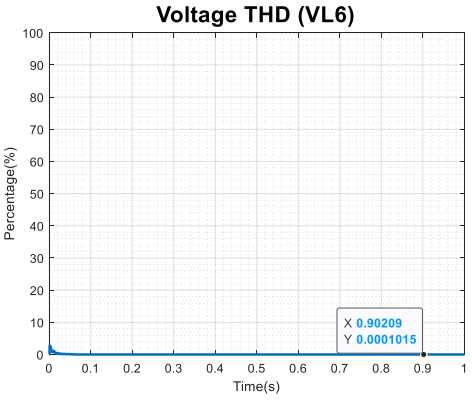

Fig 4.92A: PSCAD Voltage THD Load 6

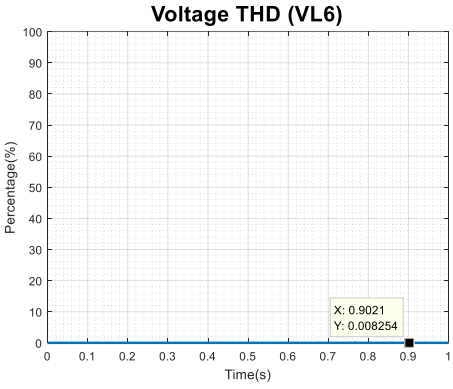

Fig 4.92B: Simulink Voltage THD Load 6

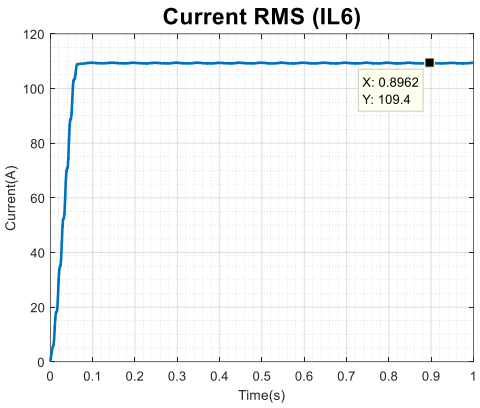

Fig 4.93A: PSCAD Current RMS Load 6

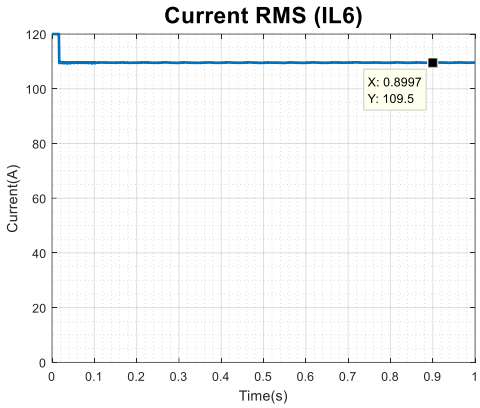

Fig 4.93B: Simulink Current RMS Load 6

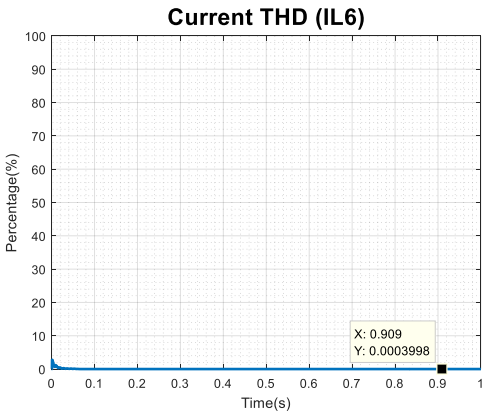

Fig 4.94A: PSCAD Current THD Load 6

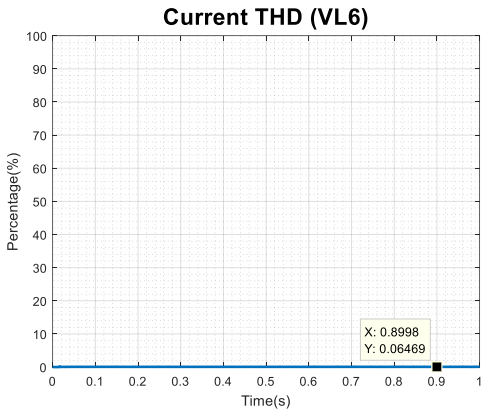

Fig 4.94B: Simulink Current THD Load 6

By analyzing figures 4.88A through 4.91B, it is evident that the output voltage and output current measured at Load 6 are similar in both simulation environments. The difference in the voltage and current between the two simulating environments is 0% and 0.0913% respectively. This further affirms that the system has been modelled uniformly and consistently in both PSAD and Matlab-Simscape. Furthermore, the total harmonic distortion measure of both current and voltage were well below 1% and the acceptable margin of error, thus indicating that the system is stable.

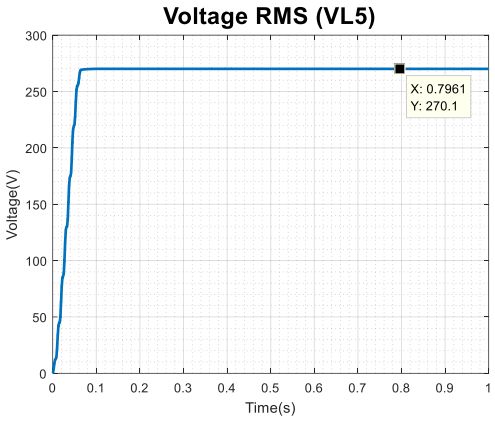

Fig 4.95A: PSCAD Voltage RMS Load 5

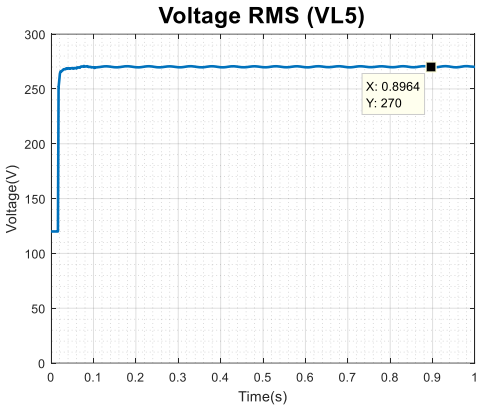

Fig 4.95B: Simulink Voltage RMS Load 5

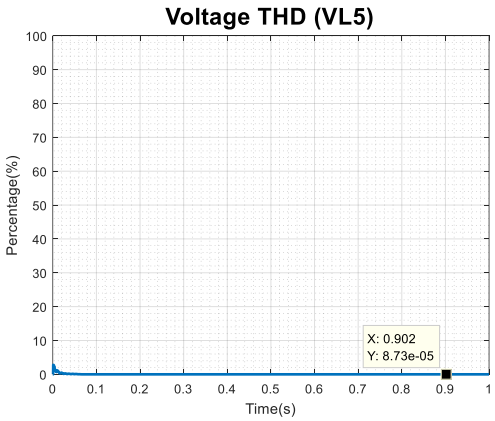

Fig 4.96A: PSCAD Voltage THD Load 5

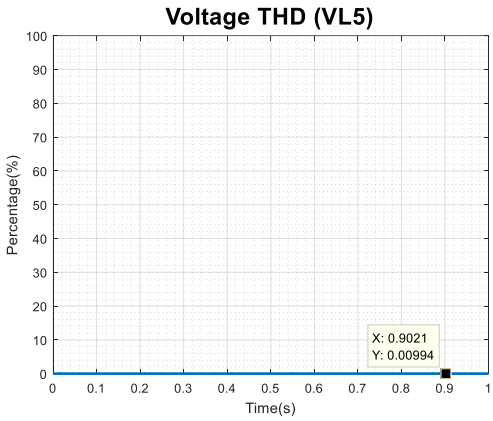

Fig 4.96B: Simulink Voltage THD Load 5

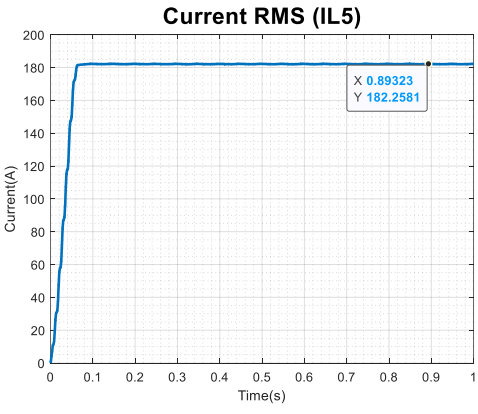

Fig 4.97A: PSCAD Current RMS Load 5

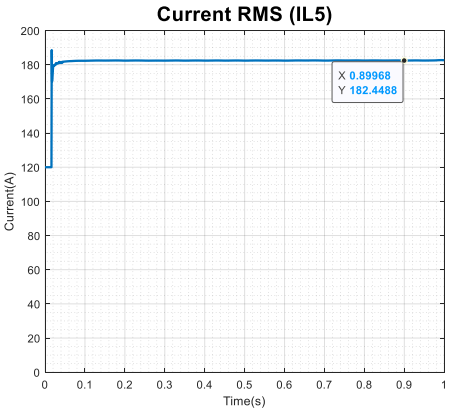

Fig 4.97B: Simulink Current RMS Load 5

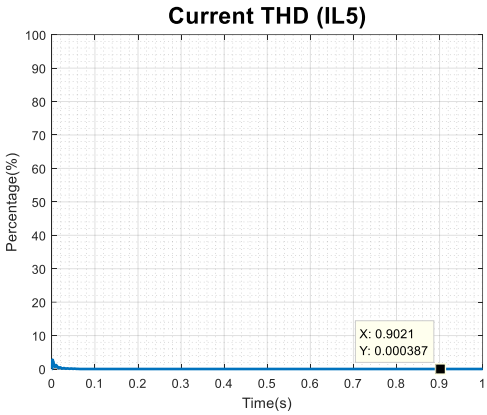

Fig 4.98A: PSCAD Current THD Load 5

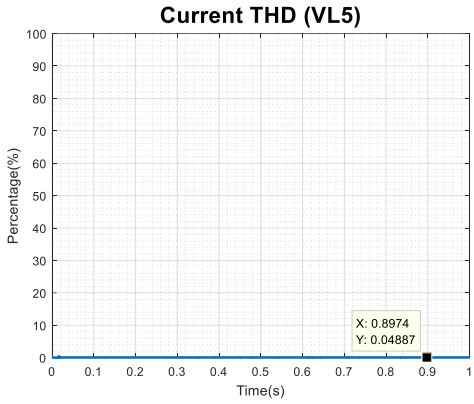

Fig 4.98B: Simulink Current THD Load 5

By analyzing figures 4.92A through 4.95B, it is evident that the output voltage and output current measured at Load 5 are similar in both simulation environments. The difference in the voltage and current between the two simulating environments is 0.0370% and 0.1642% respectively. This further affirms that the system has been modelled uniformly and consistently in both PSAD and Matlab-Simscape. The total harmonic distortion measure of both current and voltage were well below 1% and the acceptable margin of error, thus indicating that the system is stable.

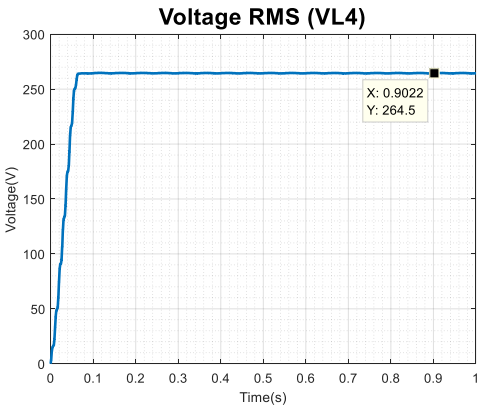

Fig 4.99A: PSCAD Voltage RMS Load 4

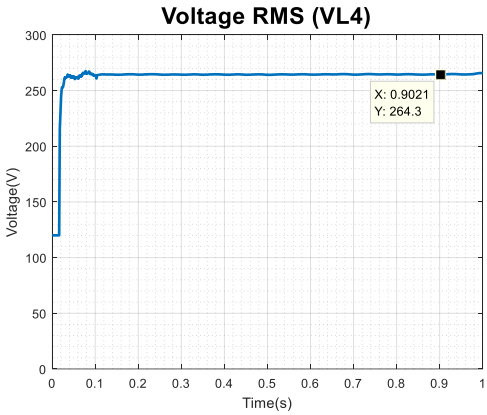

Fig 4.99B: Simulink Voltage RMS Load 4

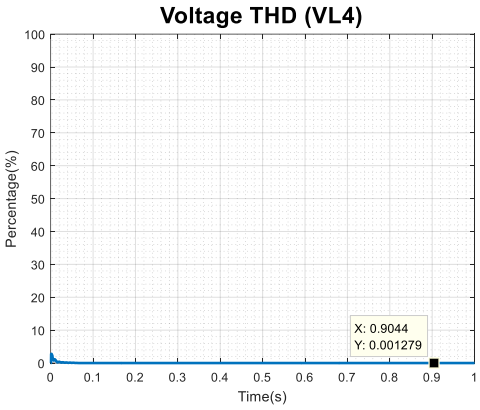

Fig 4.100A: PSCAD Voltage THD Load 4

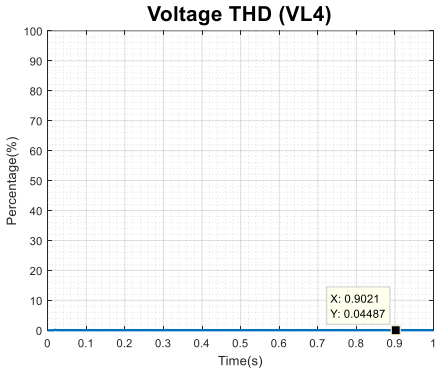

Fig 4.100B: Simulink Voltage THD Load 4

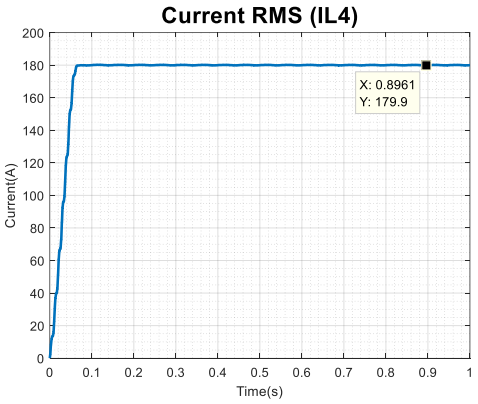

Fig 4.101A: PSCAD Current RMS Load 4

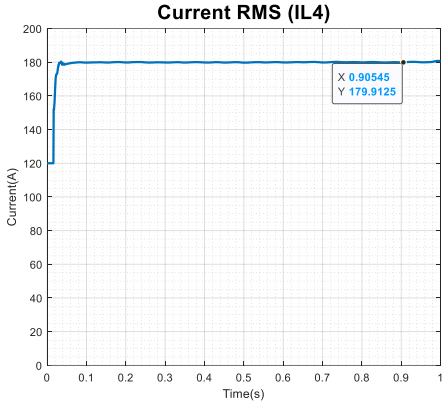

Fig 4.101B: Simulink Current RMS Load 4

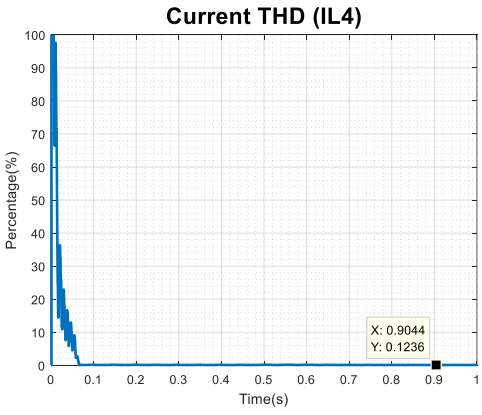

Fig 4.102A: PSCAD Current THD Load 4

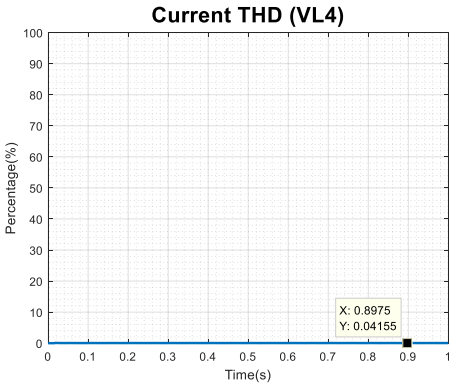

Fig 4.102A: Simulink Current THD Load 4

By analyzing figures 4.96A through 4.99B, it is evident that the output voltage and output current measured at Load 4 are similar in both simulation environments. The difference in the voltage and current between the two simulating environments is 0.0756% and 0% respectively. This further affirms that the system has been modelled uniformly and consistently in both PSAD and Matlab-Simscape. In addition, the total harmonic distortion measure of both current and voltage were well below 1% and the acceptable margin of error, thus indicating that the system is stable.

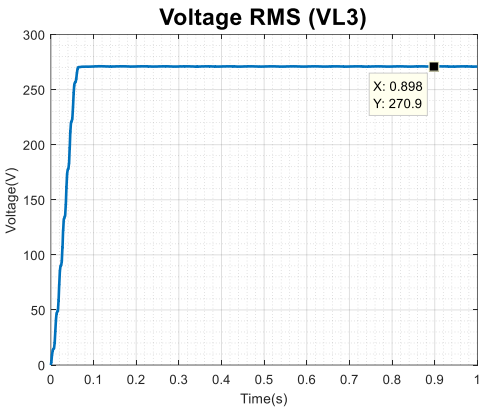

Fig 4.103A: PSCAD Voltage RMS Load 3

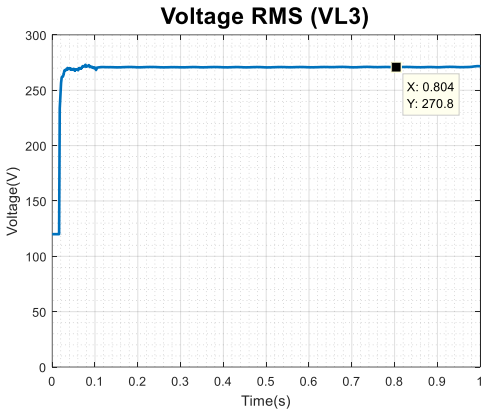

Fig 4.103B: Simulink Voltage RMS Load 3

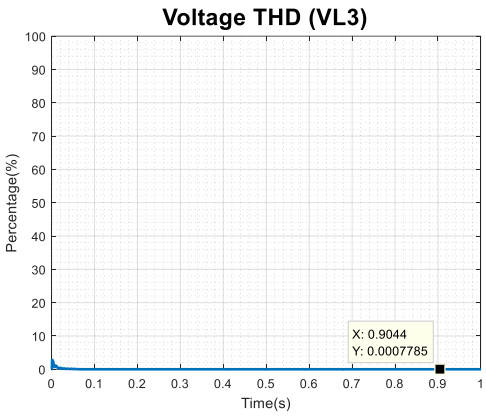

Fig 4.104A: PSCAD Voltage THD Load 3

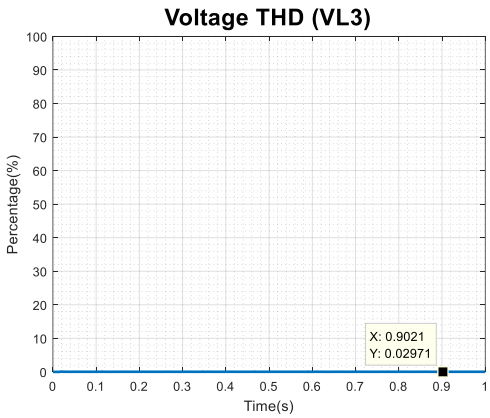

Fig 4.104B: Simulink Voltage THD Load 3

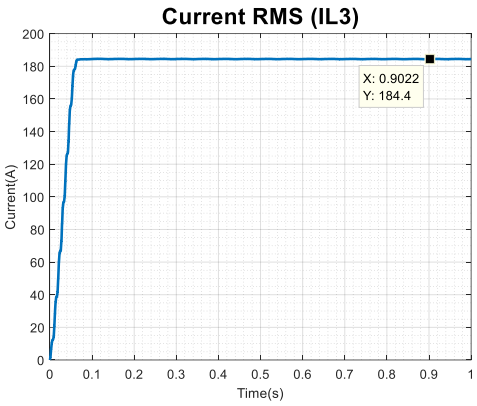

Fig 4.105A: PSCAD Current RMS Load 3

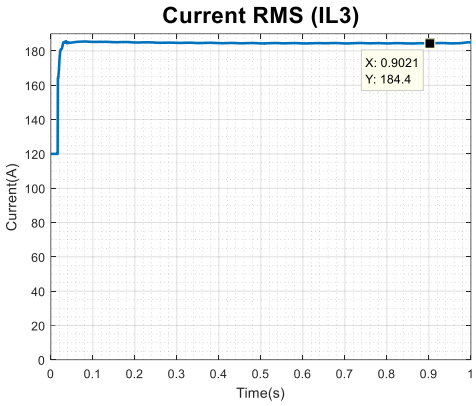

Fig 4.105B: Simulink Current RMS Load 3

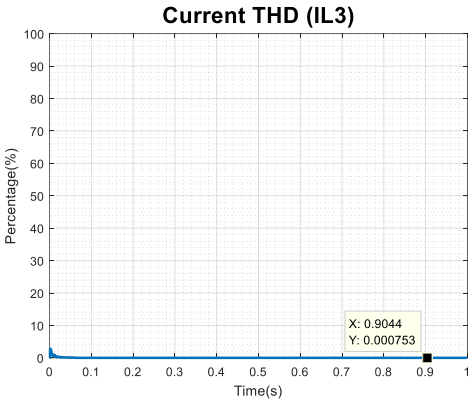

Fig 4.106A: PSCAD Current THD Load 3

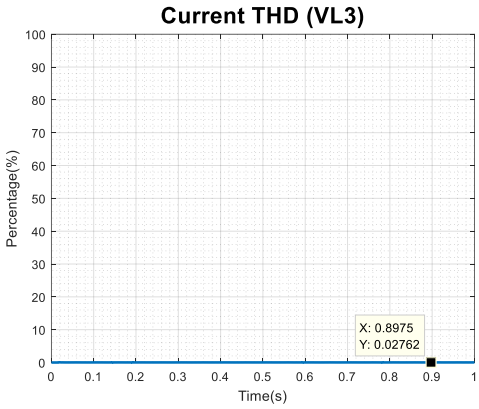

Fig 4.106B: Simulink Current THD Load 3

By analyzing figures 4.103A through 4.106B, it is evident that the output voltage and output current measured at Load 5 are similar in both simulation environments. The difference in the voltage and current between the two simulating environments is 0.0369% and 0.1642% respectively. This further affirms that the system has been modelled uniformly and consistently in both PSAD and Matlab-Simscape. Moreover, the total harmonic distortion measure of both current and voltage were well below 1% and the acceptable margin of error, thus indicating that the system is stable.

4.4. Island Mode of Operation

The objective of this section is to analyze the grid in the islanded mode of operation. The island mode of operation is the operation of the grid in the absence of the energy provided by the grid, the power demands of the loads are to be satiated by the distributed generation units. In the islanded mode of operation only crucial loads are supplied power from the Distributed Generation sources. During the island mode of operation, the network consists of three loads, namely L3, L4 and L5. The three distributed energy sources are DER-Bat, DER-PV1 and DER-PV2. Similar to the grid connected mode of operation studies in section 4.3 the system is modelled in both PSCAD and Matlab-Simscape. It is essential to perform a comprehensive study and in order to do so analysis needs to be performed at numerous nodes of interest situated all over the system. This is done in order to compare the performance of PSCAD and Matlab-Simscape on a system modelled in a similar manner in both simulation environments. Section 4.4.1 illustrates the results of the PSCAD simulation in the island mode of operation, whereas 4.4.2 depicts the results of the Matlab-Simscape simulation in the island mode operation. Fig 4.88 below depicts the CERTS microgrid testbed system in the island mode of operation, notice the disconnection of the Grid, load 6 (L6), Transformer (T1) and Transmission Line (Line16).

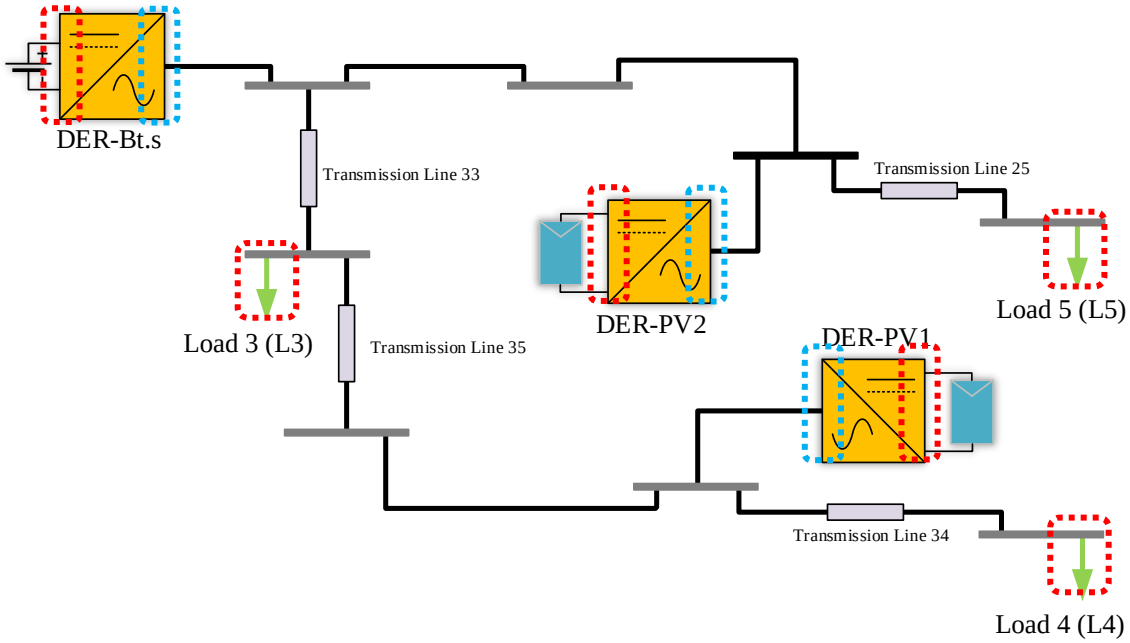

Fig 4.107: CERTS Microgrid Schematic Islanded Mode of Operation

4.4.1 PSCAD Simulation Island Mode of Operation

In this section the results obtained from PSCAD are illustrated and discussed. The points of measurement utilized were discussed in section 4.4 and are illustrated here using the single line diagram of the CERTS microgrid testbed system. The data collected through ten iterations is represented graphically and numerically, as can be seen in this section.

First the DC side voltage and DC side current generated by the distributed generation units are discussed. Followed by the AC side voltage and AC side current of inverters utilized to couple the distributed generators to the grid. Finally, the voltage and current of each of load is illustrated. In order to conduct thorough work, it was necessary to investigate the Root Mean Square and Total Harmonic Distortion of all AC values being analyzed.

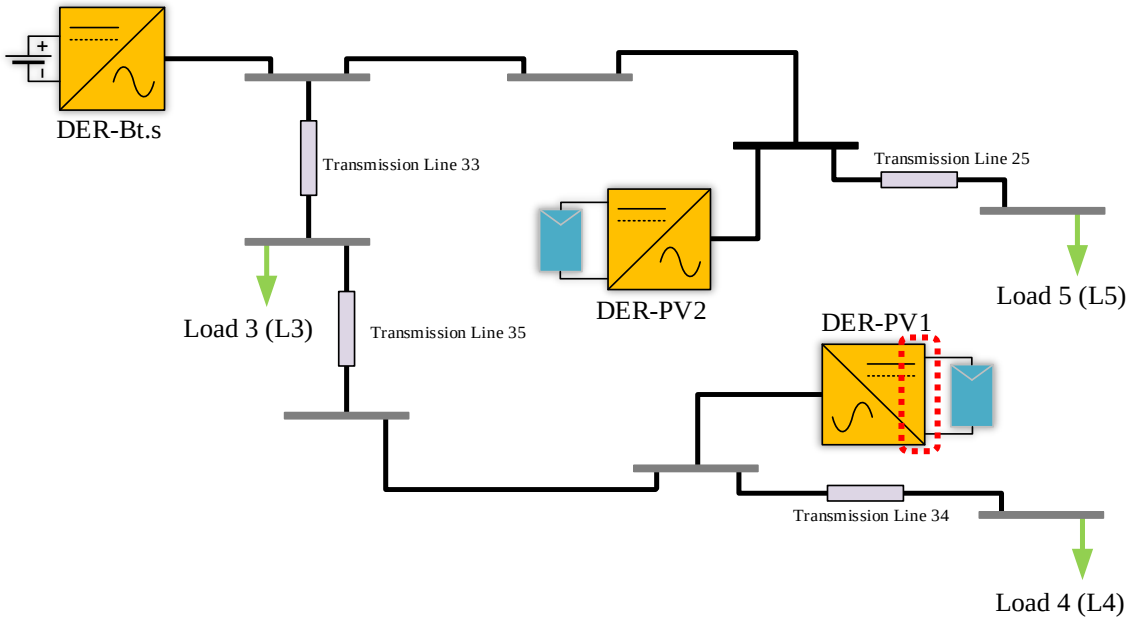

Fig 4.108: DG1 DC Side Point of Measurement

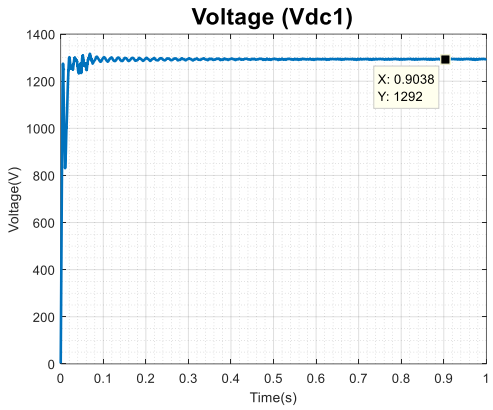

Fig 4.109: DC Link Voltage DG1

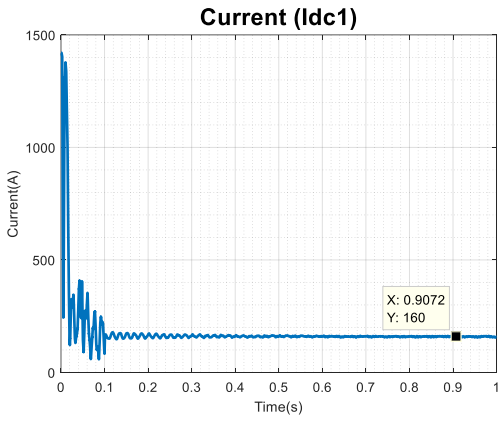

Fig 4.110: DC Link Current DG1

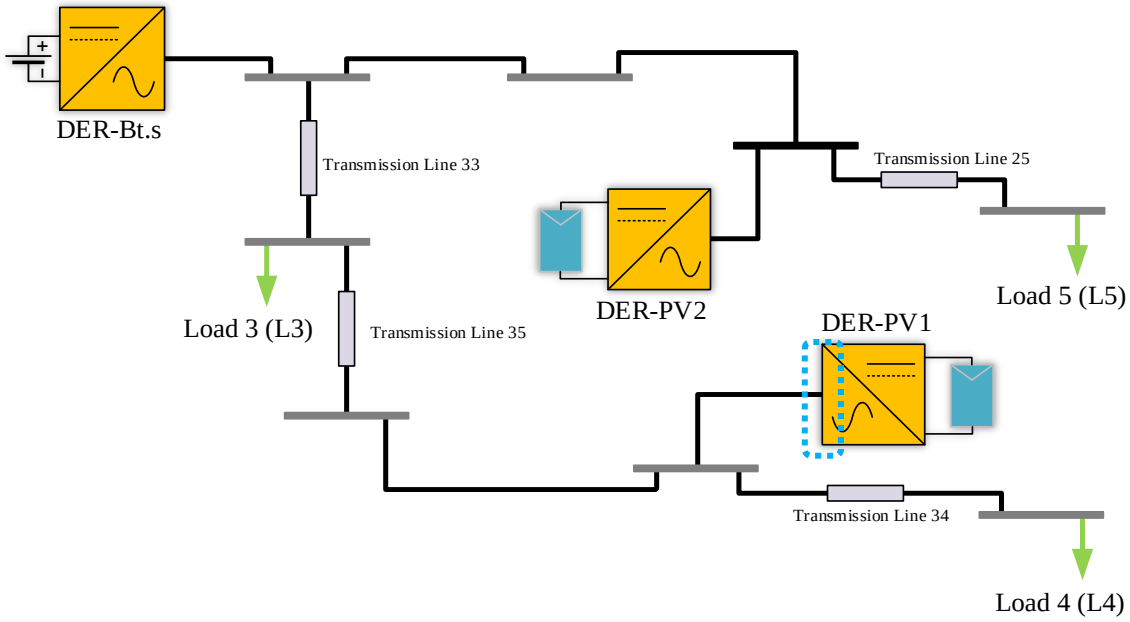

Fig 4.111: DG AC Side Point of Measurement

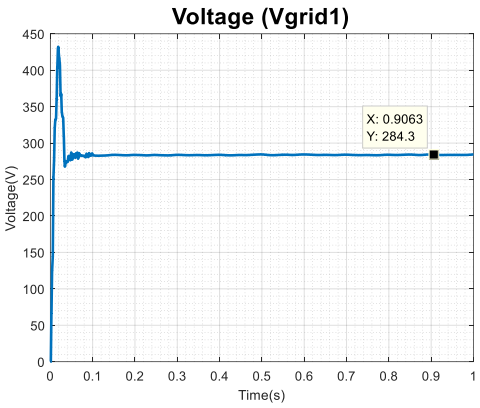

Fig 112: Voltage RMS at Point of Coupling

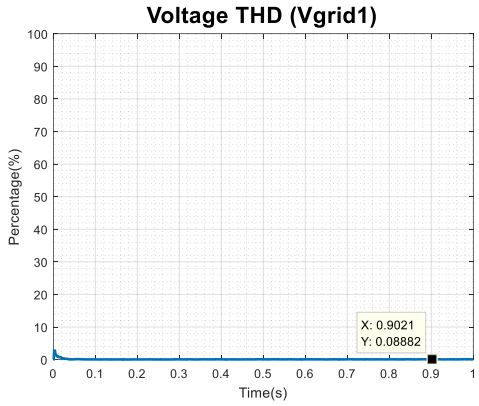

Fig 113: Voltage THD at Point of Coupling

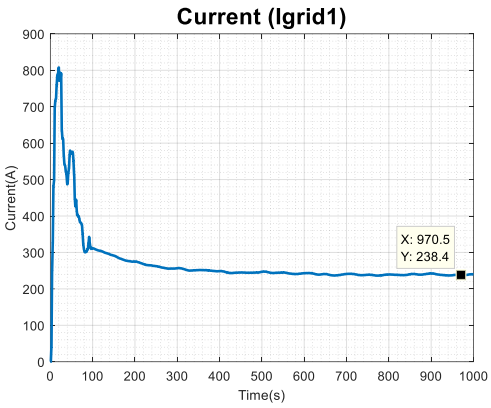

Fig 114: Current RMS at Point of Coupling

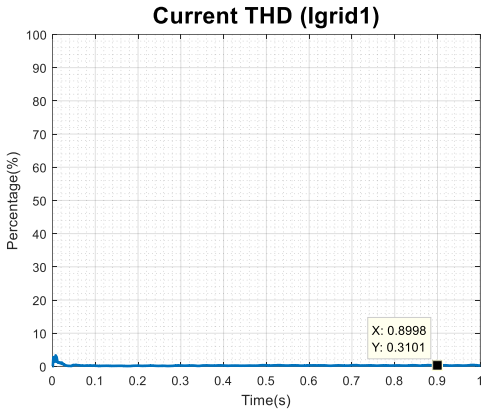

Fig 4.115: Current THD at Point of Coupling

Figure 4.108 highlights the DC side of the inverter, which is the point under study. Figures 4.109 and Figure 4.110 illustrate the output of the PSCAD results for the DC side of the inverter integrated with the second distributed generation unit (PV1) which is a photovoltaic source namely DER-PV1. Figure 4.111 highlights the AC side of the inverter which is the point under study, whereas Figures 4.112 through 4.115 indicate the output of the PSCAD results on the AC side of the inverter for the second distributed generation unit (PV1). It is evident through analysis of the figures generated that the system reaches a stable point of operation free of any transients in the neighborhood of 0.1 seconds and the total duration of the run is 1.0 second. It is clear that on the DC side of the inverter PV2 generates approximately 1,292V and 160A. The RMS voltage measured at the secondary side of the inverter at which point PV2 is incorporated into PV1 is approximately 284.3V, along with a Total Harmonic Distortion value of 0.0889%. Whereas the RMS current measured at the same point is approximately 238.4A, accompanied by a Total Harmonic Distortion value of approximately 0.03101%. The THD for both the voltage and current was very low and at an ideally acceptable level.

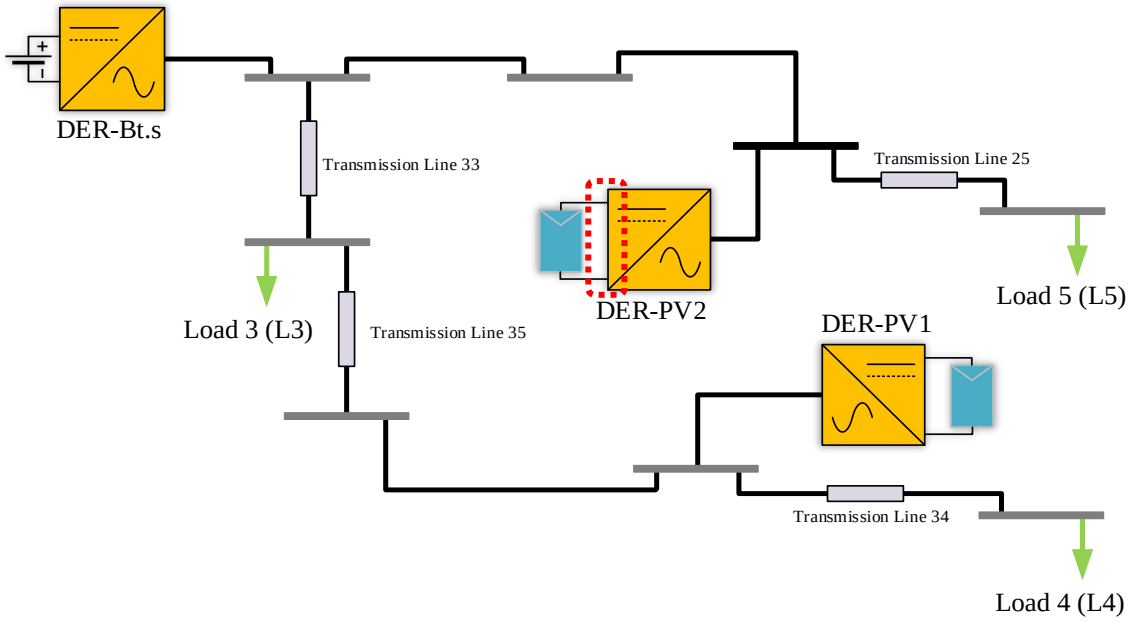

Fig 4.116: DG2 DC Side Point of Measurement

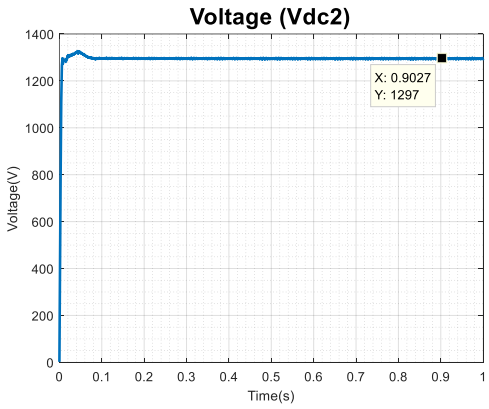

Fig 4.117: DC Link Voltage DG2

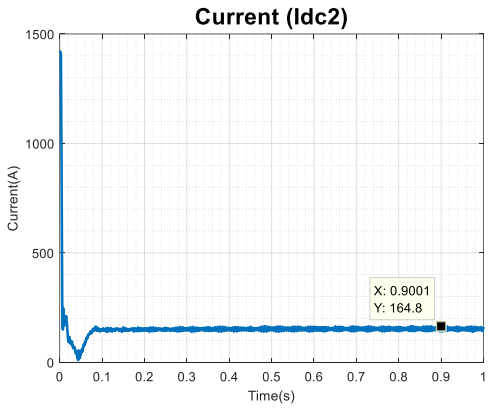

Fig 4.118: DC Link Current DG2

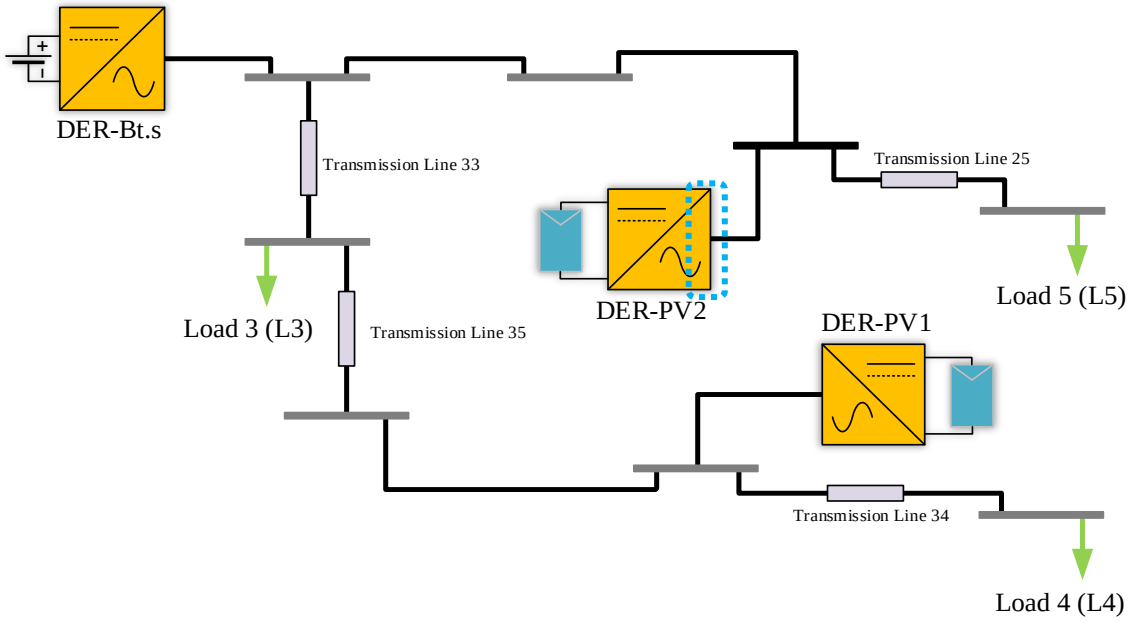

Fig 4.119: DG2 AC Side Point of Measurement

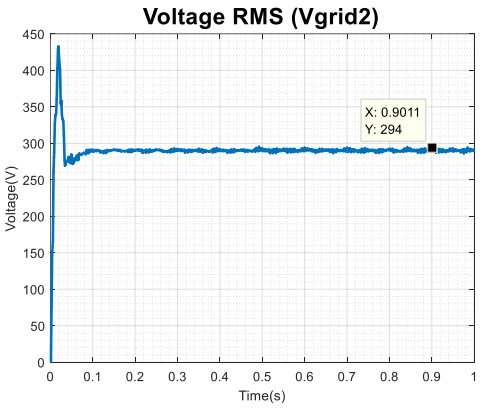

Fig 4.120: Voltage RMS at Point of Coupling

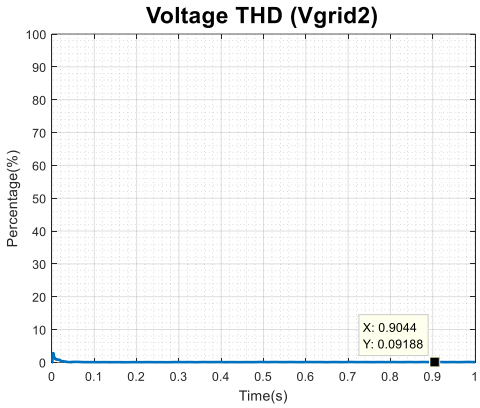

Fig 4.121: Voltage THD at Point of Coupling

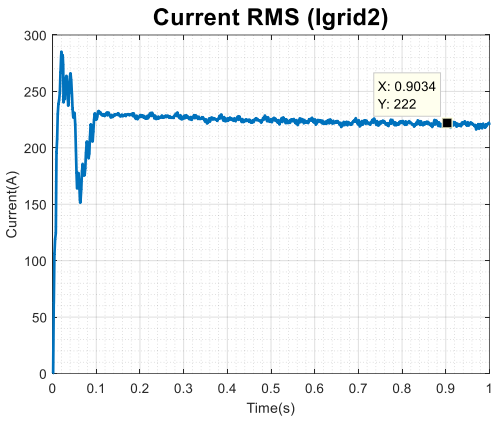

Fig 4.122: Current RMS at Point of Coupling

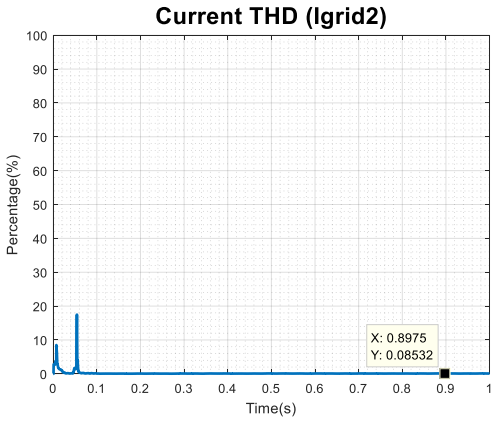

Fig 4.123: Current THD at Point of Coupling

Figure 4.116 highlights the DC side of the inverter which is the point under study. Figures 4.117 and Figure 4.118 illustrate the output of the PSCAD results for the DC side of the inverter integrated with the first distributed generation unit (PV2) which is a photovoltaic source namely DER-PV2. Figure 4.119 highlights the AC side of the inverter which is the point under study. Whereas Figures 4.120 through 4.123 indicate the output of the PSCAD results on the AC side of the inverter for the first distributed generation unit (PV1). It is evident through analysis of the figures generated that the system reaches a stable point of operation free of any transients in the neighborhood of 0.1 seconds and the total duration of the run is 1.0 second. It is clear that on the DC side of the inverter PV2 generates approximately 1297V and 164.8A. The RMS voltage measured at the secondary side of the inverter at which point PV2 is incorporated into PV2 is approximately 294V, along with a Total Harmonic Distortion value of 0.09188%. Whereas the RMS current measured at the same point is approximately 222A, accompanied by a Total Harmonic Distortion value of approximately 0.085320%. The THD for both the voltage and current was very low and at an ideally acceptable level.

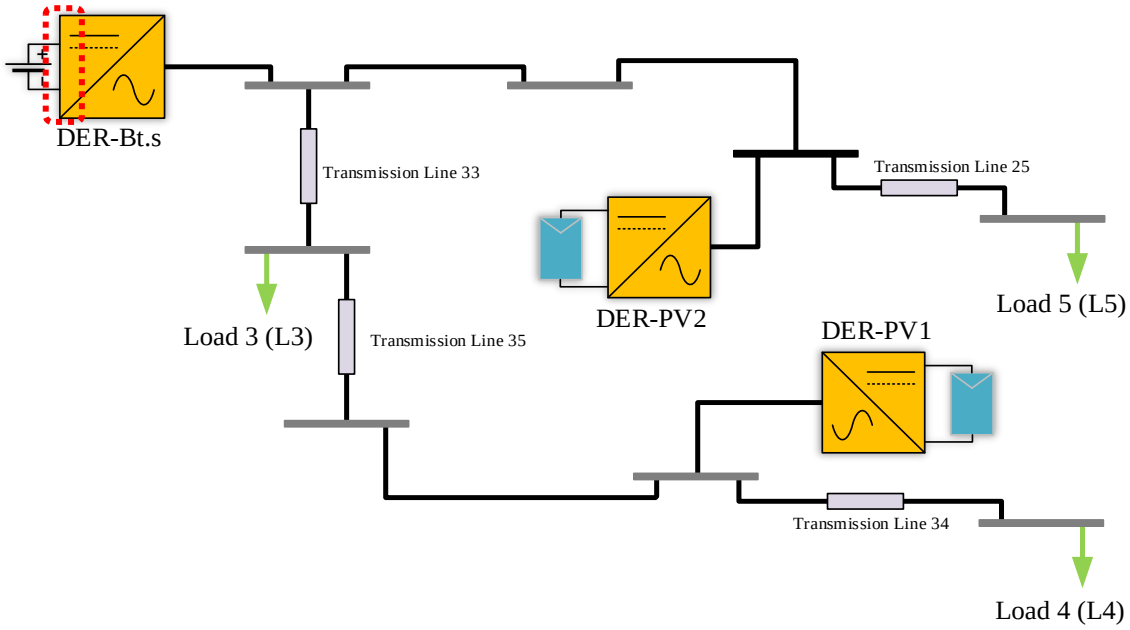

Fig 4.124: DG3 DC Side Point of Measurement

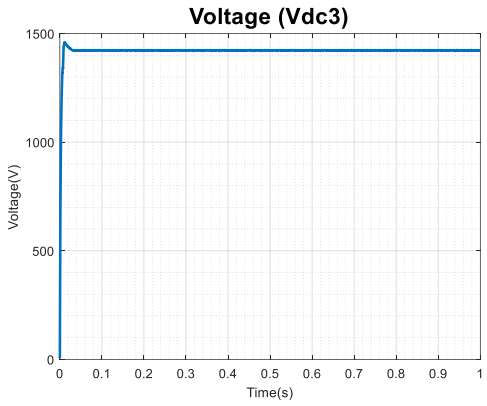

Fig 4.125: DC Link Voltage DG3

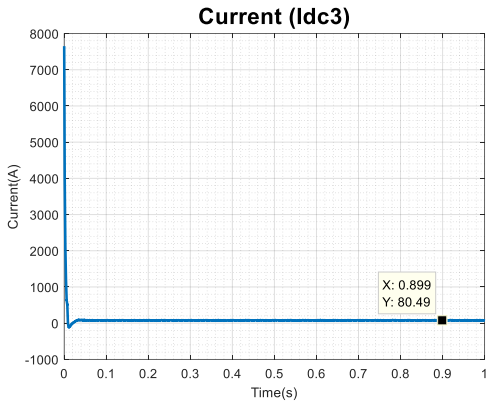

Fig 4.126: DC Link Current DG3

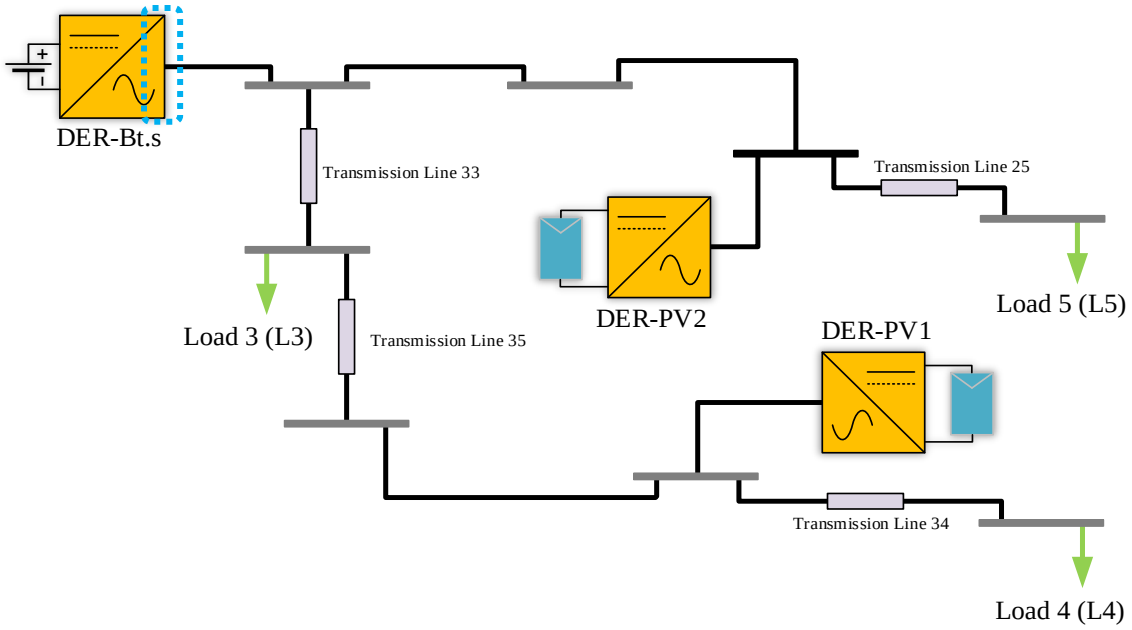

Fig 4.127: DG3 AC Side Point of Measurement

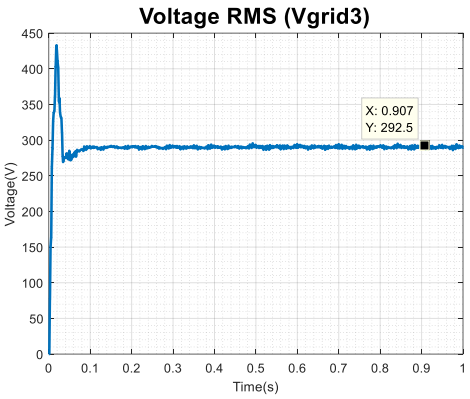

Fig 4.128: Voltage RMS at Point of Coupling

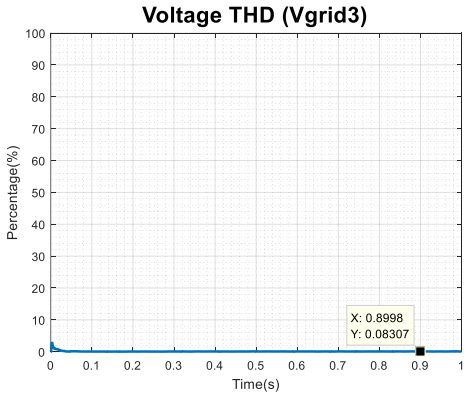

Fig 4.129: Voltage THD at Point of Coupling

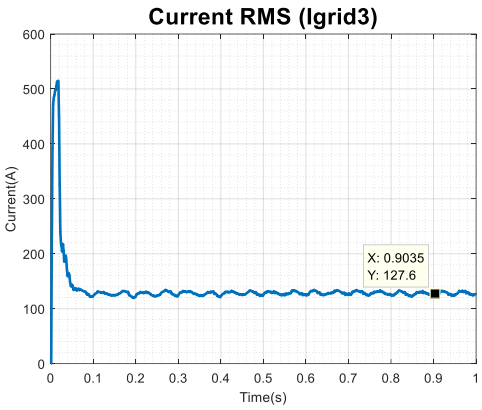

Fig 4.130: Current RMS at Point of Coupling

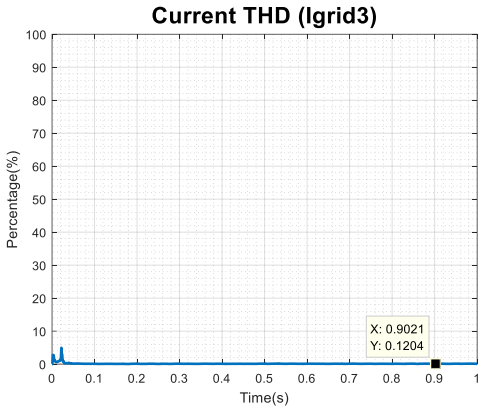

Fig 4.131: Current THD at Point of Coupling

Figure 4.124 highlights the DC side of the inverter which is the point under study. Figures 4.125 and Figure 4.126 illustrate the output of the PSCAD results for the DC side of the inverter integrated with the first distributed generation unit (Bt.S) which is a Battery Energy Storage source namely DER-Bt.S. Figure 4.126 highlights the AC side of the inverter which is the point under study, whereas Figures 4.128 through 4.131 indicate the output of the PSCAD results on the AC side of the inverter for the first distributed generation unit (Bt.S). It is evident through analysis of the figures generated that the system reaches a stable point of operation free of any transients in the neighborhood of 0.1 seconds and the total duration of the run is 1.0 second. It is clear that on the DC side of the inverter Bt.S generates approximately 1,297V and 140.2A. The RMS voltage measured at the secondary side of the inverter at which point PV1 is incorporated into Bt.S is approximately 272V, along with a Total Harmonic Distortion value of 0.0012%. Whereas the RMS current measured at the same point is approximately 218.4A, accompanied by a Total

Harmonic Distortion value of approximately 0.0220%. The THD for both the voltage and current was very low and at an ideally acceptable level.

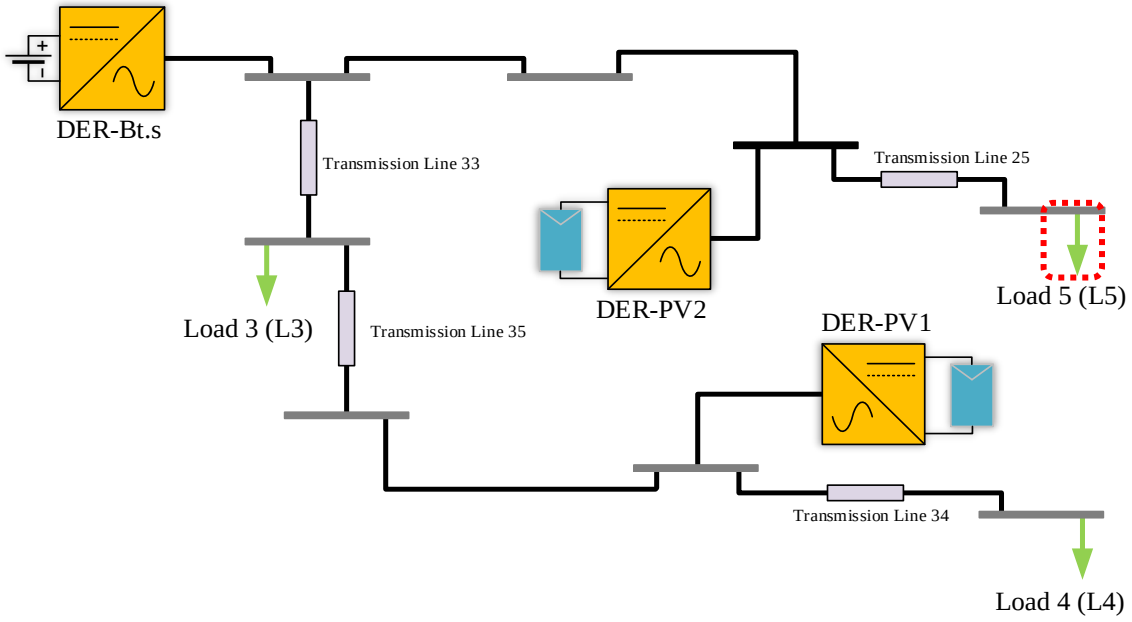

Fig 4.132: Load 5 Measurement Point

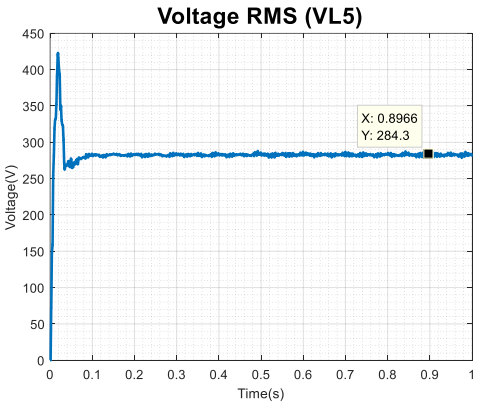

Fig 4.133: Voltage RMS at Load 5

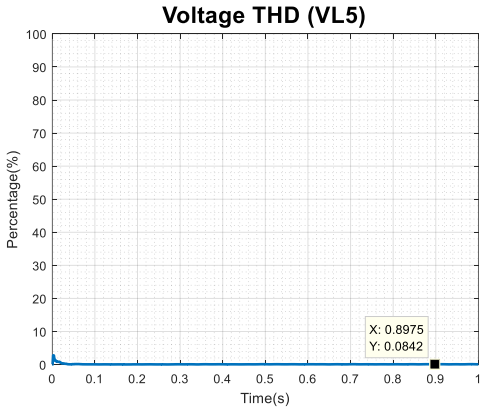

Fig 4.134 Voltage THD at Load 5

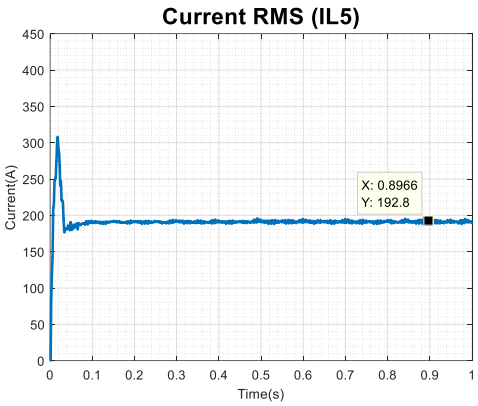

Fig 4.135: Current RMS at Load

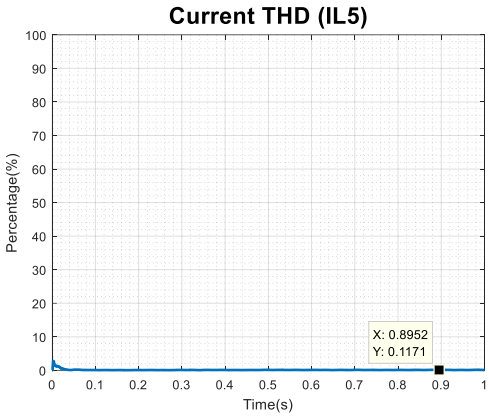

Fig 4.136: Current THD at Load

Figure 4.132 highlights Load 5, which the node under study. Figures 4.133 through figures 4.136 illustrate the output of the PSCAD results for the load side of Line25 which is the second branch of the CERTS microgrid testbed system. Between Load 5 and the Grid there is a transmission line, which results in transmission losses. It is essential to study the measurements at Load 5 to verify that the load demand is being satisfied. It is evident through analysis of the figures that the system stabilizes at 0.1 seconds and the total duration of the run is 1.0 second. The RMS voltage is 284.3V and the THD of the voltage is 0.0842%. The measurements indicate that the RMS current is approximately 192.8A and the THD is approximately 0.1171%. The THD for both the voltage and current is very low and at an ideally acceptable level.

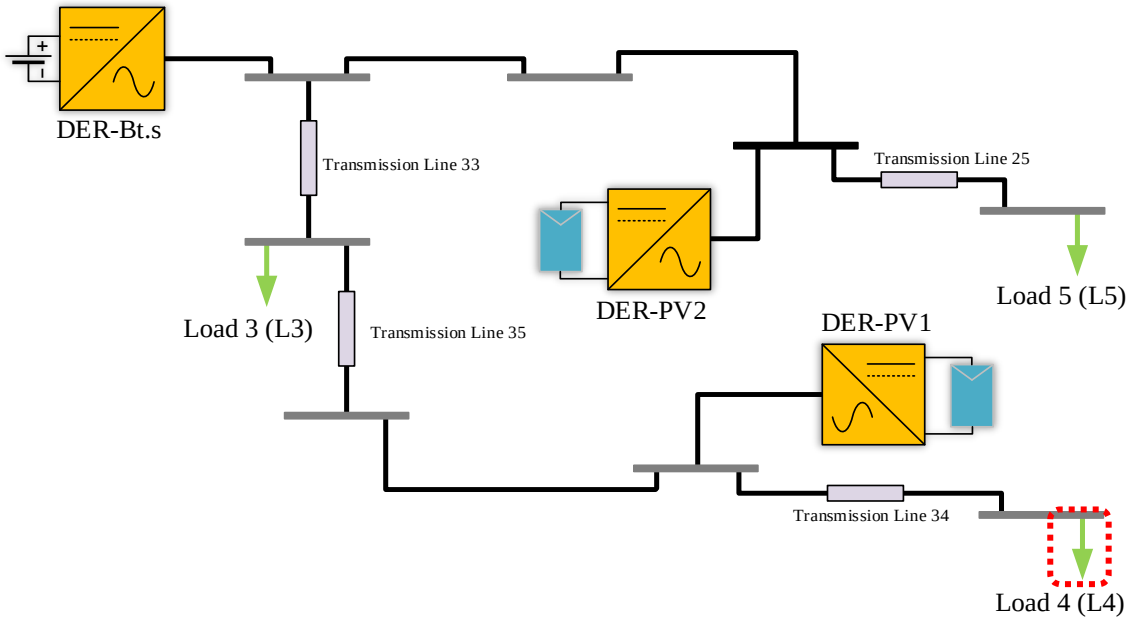

Fig 4.137: Load 4 Measurement Point

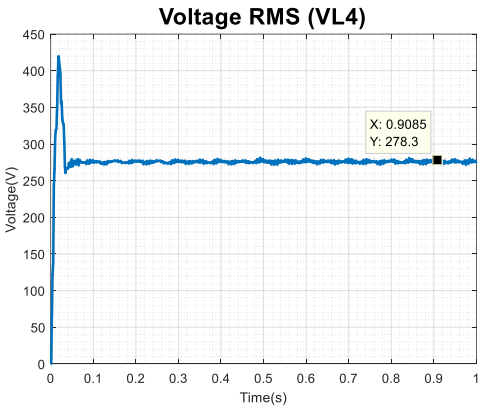

Fig. 4.138: Voltage RMS at Load 4

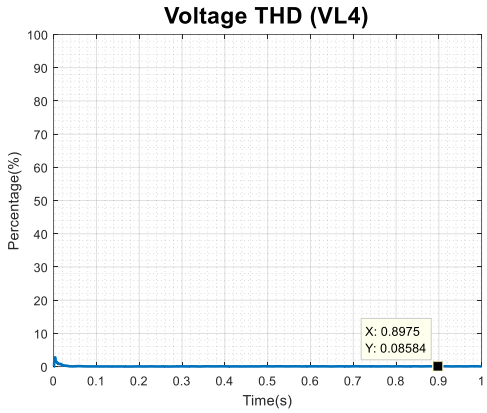

Fig 4.139: Voltage THD at Load 4

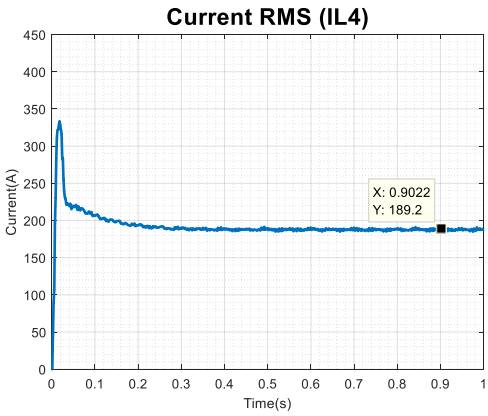

Fig 4.140: Current RMS at Load 4

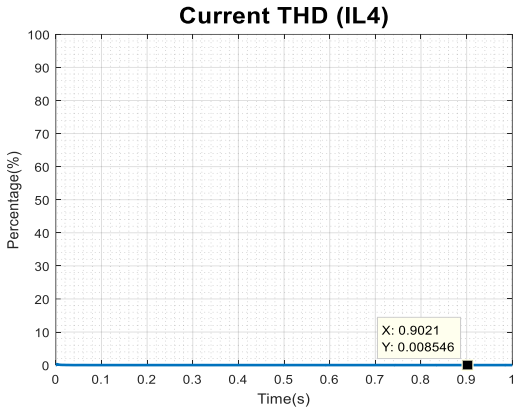

Fig 4.141: Current THD at Load 4

Figure 4.137 highlights Load 4 which the node under study. Figures 4.138 through figures 4.141 illustrate the output of the PSCAD results for the load side of Line44 which is the third branch of the CERTS microgrid testbed system. Between Load 4 and the Grid there are three transmission lines and another load which results in transmission losses. It is essential to study the measurements at Load 4 to verify that the load demand is being satisfied. It is evident through analysis of the figures that the system stabilizes at 0.1 seconds and the total duration of the run is 1.0 second. The RMS voltage is 278.3V and the THD of the voltage is 0.0858%. The measurements indicate that the RMS current is approximately 189.2A and the THD is approximately 0.0085%. The THD for both the voltage and current is very low and at an ideally acceptable level.

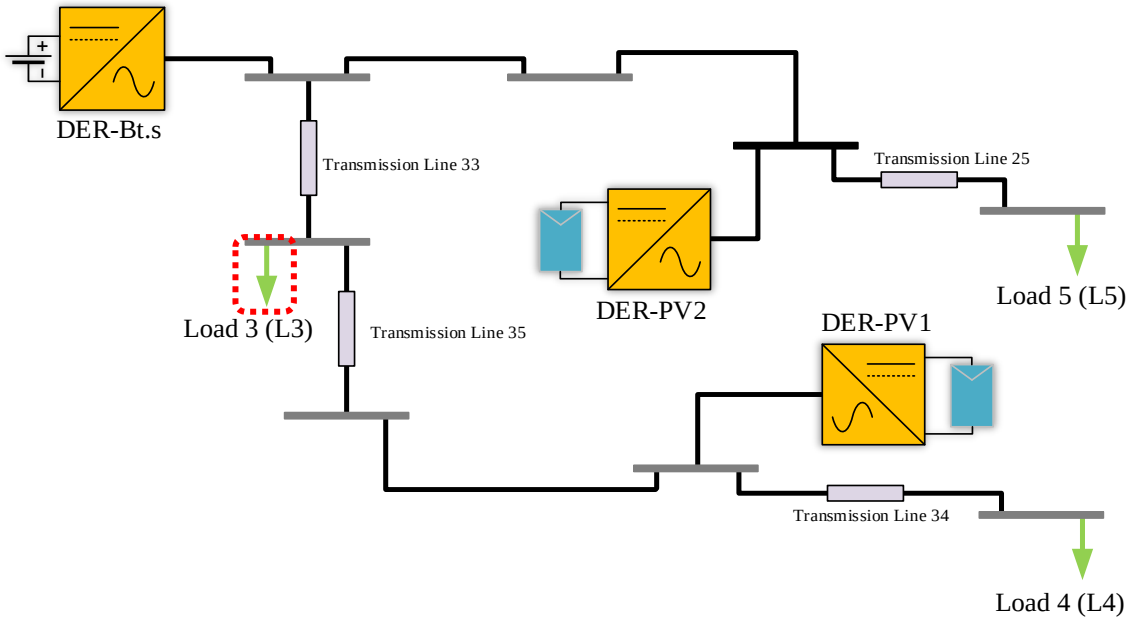

Fig 4.142. Load 3 Measurement Point

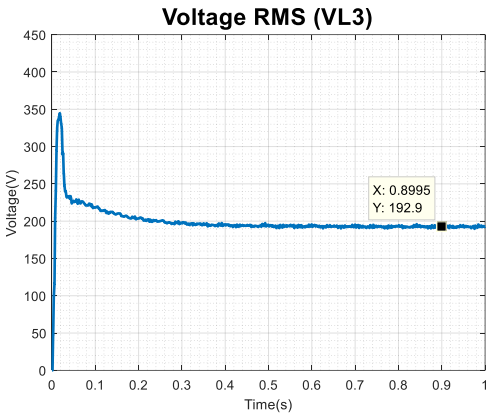

Fig 4.143: Voltage RMS at Load 3

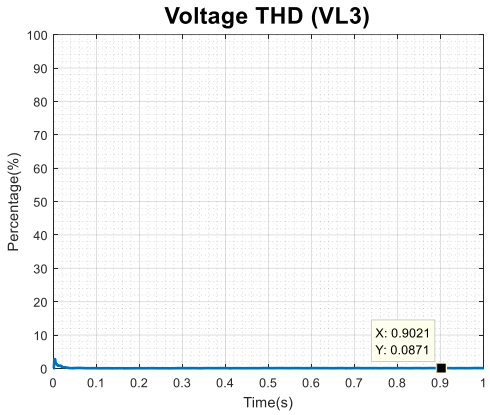

Fig 4.144: Voltage THD at Load3

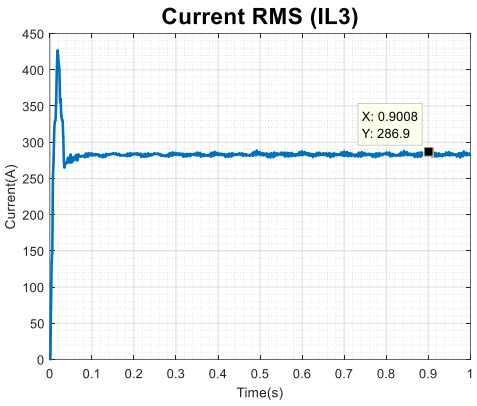

Fig 4.145: Current RMS at Load 3

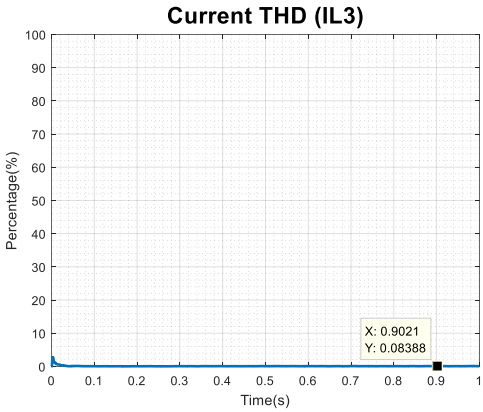

Fig 4.146: Current THD at Load 3

Figure 4.142 highlights Load 3 which the node under study. Figures 4.143 through figures 4.146 illustrate the output of the PSCAD results for the load side of Line23 which is the third branch of the CERTS microgrid testbed system. Between Load 3 and the Grid there is a transmission line which results in transmission losses. It is essential to study the measurements at Load 3 to verify that the load demand is being satisfied. It is evident through analysis of the figures that the system stabilizes at 0.1 seconds and the total duration of the run is 1.0 second. The RMS voltage is 286.9V and the THD of the voltage is 0.0838%. The measurements indicate that the RMS current is approximately 192.9A and the THD is approximately 0.0871%. The THD for both the voltage and current is very low and at an ideally acceptable level.

Table 4.9: Mean, MAD and Variance of Load 5

Load 5 PSCAD								
	Run1	**Run2**	**Run3**	**Run4**	**Run5**	**Avg of Means**	**MAD**	**Variance**
VRMS	282.555	282.555	282.555	282.555	282.555	282.5547	0	0
VTHD	0.1018	0.1018	0.1018	0.1018	0.1018	0.1018	0	0
IRMS	191.663	191.663	191.663	191.663	191.663	191.6627	0	0
ITHD	0.1342	0.1342	0.1342	0.1342	0.1342	0.1342	0	0

Table 4.10: Mean, MAD and Variance of Load 4

Load 4 PSCAD								
	Run1	**Run2**	**Run3**	**Run4**	**Run5**	**Avg of Means**	**MAD**	**Variance**
VRMS	276.104	276.104	276.104	276.104	276.104	276.1037	0	0
VTHD	0.1024	0.1024	0.1024	0.1024	0.1024	0.1024	0	0
IRMS	192.666	192.666	192.666	192.666	192.666	192.666	0	0
ITHD	0.9778	0.9778	0.9778	0.9778	0.9778	0.9778	0	0

Table 4.11: Mean, MAD and Variance of Load 3

Load 3 PSCAD								
	Run1	**Run2**	**Run3**	**Run4**	**Run5**	**Avg of Means**	**MAD**	**Variance**
VRMS	199.56	199.56	199.56	199.56	199.56	199.5597	0	0
VTHD	0.1012	0.1012	0.1012	0.1012	0.1012	0.1012	0	0
IRMS	283.066	283.066	283.066	283.066	283.066	283.0656	0	0
	0.09662	0.09662	0.09662	0.09662	0.09662	0.09662	0	0

4.4.2 Matlab-Simscape Simulation Island Mode of Operation

In this section the results obtained from Matlab-Simscape are illustrated and discussed. The points of measurement utilized were discussed in section 4.2 and are illustrated here using the single line diagram of the CERTS microgrid testbed system. The data collected through ten iterations is represented graphically and numerically, as can be seen in this section.

First the DC side voltage and DC side current generated by the distributed generation units are discussed. Followed by the AC side voltage and AC side current of inverters utilized to couple the distributed generators to the grid. Finally, the voltage and current of each of load is illustrated. In order to conduct thorough work, it was necessary to investigate the Root Mean Square and Total Harmonic Distortion of all AC values being analyzed.

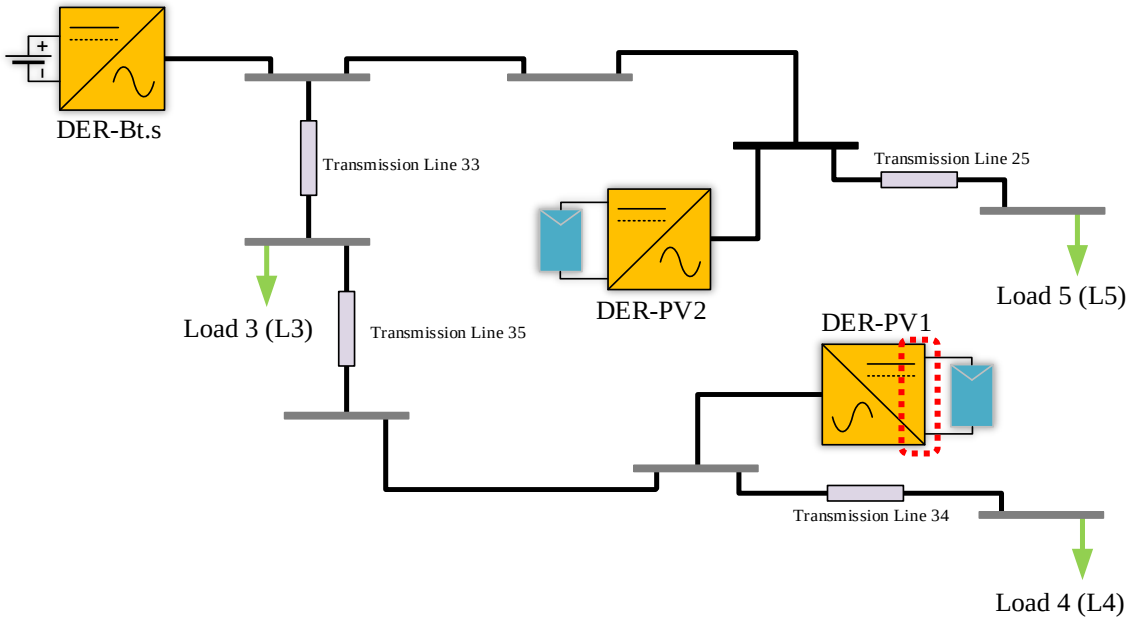

Fig 4.147: DG1 DC Side Point of Measurement

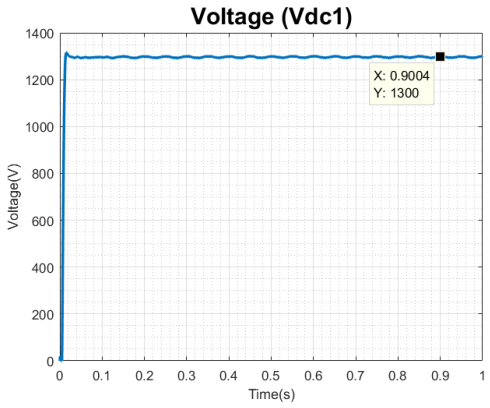

Fig 4.148: DC Link Voltage DG1

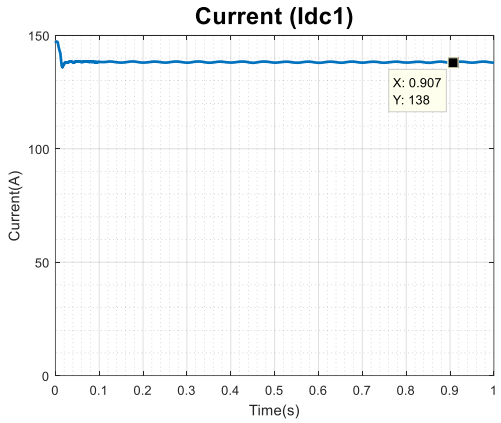

Fig 4.149: DC Link Current DG1

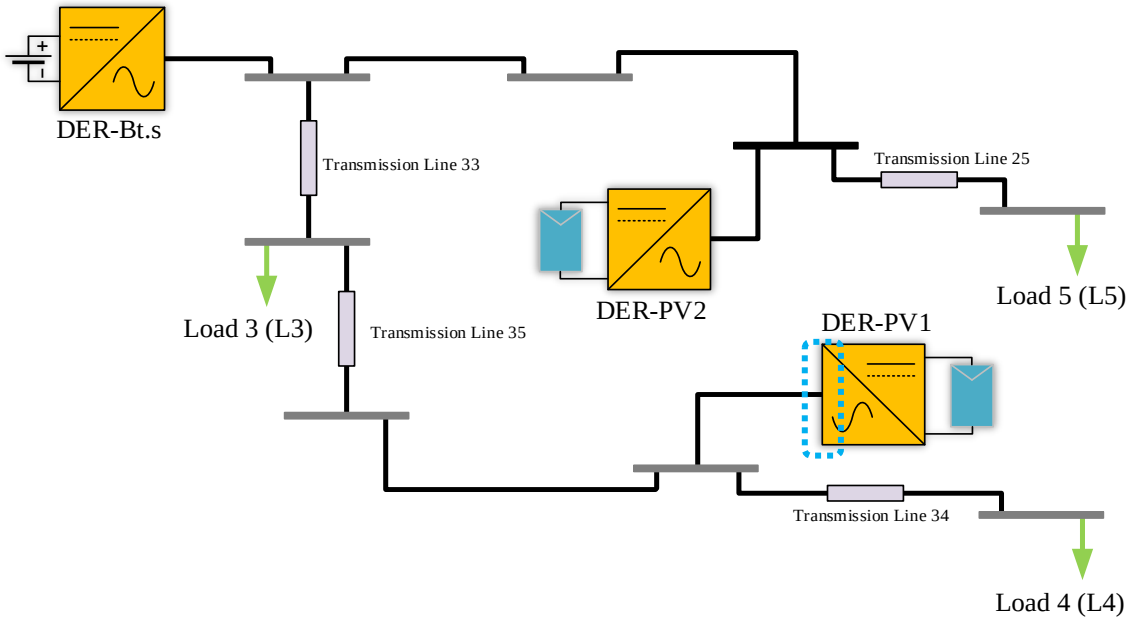

Fig 4.150: DG1 AC Side Point of Measurement

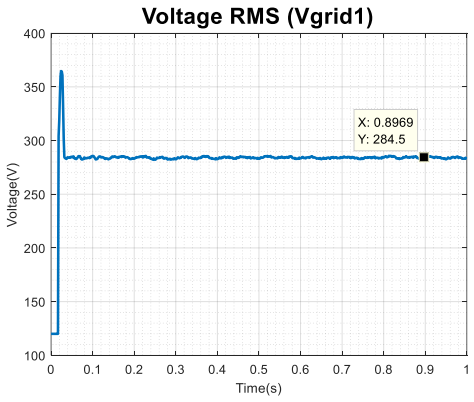

Fig 4.151: Voltage RMS at Point of Coupling

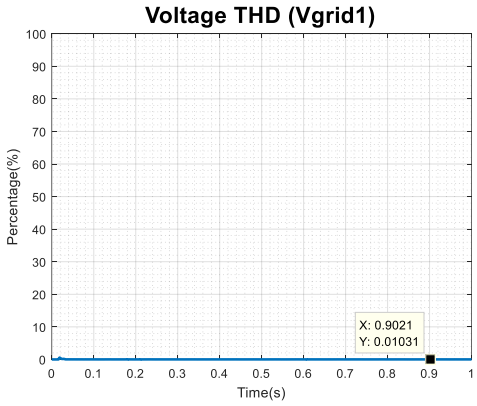

Fig 4.152: Voltage THD at Point of Coupling

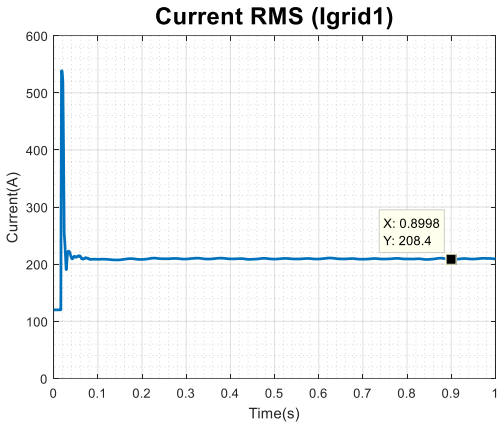

Fig 4.153: Current RMS at Point of Coupling

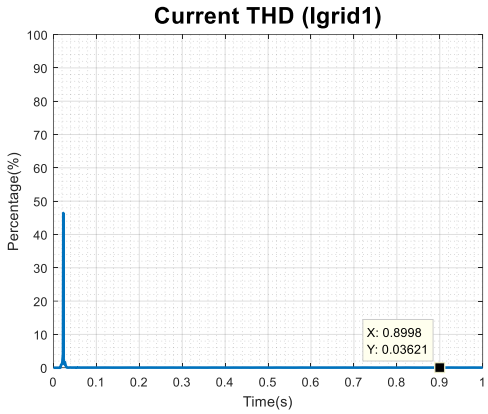

Fig 4.154: Current THD at Point of Coupling

Figure 4.147 highlights the DC side of the inverter which is the point under study. Figures 4.148 and Figure 4.149 illustrate the output of the PSCAD results for the DC side of the inverter integrated with the second distributed generation unit (PV1), which is a photovoltaic source namely PV1. Figure 4.150 highlights the AC side of the inverter which is the point under study. Whereas Figures 4.151 through 4.154 indicate the output of the PSCAD results on the AC side of the inverter for the second distributed generation unit (PV1). It is evident through analysis of the figures generated that the system reaches a stable point of operation free of any transients in the neighborhood of 0.1 seconds and the total duration of the run is 1.0 second. It is clear that on the DC side of the inverter PV1 generates approximately 1,300V and 138A. The RMS voltage measured at the secondary side of the inverter at which point PV1 is incorporated into PV1 is approximately 284.5V, along with a Total Harmonic Distortion value of 0.0103%. Whereas the RMS current measured at the same point is approximately 208.4A, accompanied by a Total Harmonic Distortion value of approximately 0.0362%. The THD for both the voltage and current was very low and at an ideally acceptable level.

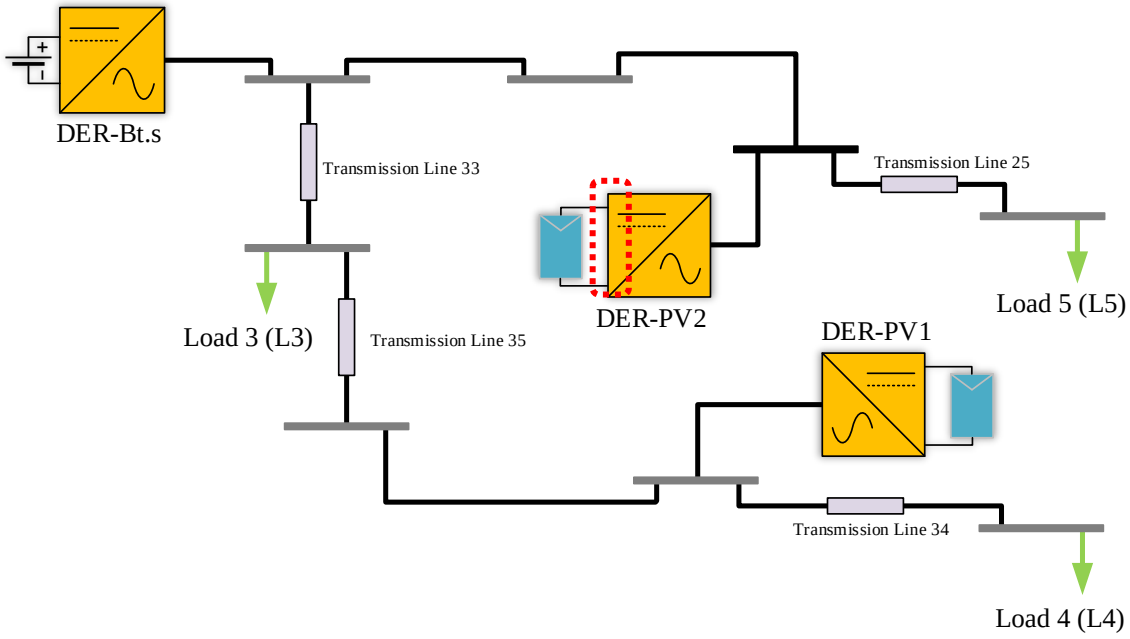

Fig 4.155: DG2 DC Side Point of Measurement

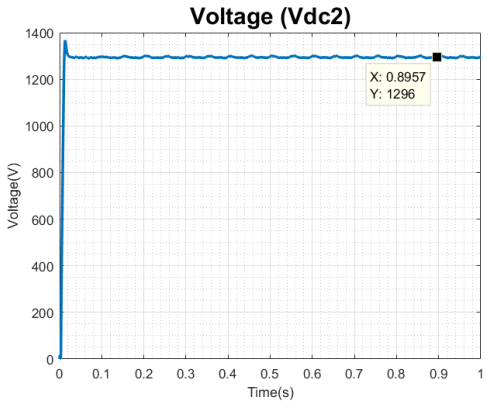

Fig 4.156: DC Link Voltage DG2

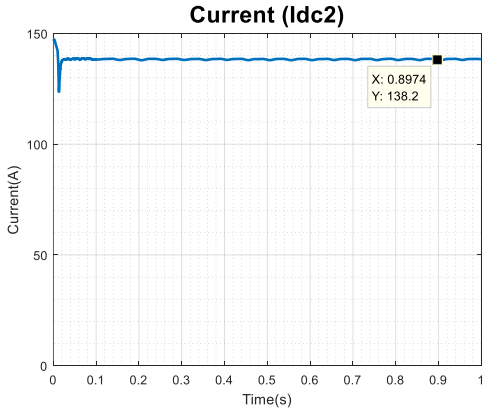

Fig 4.157: DC Link Current DG2

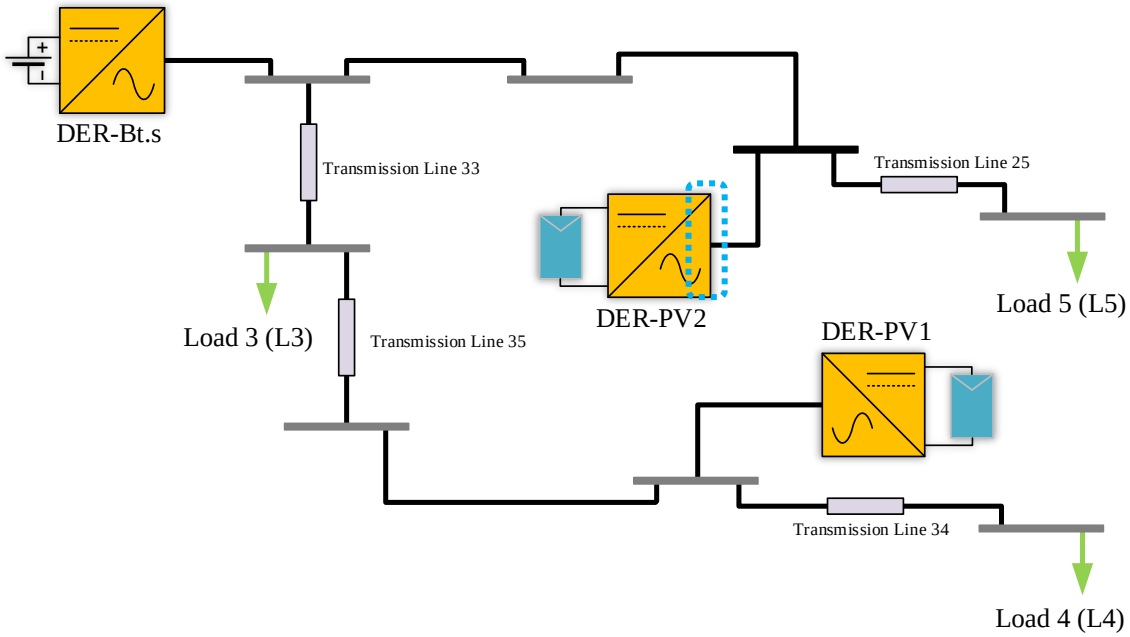

Fig 4.158: DG2 AC Side Point of Measurement

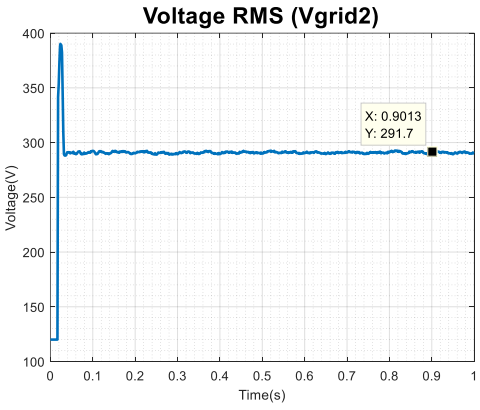

Fig 4.159: Voltage RMS at Point of Coupling

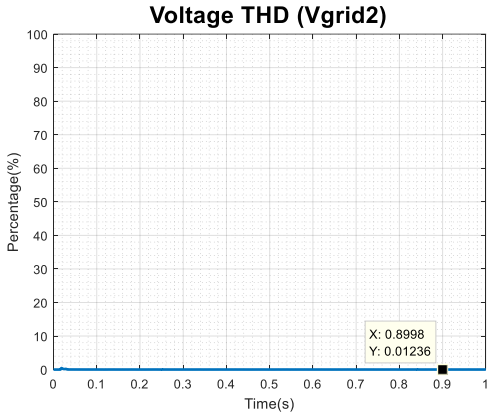

Fig 4.160: Voltage THD at Point of Coupling

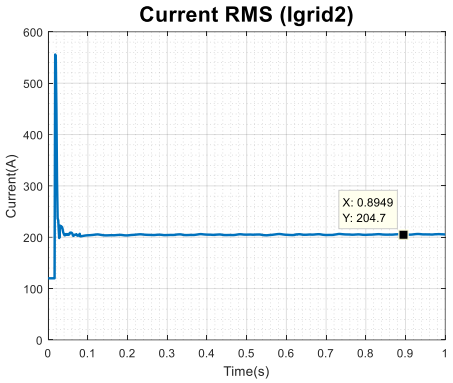

Fig 4.161: Current RMS at Point of Coupling

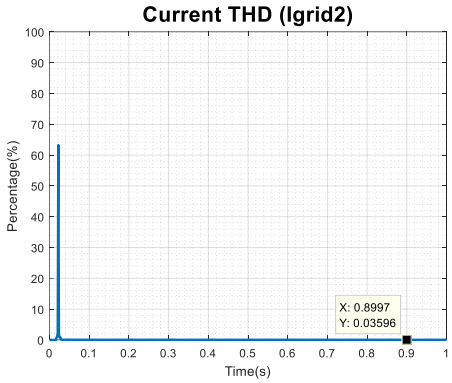

Fig 4.162: Current THD at Point of Coupling

Figure 4.155 highlights the DC side of the inverter, which is the point under study. Figures 4.156 and Figure 4.157 illustrate the output of the PSCAD results for the DC side of the inverter integrated with the first distributed generation unit (PV2) which is a photovoltaic source namely PV2. Figure 4.158 highlights the AC side of the inverter which is the point under study. Whereas Figures 4.159 through 4.162 indicate the output of the PSCAD results on the AC side of the inverter for the first distributed generation unit (PV1). It is evident through analysis of the figures generated that the system reaches a stable point of operation free of any transients in the neighborhood of 0.1 seconds and the total duration of the run is 1.0 second. It is clear that on the DC side of the inverter PV2 generates approximately 1296 and 138.2A. The RMS voltage measured at the secondary side of the inverter at which point PV2 is incorporated into PV2 is approximately 291.7V, along with a Total Harmonic Distortion value of 0.0123%, whereas the RMS current measured at the same point is approximately 204.7A, accompanied by a Total Harmonic Distortion value of approximately 0.0359%. The THD for both the voltage and current was very low and at an ideally acceptable level.

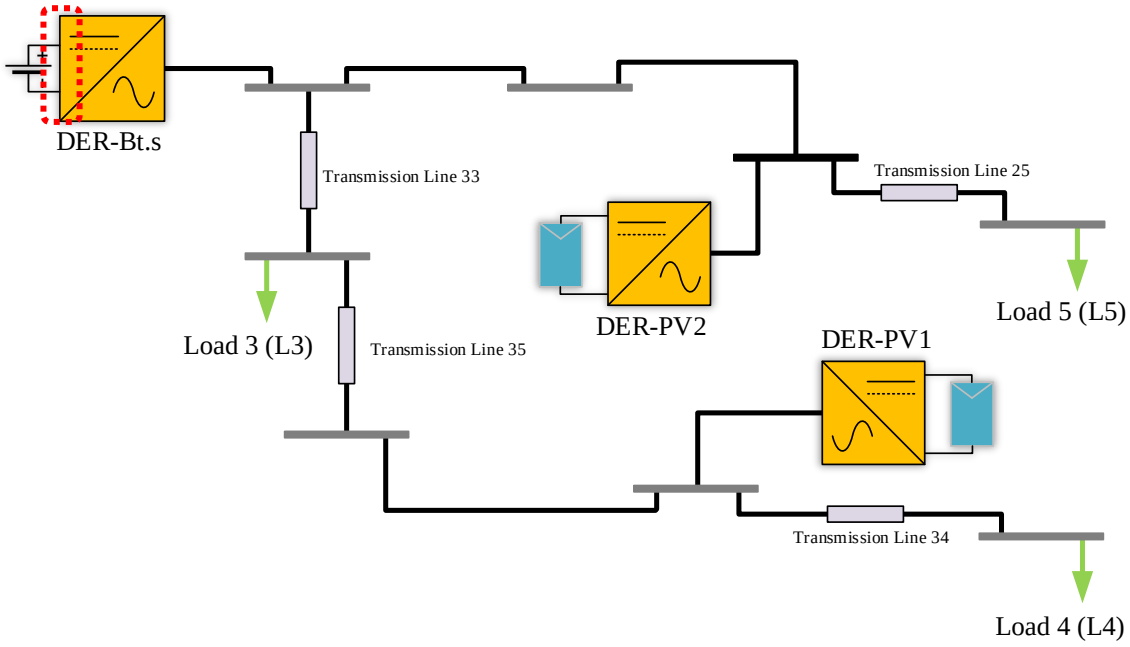

Fig 4.163: DG3 DC Side Point of Measurement

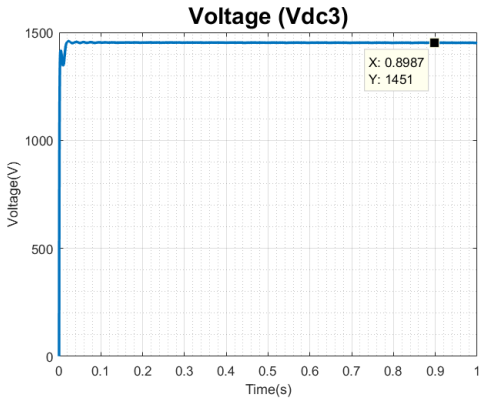

Fig 4.164: DC Link Voltage DG3

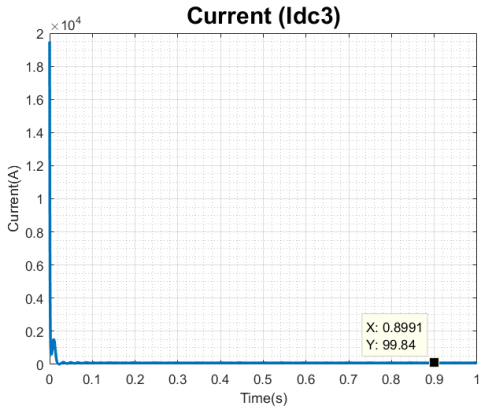

Fig 4.165: DC Link Current DG3

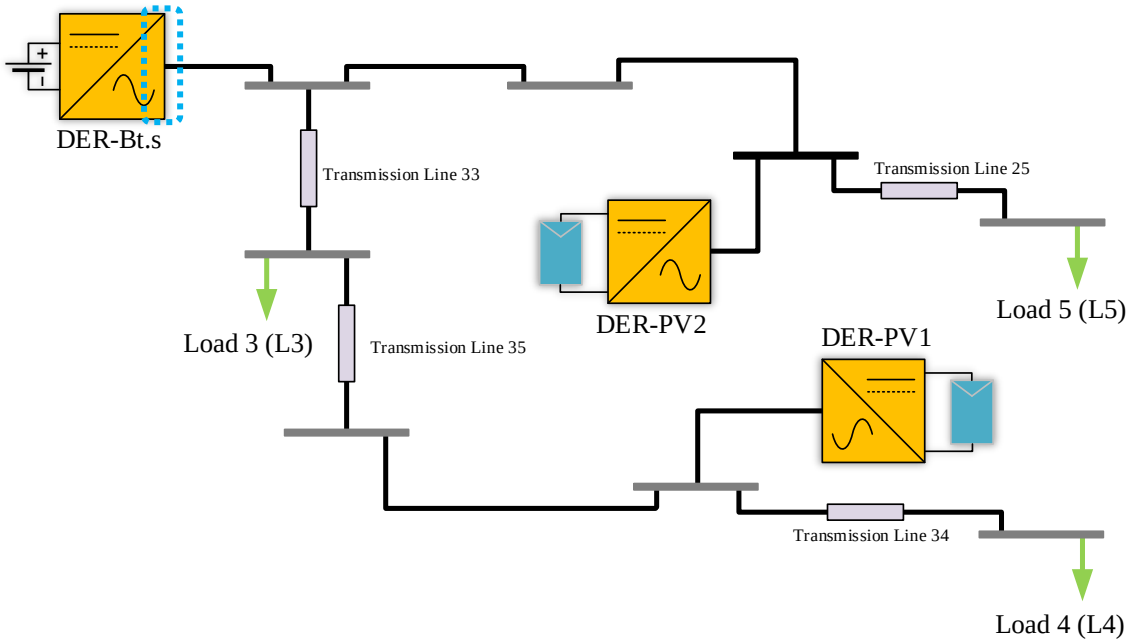

Fig 4.166: DG3 AC Side Point of Measurement

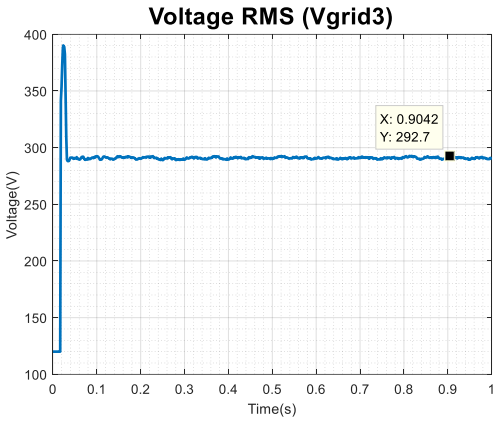

Fig 4.167: Voltage RMS at Point of Coupling

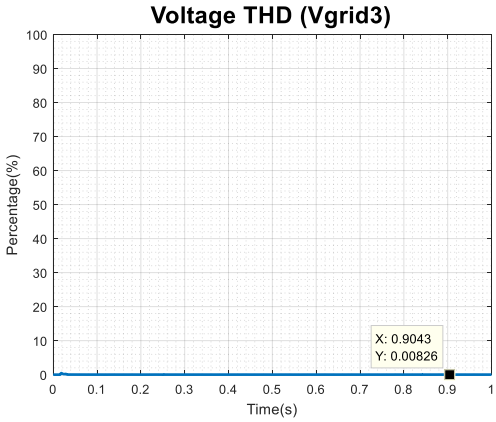

Fig 4.168: Voltage THD at Point of Coupling

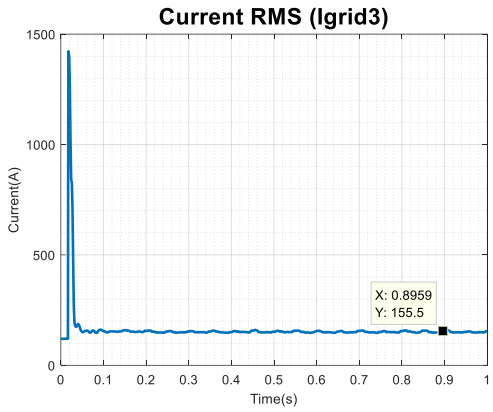

Fig 4.169: Current RMS at Point of Coupling

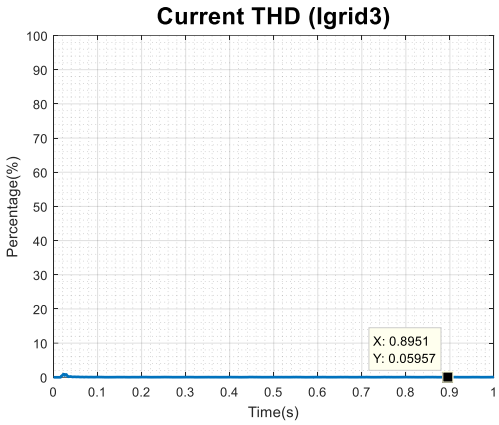

Fig 4.170: Current THD at Point of Coupling

Figure 4.163 highlights the DC side of the inverter which is the point under study. Figures 4.164 and Figure 4.165 illustrate the output of the PSCAD results for the DC side of the inverter integrated with the first distributed generation unit (Bt.S) which is a Battery Energy Storage source namely DER-Bt.S. Figure 4.166 highlights the AC side of the inverter which is the point under study. Whereas Figures 4.167 through 4.170 indicate the output of the PSCAD results on the AC side of the inverter for the first distributed generation unit (Bt.S). It is evident through analysis of the figures generated that the system reaches a stable point of operation free of any transients in the neighborhood of 0.1 seconds and the total duration of the run is 1.0 second. It is clear that on the DC side of the inverter Bt.S generates approximately 1451V and 99.84A. The RMS voltage measured at the secondary side of the inverter at which point PV1 is incorporated into Bt.S is approximately 292.7V, along with a Total Harmonic Distortion value of 0.0083%. Whereas the RMS current measured at the same point is approximately 155.5A, accompanied by a Total Harmonic Distortion value of approximately 0.0596%. The THD for both the voltage and current was very low and at an ideally acceptable level.

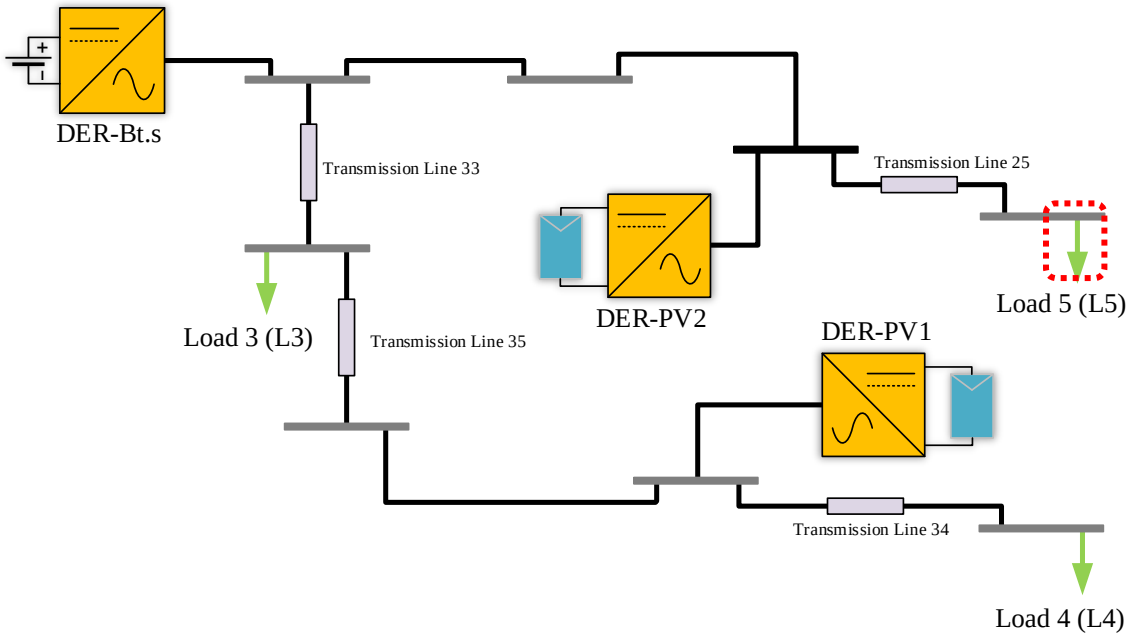

Fig 4.171: Load 5 Measurement Point

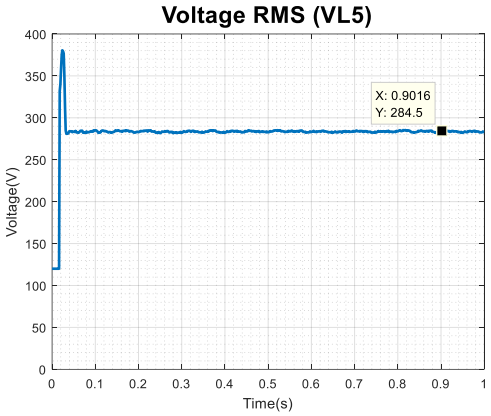

Fig 4.172: Voltage RMS at Load 5

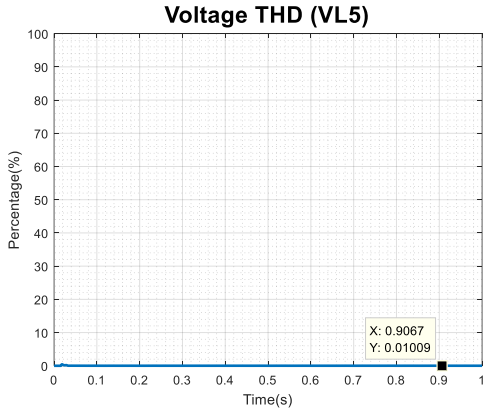

Fig 4.173: Voltage THD at Load 5

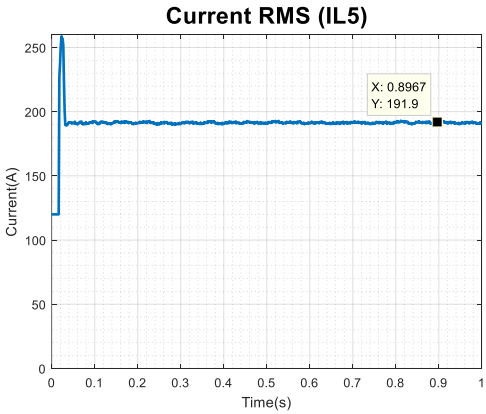

Fig 4.174: Current RMS at Load 5

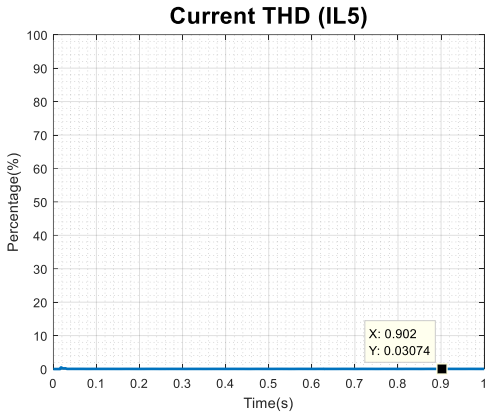

Fig 4.175: Current THD at Load 5

Figure 4.171 highlights Load 5 which the node under study. Figures 4.172 through figures 4.175 illustrate the output of the PSCAD results for the load side of Line25 which is the second branch of the CERTS microgrid testbed system. Between Load 5 and the Grid there is a transmission line which results in transmission losses. It is essential to study the measurements at Load 5 to verify that the load demand is being satisfied. It is evident through analysis of the figures that the system stabilizes at 0.1 seconds and the total duration of the run is 1.0 second. The RMS voltage is 284.5V and the THD of the voltage is 0.0100%. The measurements indicate that the RMS current is approximately 191.9A and the THD is approximately 0.0307%. The THD for both the voltage and current is very low and at an ideally acceptable level.

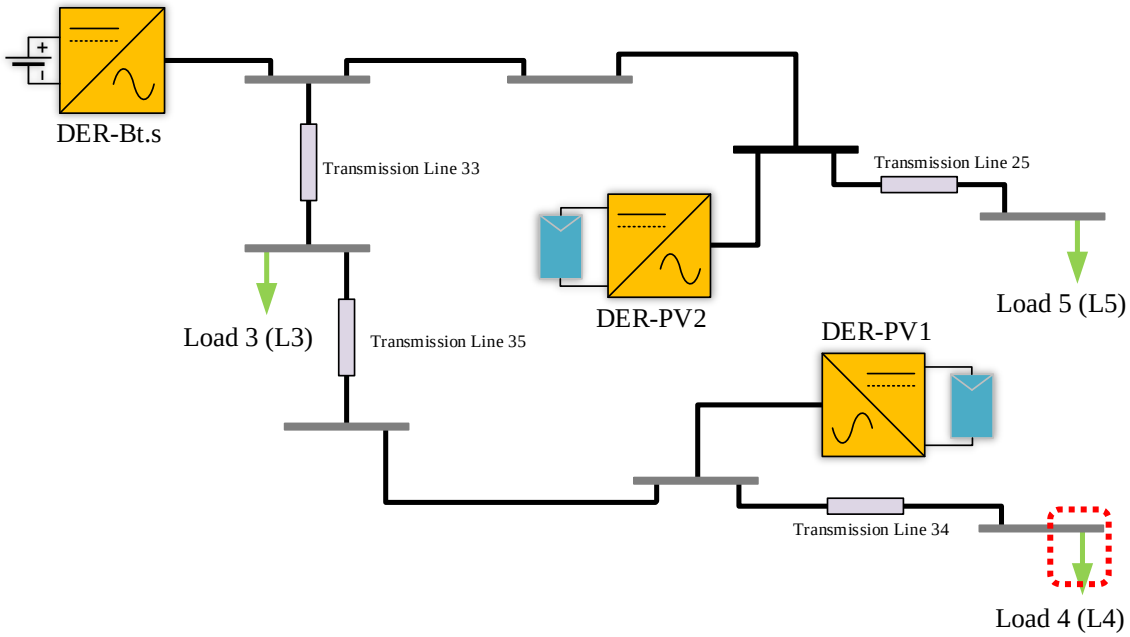

Fig 4.176: Load 4 Measurement Point

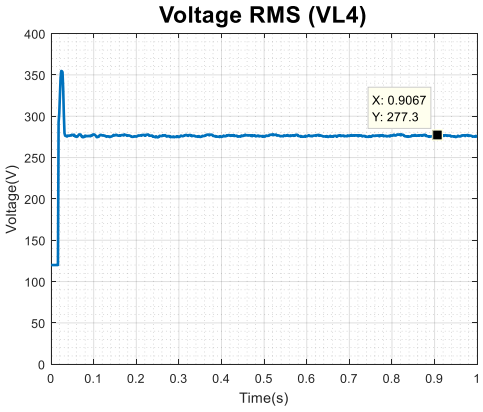

Fig 4.177: Voltage RMS at Load 4

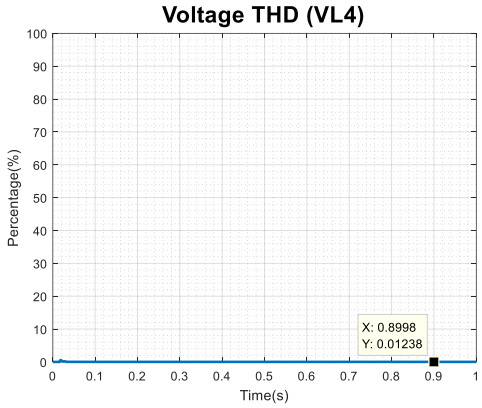

Fig 4.178: Voltage THD at Load 4

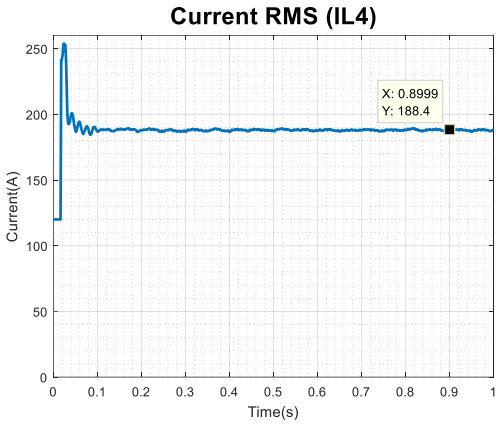

Fig 4.179: Current RMS at Load 4

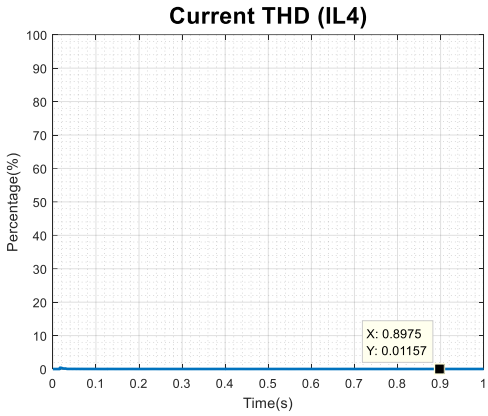

Fig 4.180: Current THD at Load 4

Figure 4.176 highlights Load 4 which the node under study. Figures 4.177 through figures 4.180 illustrate the output of the PSCAD results for the load side of Line44 which is the third branch of the CERTS microgrid testbed system. Between Load 4 and the Grid there are three transmission lines and another load which results in transmission losses. It is essential to study the measurements at Load 4 to verify that the load demand is being satisfied. It is evident through analysis of the figures that the system stabilizes at 0.1 seconds and the total duration of the run is 1.0 second. The RMS voltage is 277.3V and the THD of the voltage is 0.0124%. The measurements indicate that the RMS current is approximately 188.4A and the THD is approximately 0.0116%. The THD for both the voltage and current is very low and at an ideally acceptable level.

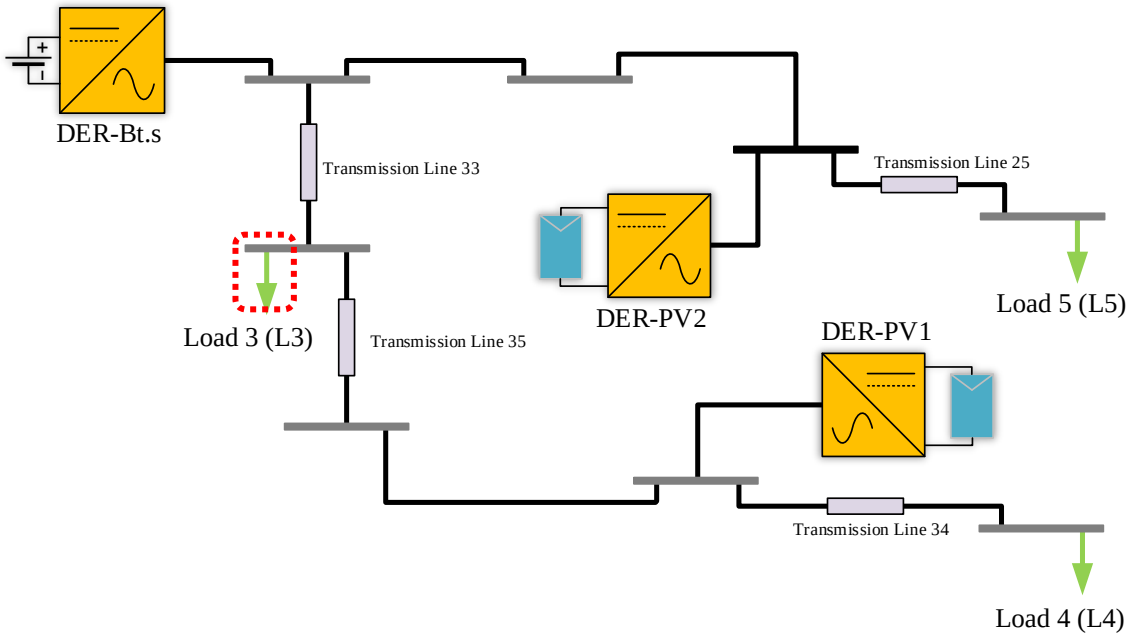

Fig 4.181: Load 3 Measurement Point

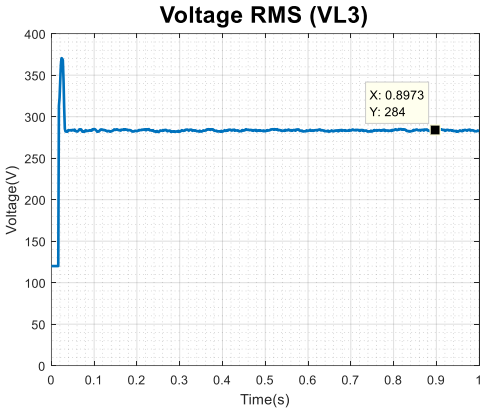

Fig 4.182: Voltage RMS at Load 3

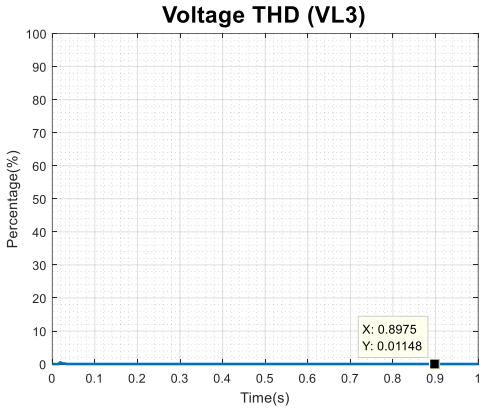

Fig 4.183: Voltage THD at Load 3

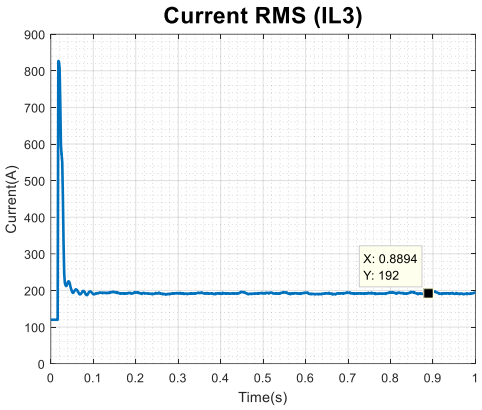

Fig 4.184: Current RMS at Load 3

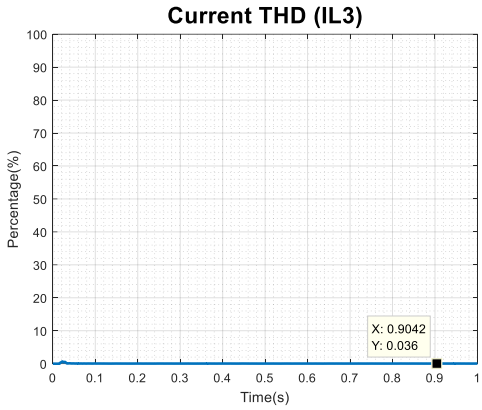

Fig 4.185: Current THD at Load 3

Figure 4.181 highlights Load 3 which the node under study. Figures 4.182 through figures 4.185 illustrate the output of the PSCAD results for the load side of Line23 which is the third branch of the CERTS microgrid testbed system. Between Load 3 and the Grid there is a transmission line which results in transmission losses. It is essential to study the measurements at Load 3 to verify that the load demand is being satisfied. It is evident through analysis of the figures that the system stabilizes at 0.1 seconds and the total duration of the run is 1.0 second. The RMS voltage is 284V and the THD of the voltage is 0.0115%. The measurements indicate that the RMS current is approximately 192A and the THD is approximately 0.0360%. The THD for both the voltage and current is very low and at an ideally acceptable level.

Table 4.12: Mean, MAD and Variance of Load 5

Load 5 Simulink								
	Run1	**Run2**	**Run3**	**Run4**	**Run5**	**Avg of Means**	**MAD**	**Variance**
VRMS	282.22	282.22	282.225	282.22	282.22	282.22094	0.001504	4.418E-06
VTHD	0.0174	0.0174	0.0174	0.0174	0.0174	0.0174	0	0
IRMS	190.98	190.98	190.98	190.98	190.98	190.98	0	0
ITHD	0.0397	0.0397	0.0397	0.0397	0.0397	0.0397	0	0

Table 4.13: Mean, MAD and Variance of Load 4

Load 4 Simulink								
	Run1	**Run2**	**Run3**	**Run4**	**Run5**	**Avg of Means**	**MAD**	**Variance**
VRMS	274.771	274.771	274.771	274.771	274.771	274.7711	0	0
VTHD	0.0176	0.0176	0.0176	0.0176	0.0176	0.0176	0	0
IRMS	188.008	188.008	188.008	188.008	188.008	188.0084	0	0
ITHD	0.0169	0.0169	0.0169	0.0169	0.0169	0.0169	0	0

Table 4.14: Mean, MAD and Variance of Load 3

Load 3 Simulink								
	Run1	**Run2**	**Run3**	**Run4**	**Run5**	**Avg of Means**	**MAD**	**Variance**
VRMS	284.829	284.829	284.829	284.829	284.829	284.8294	0	0
VTHD	0.0169	0.0169	0.0169	0.0169	0.0169	0.0169	0	0
IRMS	198.017	198.017	198.017	198.017	198.017	198.017	0	0
ITHD	0.0473	0.0473	0.0473	0.0473	0.0473	0.0473	0	0

4.4.3 PSCAD and Simulink in Island Mode Comparative Study

In order to analyze and compare the performance of both PSCAD and Matlab-Simscape simulating the CERTS microgrid testbed system in the grid connected mode of operation. In sections 4.3.1 and 4.3.2 the results of the simulation in individual software was illustrated. In this chapter the results are compared and explored side by side in order to determine which of the two software performs better. In order to do so there needs to be a comparison made at the voltage and current readings at each of the four loads. The root mean square (RMS) and total harmonic distortion (THD) are calculated and demonstrated at each of the loads. This is done in order to demonstrate which of the software provide a more robust solution to the system. The CERTS microgrid testbed System was modelled identically in both PSCAD and Matlab-Simscape while following the same parameters for each of the components utilized.

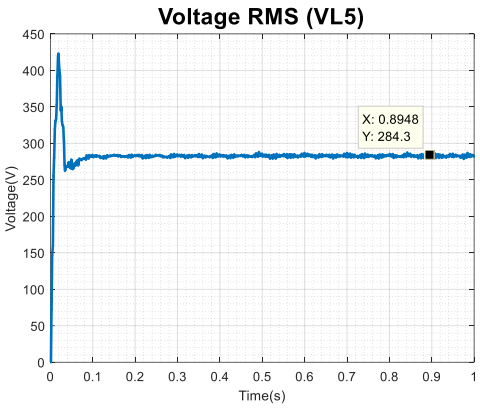

Fig 4.186A: PSCAD Voltage RMS Load 5

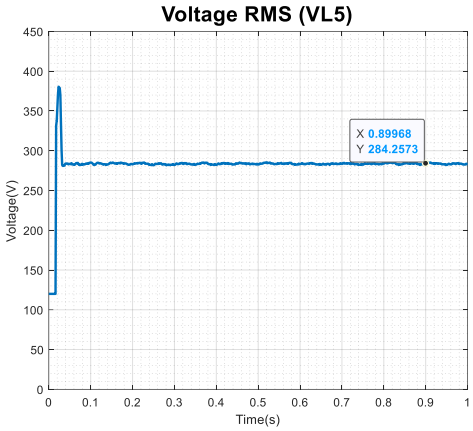

Fig 4.186B: Simulink Voltage RMS Load 5

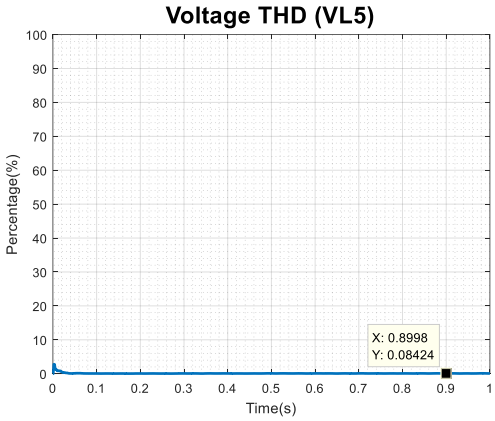

Fig 4.187A: PSCAD Voltage THD Load 5

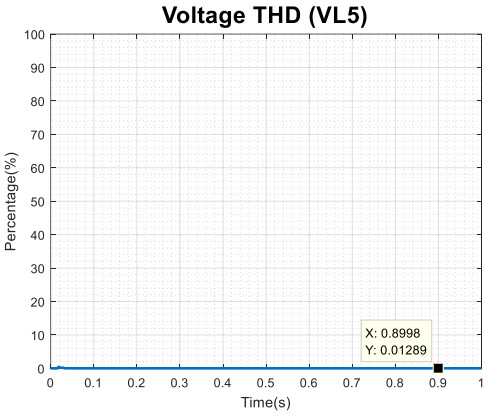

Fig 4.187B: Simulink Voltage THD Load 5

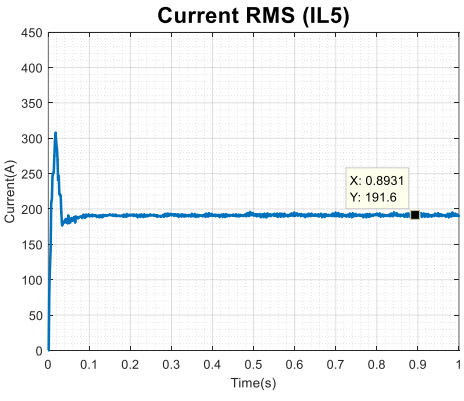

Fig 4.188A: PSCAD Current RMS Load 5

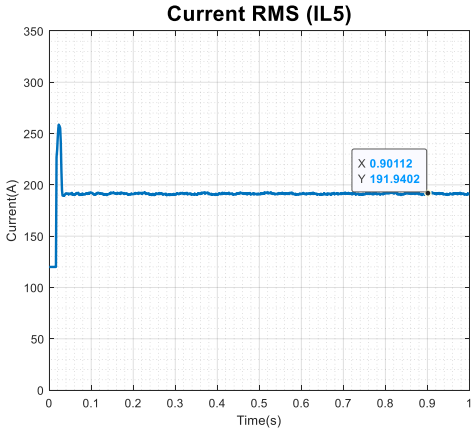

Fig 4.188B: Simulink Current RMS Load 5

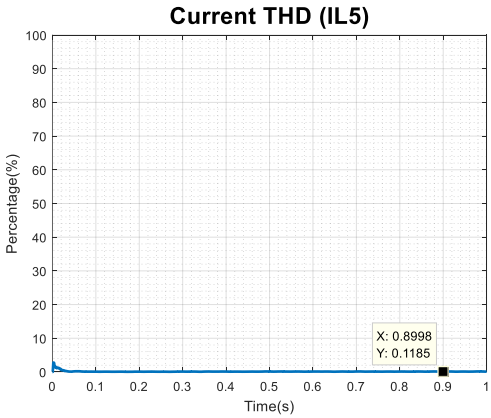

Fig 4.189A: PSCAD Current THD Load 5

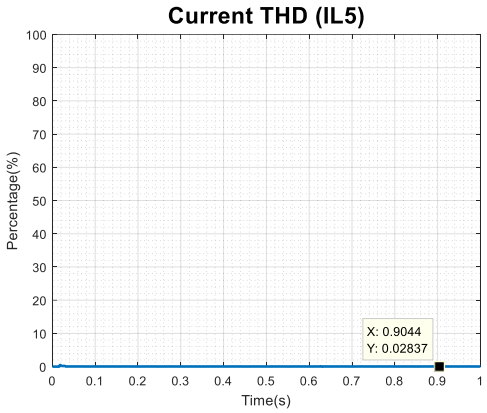

Fig 4.189B: Simulink Current THD Load 5

By analyzing figures 4.186A through 4.189B, it is evident that the output voltage and output current measured at Load 5 are similar in both simulation environments. The difference in the voltage and current between the two simulating environments is 0.0703% and 0.1563% respectively. This further affirms that the system has been modelled uniformly and consistently in both PSAD and Matlab-Simscape. Furthermore, the total harmonic distortion measure of both current and voltage were well below 1% and the acceptable margin of error, thus indicating that the system is stable.

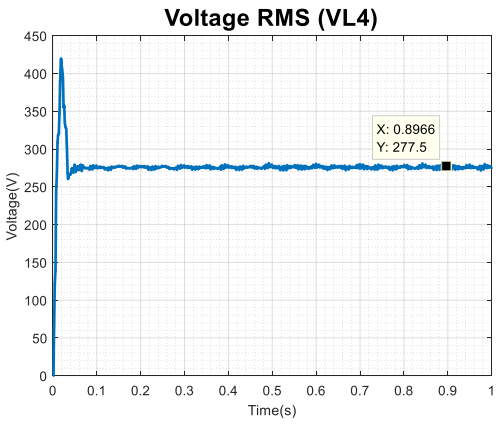

Fig 4.190A: PSCAD Voltage RMS Load 4

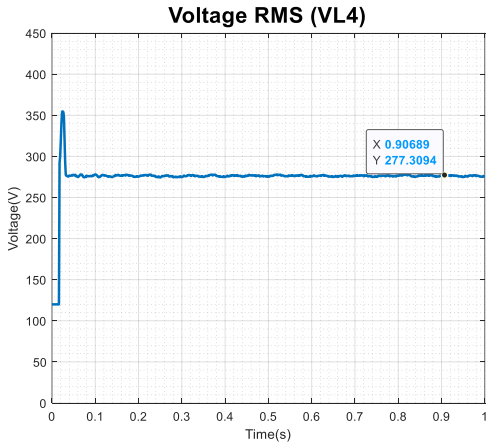

Fig 4.190B: Simulink Voltage RMS Load 4

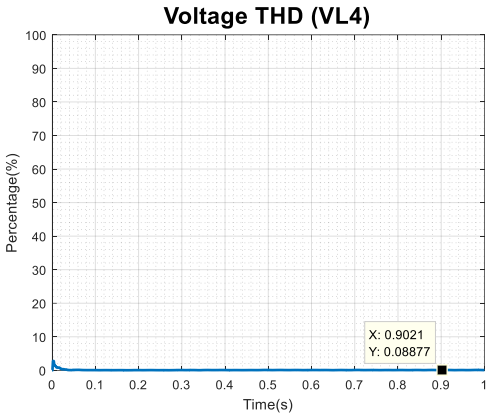

Fig 4.191A: PSCAD Voltage THD Lo 4

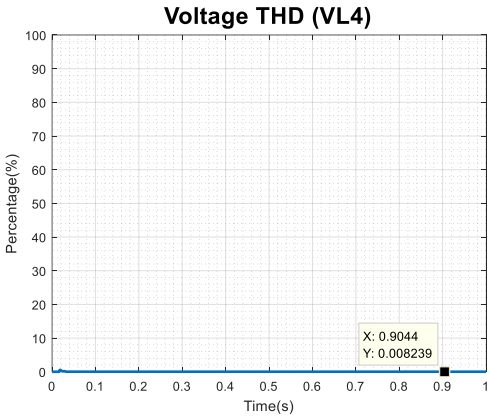

Fig 4.191B: Simulink Voltage THD Lo 4

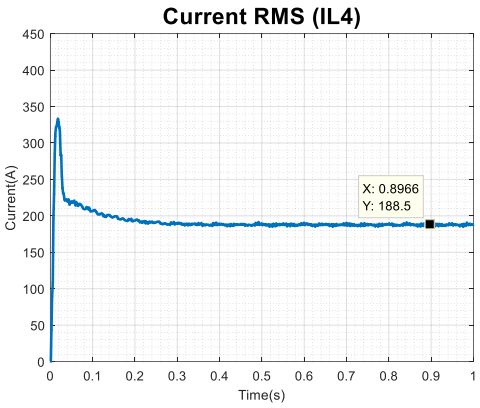

Fig 4.192A: PSCAD Current RMS Load 4

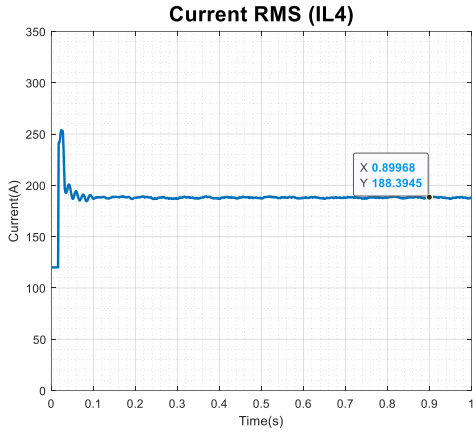

Fig 4.192B: Simulink Current RMS Load 4

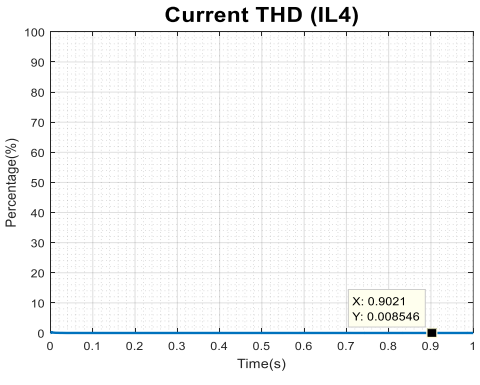

Fig 4.193A: PSCAD Current THD Load 4

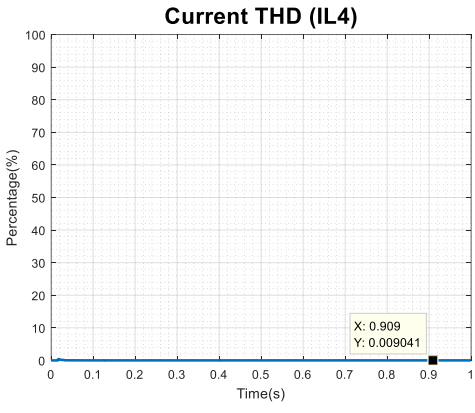

Fig 4.193A: Simulink Current THD Load 4

By analyzing figures 4.190A through 4.193B, it is evident that the output voltage and output current measured at Load 4 are similar in both simulation environments. The difference in the voltage and current between the two simulating environments is 0.0721% and 0.0531% respectively. This further affirms that the system has been modelled uniformly and consistently in both PSAD and Matlab-Simscape. Furthermore, the total harmonic distortion measure of both current and voltage were well below 1% and the acceptable margin of error, thus indicating that the system is stable.

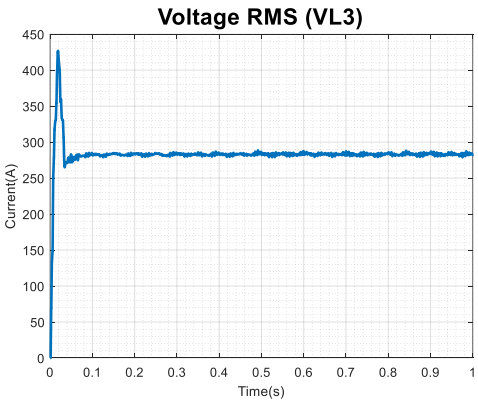

Fig 4.194A: PSCAD Voltage RMS Load 3

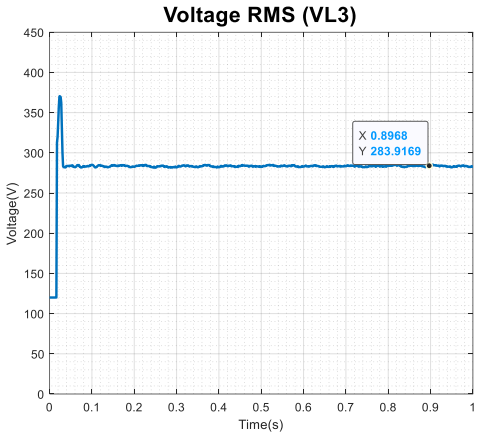

Fig 4.194B: Simulink Voltage RMS Load 3

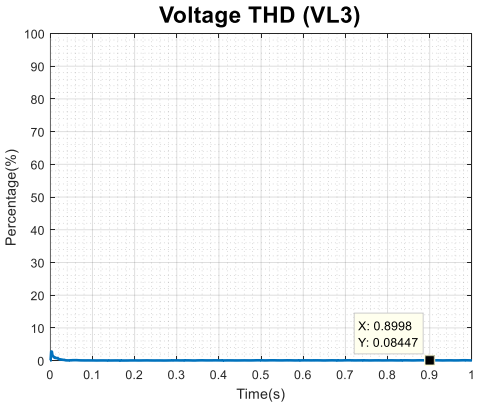

Fig 4.195A: PSCAD Voltage THD Load 3

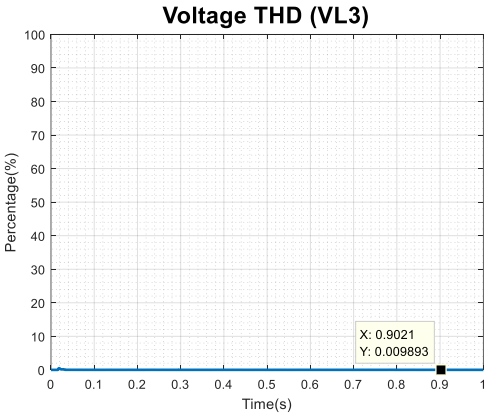

Fig 4.195B: Simulink Voltage THD Load 3

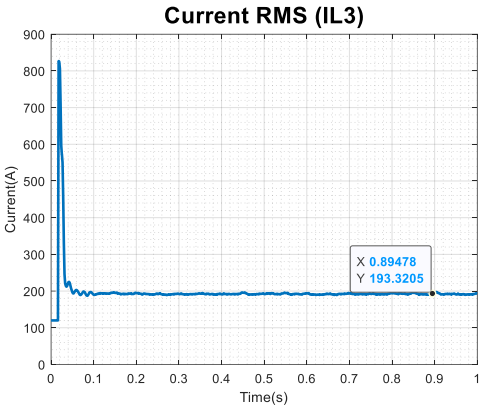

Fig 4.196A: PSCAD Current RMS Load 3

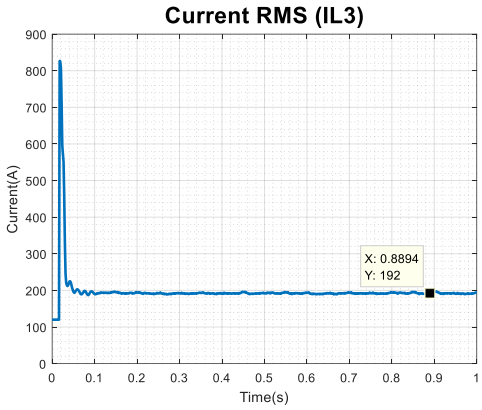

Fig 4.196B: Simulink Current THD Load 3

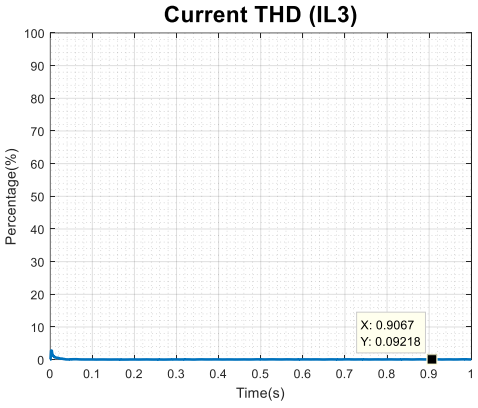

Fig 4.197A: PSCAD Current THD Load 3

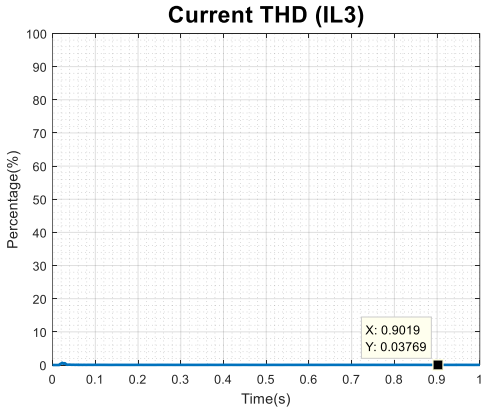

Fig 4.197B: Simulink Current THD Load 3

By analyzing figures 4.194A through 4.197B, it is evident that the output voltage and output current measured at Load 3 are similar in both simulation environments. The difference in the voltage and current between the two simulating environments is 0.2465% and 0.7752% respectively. This further affirms that the system has been modelled uniformly and consistently in both PSAD and Matlab-Simscape. Additionally, the total harmonic distortion measure of both current and voltage were well below 1% and the acceptable margin of error, thereby indicating that the system is stable.

5. Conclusion and Recommendations

5.1. Conclusion

This research identifies effective modelling and simulation methodologies necessary to uniformly represent the CERTS microgrid testbed system in two different simulation platforms. The issue of inconsistency in the output quantities (voltage and current) of the modelled system is highlighted and addressed. The framework necessary to measure and adjust the performance in both simulation platforms in a quantitative and qualitative manner was introduced. Moreover, the methodology necessary to model the various components of the CERTS microgrid testbed system in a uniform and interchangeable manner was proposed. Hence, all components are modelled systematically in both the simulation platforms, while overcoming the difference in the input parameters required for each component. Along with the differences in the input parameters, the unit associated with the quantity being utilized was unified. The equivalent modelling of the components was made possible by employing an equivalent model approach for the transmission lines and the loads.

The detailed investigation provided shows that, it is important to utilize constant impedance model which are implemented by linear components, in order to ensure that both the platforms remain within the linear mode of operation throughout the entire simulation. That is, PSCAD operates in the linear mode of operation but changes over to non-linear characteristic within ±20% of the rated RMS voltage, minimum of 10, frequency index of reactive power and frequency index of active power. The switching between linear and non-linear characteristics has an impact on the output parameters under study. Whereas Matlab-Simscape ensures that the execution of the model is kept in the linear

mode of operation (with the proper solver selected). This is done by relaying on the steady state design parameters such as rated active power, rated reactive power and rated RMS voltage (L-G RMS). In other words, values of the reactances are deduced from the reactive power equations of each load. While the resistances are deduced from the active power equations. Finally, the properties of each components in each software have been highlighted in detail to facilitate the transition between each platform.

The CERTS microgrid was studied in both the grid connected mode of operation and the island mode of operation. The points of measurement were chosen to be the loads associated with the microgrid and the PCC of each of the distributed generation units. In order to verify the performance of both simulating environments, voltage, current, and their THD at the important nodes within the microgrid and the connected power system have been monitored and logged. Furthermore, the means, variance and MAD have been calculated in order to evaluate the robustness of the solutions provided by each of the simulation platforms and to demonstrate their reliability and consistency.

The detailed comparison of the performance of the two simulation platforms shows that both environments (PSCAD and Matlab-Simscape) produced similar results within the acceptable margin of error in both island mode of operation and grid connected mode of operation. The data presented in Chapter 4 concludes that the voltage and current at each of the points of measurement were within the acceptable margin of error. The RMS voltages and currents were within 1% margin of error, and the THD for the measured voltages and currents were also within 1% margin of error. Furthermore, the analysis of the test data shows that the variances calculated for the various runs is very low and are accompanied by a very low MAD. Based on the illustrated data (shown in the tables for

five runs), it was evident that the system was providing a robust solution in both modes of operation.

It was evident from the data that the results produced by both simulation platforms (PSCAD and Matlab-Simscape) maintained a percentage error below 1%, which verifies that the system was modelled uniformly in both PSAD and Matlab-Simscape. Furthermore, the obtained results show the impact of the microgrid on the connected power system at the PCC as there are harmonics injected into the grid (i.e. a by-product of the utilization of switching devices used to tie the DGs into the grid network). This was verified by analyzing the RMS and THD values associated with each of the selected points of measurement. Moreover, the analysis of the test data shows that the THD measured at all points of measurement was below the 1% mark, which complies with IEEE standards for grid connected DG.

5.2. Recommendations

Based on the work established in this thesis, a few recommendations can be formulated. The first, would be to further broaden the scope of the CERTS microgrid testbed system by modelling distributed generation sources other than the ones studied in this thesis, such as inertial generators, fly wheels, wind turbine and thermal generation. The second, would be to implement different types of loads in the microgrid such as the constant power load and the effect such loads would have on the stability of the microgrid system.

In order to model such different types of loads and distributed generators, the foundational knowledge of each of these components are essential. It is of importance to compare the existing models of these components in PSCAD and Matlab-Simscape to determine what could be causing the offsets. More importantly, the control schemes

associated with the distributed generation will have to be altered and tailored for the distributed generation type employed. As for the constant power loads, detailed attention would have to be carried out in order to ensure that the loads are being modelled uniformly and equally in both PSCAD and Matlab-Simscape. They form crucial part of the microgrid as they represent critical loads such as; hospital equipment, airport equipment or other such equipment which must supplied with uninterrupted power.

Furthermore, one more recommendation is worth mentioning. Although the step size for the steady state analysis conducted in this study was determined based on the Nyquist Criteria. It would, however, be of high importance in the case of the transient response of the system in both simulation platforms. This is why a greater emphasis should be utilized when selecting the time step for a transient study as the transients can have large frequency deviations.

5.3. Future Work

To build on the study performed in this work, a few extra topics can be explored. A transient study can be performed in order to investigate the impact that different faults may have on the microgrid. Also, this study can be extended to investigate system dynamics under AC and / or DC faults. Hence, more adjustment in the components modelling in both PSCAD and Matlab-Simscape might be needed. Moreover, machine learning techniques can be invoked to explore the avenue of fault classification in a microgrid.

A very interesting topic which can be explored is the detection of incipient faults, incipient faults are very small variations in the power supply that last for short duration of time but can become problematic and lead to full fledge faults. This prospect can be

explored by utilizing tools such as machine learning and wavelet analysis. As wavelets enable detailed studies of signals and can be used to detect the smallest of variations in any signal and can help with feature extraction to be used by various machine learning techniques. Along with the incorporation of optimization techniques to help attain better features, to be used in the machine learning algorithms. Finally, more test beds would be included to the study to verify and adjust the models used in other applications such as high voltage DC transmission lines.

Furthermore, this work can be further expanded through the incorporation of different types of distributed generation. This work emphasized the usage of photovoltaic arrays and battery energy storage in the form of a battery. Other distributed generation types such as wind turbines, inertial generators like diesel generators and petrol generators can be included in this study. The key aspect to be studied would be the characteristics of the various DGs and how these characteristics can be modelled uniformly in both PSCAD and Matlab-Simscape.

References

[1] "Applying FBD-power theory to analysing effective lighting devices' impact on power quality and electric grid efficiency." [Online]. Available: http://www.scielo.org.co/scielo.php?script=sci_arttext&pid=S0120-56092011000500017. [Accessed: 15-Dec-2019].

[2] T. S. A. A. Sewilam, "Automated wavelet-based fault detection and diagnosis for smart distribution systems and microgrids," Aug. 2017.

[3] I. Colak, "Introduction to smart grid," in *2016 International Smart Grid Workshop and Certificate Program (ISGWCP)*, Istanbul, Turkey, 2016, pp. 1–5, doi: 10.1109/ISGWCP.2016.7548265.

[4] "Figure 1. Smart grid architecture with modern communications technologies," *ResearchGate*. [Online]. Available: https://www.researchgate.net/figure/Smart-grid-architecture-with-modern-communications-technologies_fig1_322555918. [Accessed: 15-Dec-2019].

[5] C. E. Association, "THE SMART GRID: A PRAGMATIC APPROACH A 'State-of-Play' Discussion Paper Presented by the Canadian Electricity Association," *electricity.ca*, May-2017. [Online]. Available: https://electricity.ca/wp-content/uploads/2017/05/SmartGridpaperEN.pdf.

[6] H. Yenginer, C. Cetiz, and E. Dursun, "A review of energy management systems for smart grids," in *2015 3rd International Istanbul Smart Grid Congress and Fair (ICSG)*, Istanbul, Turkey, 2015, pp. 1–4, doi: 10.1109/SGCF.2015.7354918.

[7] A. Sharma, B. K. Saxena, and K. V. S. Rao, "Comparison of smart grid development in five developed countries with focus on smart grid implementations in India," in *2017 International Conference on Circuit ,Power and Computing Technologies (ICCPCT)*, Kollam, India, 2017, pp. 1–6, doi: 10.1109/ICCPCT.2017.8074195.

[8] V. C. Gungor *et al.*, "Smart Grid Technologies: Communication Technologies and Standards," *IEEE Trans. Ind. Inf.*, vol. 7, no. 4, pp. 529–539, Nov. 2011, doi: 10.1109/TII.2011.2166794.

[9] J. McClean and V. Polsoni, "at PowerStream: Operations to Micro Grid," p. 57.

[10] Z. Davar, "Scale Microgrids: Cleantech Solutions For California Wildfires," *Medium*, 16-Jul-2019. [Online]. Available: https://medium.com/cleantech-rising/scale-microgrids-cleantech-solutions-for-california-wildfires-cleantech-rising-b85356cfa30a. [Accessed: 15-Dec-2019].

[11] A. K. Srivastava, A. A. Kumar, and N. N. Schulz, "Impact of Distributed Generations With Energy Storage Devices on the Electric Grid," *IEEE Systems Journal*, vol. 6, no. 1, pp. 110–117, Mar. 2012, doi: 10.1109/JSYST.2011.2163013.

[12] J. T. Bialasiewicz, "Renewable Energy Systems With Photovoltaic Power Generators: Operation and Modeling," *IEEE Transactions on Industrial Electronics*, vol. 55, no. 7, pp. 2752–2758, Jul. 2008, doi: 10.1109/TIE.2008.920583.

[13] S. W. Mohod and M. V. Aware, "A STATCOM-Control Scheme for Grid Connected Wind Energy System for Power Quality Improvement," *IEEE Systems Journal*, vol. 4, no. 3, pp. 346–352, Sep. 2010, doi: 10.1109/JSYST.2010.2052943.

[14] A. M. Azmy and I. Erlich, "Impact of distributed generation on the stability of electrical power system," in *IEEE Power Engineering Society General Meeting, 2005*, 2005, pp. 1056-1063 Vol. 2, doi: 10.1109/PES.2005.1489354.

[15] M. Reza, P. H. Schavemaker, J. G. Slootweg, W. L. Kling, and L. van der Sluis, "Impacts of distributed generation penetration levels on power systems transient stability," in *IEEE Power Engineering Society General Meeting, 2004.*, 2004, pp. 2150-2155 Vol.2, doi: 10.1109/PES.2004.1373261.
[16] J. Xu, Q. Qian, B. Zhang, and S. Xie, "Harmonics and Stability Analysis of Single-Phase Grid-Connected Inverters in Distributed Power Generation Systems Considering Phase-Locked Loop Impact," *IEEE Transactions on Sustainable Energy*, vol. 10, no. 3, pp. 1470–1480, Jul. 2019, doi: 10.1109/TSTE.2019.2893679.
[17] J. Xu, S. Xie, Q. Qian, and B. Zhang, "Adaptive Feedforward Algorithm Without Grid Impedance Estimation for Inverters to Suppress Grid Current Instabilities and Harmonics Due to Grid Impedance and Grid Voltage Distortion," *IEEE Transactions on Industrial Electronics*, vol. 64, no. 9, pp. 7574–7586, Sep. 2017, doi: 10.1109/TIE.2017.2711523.
[18] X. Wu, X. Li, X. Yuan, and Y. Geng, "Grid Harmonics Suppression Scheme for LCL-Type Grid-Connected Inverters Based on Output Admittance Revision," *IEEE Transactions on Sustainable Energy*, vol. 6, no. 2, pp. 411–421, Apr. 2015, doi: 10.1109/TSTE.2014.2384509.
[19] "IEEE Recommended Practice and Requirements for Harmonic Control in Electric Power Systems," *IEEE Std 519-2014 (Revision of IEEE Std 519-1992)*, pp. 1–29, Jun. 2014, doi: 10.1109/IEEESTD.2014.6826459.
[20] A. Picciariello, K. Alvehag, and L. Söder, "Impact of Network Regulation on the Incentive for DG Integration for the DSO: Opportunities for a Transition Toward a Smart Grid," *IEEE Transactions on Smart Grid*, vol. 6, no. 4, pp. 1730–1739, Jul. 2015, doi: 10.1109/TSG.2015.2409313.
[21] T. Ackermann, "Distributed generation: a definition," *Electric Power Systems Research*, p. 10, 2001.
[22] D. Trebolle and T. Gómez, "Reliability Options in Distribution Planning Using Distributed Generation," *IEEE Latin America Transactions*, vol. 8, no. 5, pp. 557–564, Sep. 2010, doi: 10.1109/TLA.2010.5623509.
[23] V. H. M. Quezada, J. R. Abbad, and T. G. S. Roman, "Assessment of energy distribution losses for increasing penetration of distributed generation," *IEEE Transactions on Power Systems*, vol. 21, no. 2, pp. 533–540, May 2006, doi: 10.1109/TPWRS.2006.873115.
[24] "Development of dispersed generation and consequences for power systems," *e-cigre*. [Online]. Available: https://e-cigre.org/publication/ELT_215_3-development-of-dispersed-generation-and-consequences-for-power-systems. [Accessed: 15-Dec-2019].
[25] J. de Joode, J. C. Jansen, A. J. van der Welle, and M. J. J. Scheepers, "Increasing penetration of renewable and distributed electricity generation and the need for different network regulation," *Energy Policy*, vol. 37, no. 8, pp. 2907–2915, 2009.
[26] S. J. Steffel, P. R. Caroselli, A. M. Dinkel, J. Q. Liu, R. N. Sackey, and N. R. Vadhar, "Integrating Solar Generation on the Electric Distribution Grid," *IEEE Transactions on Smart Grid*, vol. 3, no. 2, pp. 878–886, Jun. 2012, doi: 10.1109/TSG.2012.2191985.

[27] M. E. Baran, H. Hooshyar, Z. Shen, and A. Huang, “Accommodating High PV Penetration on Distribution Feeders,” *IEEE Transactions on Smart Grid*, vol. 3, no. 2, pp. 1039–1046, Jun. 2012, doi: 10.1109/TSG.2012.2190759.
[28] F. Blaabjerg, Y. Yang, D. Yang, and X. Wang, “Distributed Power-Generation Systems and Protection,” *Proceedings of the IEEE*, vol. 105, no. 7, pp. 1311–1331, Jul. 2017, doi: 10.1109/JPROC.2017.2696878.
[29] H. Margossian, G. Deconinck, and J. Sachau, “Distribution network protection considering grid code requirements for distributed generation,” *Transmission Distribution IET Generation*, vol. 9, no. 12, pp. 1377–1381, 2015, doi: 10.1049/iet-gtd.2014.0987.
[30] “Regulations for grid connection | Energinet.” [Online]. Available: https://en.energinet.dk/Electricity/Rules-and-Regulations/Regulations-for-grid-connection. [Accessed: 15-Dec-2019].
[31] “Simscape Electrical - MATLAB & Simulink.” [Online]. Available: https://www.mathworks.com/products/simscape-electrical.html. [Accessed: 15-Dec-2019].
[32] “PSCAD Overview | PSCAD.” [Online]. Available: https://hvdc.ca/pscad/. [Accessed: 15-Dec-2019].
[33] “Home,” *RTDS Technologies*. [Online]. Available: https://www.rtds.com/. [Accessed: 15-Dec-2019].
[34] A. Zahedi, “Developing a system model for future smart grid,” in *2011 IEEE PES Innovative Smart Grid Technologies*, Perth, WA, 2011, pp. 1–5, doi: 10.1109/ISGT-Asia.2011.6167326.
[35] T. Chakravorti, R. K. Patnaik, and P. K. Dash, “Advanced signal processing techniques for multiclass disturbance detection and classification in microgrids,” *IET Science, Measurement & Technology*, vol. 11, no. 4, pp. 504–515, Jul. 2017, doi: 10.1049/iet-smt.2016.0432.
[36] M. Farrokhabadi, S. Konig, C. A. Canizares, K. Bhattacharya, and T. Leibfried, “Battery Energy Storage System Models for Microgrid Stability Analysis and Dynamic Simulation,” *IEEE Trans. Power Syst.*, vol. 33, no. 2, pp. 2301–2312, Mar. 2018, doi: 10.1109/TPWRS.2017.2740163.
[37] M. Farrokhabadi, C. A. Canizares, and K. Bhattacharya, “Frequency Control in Isolated/Islanded Microgrids Through Voltage Regulation,” *IEEE Trans. Smart Grid*, vol. 8, no. 3, pp. 1185–1194, May 2017, doi: 10.1109/TSG.2015.2479576.
[38] R. Majumder, A. Ghosh, G. Ledwich, and F. Zare, “Load sharing and power quality enhanced operation of a distributed microgrid,” *IET Renew. Power Gener.*, vol. 3, no. 2, p. 109, 2009, doi: 10.1049/iet-rpg:20080001.
[39] M. A. Zamani, A. Yazdani, and T. S. Sidhu, “A Control Strategy for Enhanced Operation of Inverter-Based Microgrids Under Transient Disturbances and Network Faults,” *IEEE Trans. Power Delivery*, vol. 27, no. 4, pp. 1737–1747, Oct. 2012, doi: 10.1109/TPWRD.2012.2205713.
[40] Xiong Liu, Peng Wang, and Poh Chiang Loh, “A Hybrid AC/DC Microgrid and Its Coordination Control,” *IEEE Trans. Smart Grid*, vol. 2, no. 2, pp. 278–286, Jun. 2011, doi: 10.1109/TSG.2011.2116162.
[41] A. Colet-Subirachs, A. Ruiz-Alvarez, O. Gomis-Bellmunt, F. Alvarez-Cuevas-Figuerola, and A. Sudria-Andreu, “Centralized and Distributed Active and Reactive

Power Control of a Utility Connected Microgrid Using IEC61850," *IEEE Systems Journal*, vol. 6, no. 1, pp. 58–67, Mar. 2012, doi: 10.1109/JSYST.2011.2162924.
[42] M. Ramezani, S. Li, and Y. Sun, "Combining droop and direct current vector control for control of parallel inverters in microgrid," *IET Renewable Power Generation*, vol. 11, no. 1, pp. 107–114, Jan. 2017, doi: 10.1049/iet-rpg.2016.0107.
[43] O. Khan, S. Acharya, M. Al Hosani, and M. S. El Moursi, "Hill Climbing Power Flow Algorithm for Hybrid DC/AC Microgrids," *IEEE Trans. Power Electron.*, vol. 33, no. 7, pp. 5532–5537, Jul. 2018, doi: 10.1109/TPEL.2017.2779238.
[44] S. K. Kollimalla and M. K. Mishra, "Variable Perturbation Size Adaptive P O MPPT Algorithm for Sudden Changes in Irradiance," *IEEE Transactions on Sustainable Energy*, vol. 5, no. 3, pp. 718–728, Jul. 2014, doi: 10.1109/TSTE.2014.2300162.
[45] H. H. Zeineldin, M. S. El Moursi, and M. H. Syed, "Hybrid micro-grid operation characterisation based on stability and adherence to grid codes," *IET Generation, Transmission & Distribution*, vol. 8, no. 3, pp. 563–572, Mar. 2014, doi: 10.1049/iet-gtd.2013.0230.
[46] B. John, A. Ghosh, F. Zare, and S. Rajakaruna, "Improved control strategy for accurate load power sharing in an autonomous microgrid," *IET Generation, Transmission & Distribution*, vol. 11, no. 17, pp. 4384–4390, Nov. 2017, doi: 10.1049/iet-gtd.2017.0499.
[47] M. Hamzeh, A. Ghazanfari, H. Mokhtari, and H. Karimi, "Integrating Hybrid Power Source Into an Islanded MV Microgrid Using CHB Multilevel Inverter Under Unbalanced and Nonlinear Load Conditions," *IEEE Trans. Energy Convers.*, vol. 28, no. 3, pp. 643–651, Sep. 2013, doi: 10.1109/TEC.2013.2267171.
[48] "MAS based distributed automatic generation control for cyber-physical microgrid system," *IEEE/CAA J. Autom. Sinica*, vol. 3, no. 1, pp. 78–89, Jan. 2016, doi: 10.1109/JAS.2016.7373765.
[49] M. O. Faruque, Y. Zhang, and V. Dinavahi, "Detailed Modeling of CIGRÉ HVDC Benchmark System Using PSCAD/EMTDC and PSB/SIMULINK," *IEEE Trans. Power Delivery*, vol. 21, no. 1, pp. 378–387, Jan. 2006, doi: 10.1109/TPWRD.2005.852376.
[50] S. W. Mohod and M. V. Aware, "Micro Wind Power Generator With Battery Energy Storage for Critical Load," *IEEE Systems Journal*, vol. 6, no. 1, pp. 118–125, Mar. 2012, doi: 10.1109/JSYST.2011.2163015.
[51] A. H. Kasem Alaboudy, H. H. Zeineldin, and J. Kirtley, "Microgrid Stability Characterization Subsequent to Fault-Triggered Islanding Incidents," *IEEE Trans. Power Delivery*, vol. 27, no. 2, pp. 658–669, Apr. 2012, doi: 10.1109/TPWRD.2012.2183150.
[52] A. A. A. Radwan and Y. A.-R. I. Mohamed, "Modeling, Analysis, and Stabilization of Converter-Fed AC Microgrids With High Penetration of Converter-Interfaced Loads," *IEEE Trans. Smart Grid*, vol. 3, no. 3, pp. 1213–1225, Sep. 2012, doi: 10.1109/TSG.2012.2183683.
[53] N. Eghtedarpour and E. Farjah, "Power Control and Management in a Hybrid AC/DC Microgrid," *IEEE Trans. Smart Grid*, vol. 5, no. 3, pp. 1494–1505, May 2014, doi: 10.1109/TSG.2013.2294275.

[54] A. Ketabi, S. S. Rajamand, and M. Shahidehpour, “Power sharing in parallel inverters with different types of loads,” *IET Generation, Transmission & Distribution*, vol. 11, no. 10, pp. 2438–2447, Jul. 2017, doi: 10.1049/iet-gtd.2016.0570.
[55] “New Model of a Converter-Based Generator Using Electrostatic Synchronous Machine Concept,” *IEEE Trans. Energy Convers.*, vol. 29, no. 2, pp. 344–353, Jun. 2014, doi: 10.1109/TEC.2014.2303827.
[56] A. Yazdani and P. P. Dash, “A Control Methodology and Characterization of Dynamics for a Photovoltaic (PV) System Interfaced With a Distribution Network,” *IEEE Transactions on Power Delivery*, vol. 24, no. 3, pp. 1538–1551, Jul. 2009, doi: 10.1109/TPWRD.2009.2016632.
[57] E. Alegria, T. Brown, E. Minear, and R. H. Lasseter, “CERTS Microgrid Demonstration With Large-Scale Energy Storage and Renewable Generation,” *IEEE Transactions on Smart Grid*, vol. 5, no. 2, pp. 937–943, Mar. 2014, doi: 10.1109/TSG.2013.2286575.
[58] J. Eto *et al.*, “The CERTS Microgrid Concept, as Demonstrated at the CERTS/AEP Microgrid Test Bed,” 2018. .
[59] *Smart Power Distribution Systems*. Elsevier, 2019.
[60] H. Saadat, *Power System Analysis*, Third. PSA Publishing LLC.
[61] “Voltage-Sourced Converters in Power Systems : Modeling, Control, and Applications | Wiley,” *Wiley.com*. [Online]. Available: https://www.wiley.com/en-ca/Voltage+Sourced+Converters+in+Power+Systems+%3A+Modeling%2C+Control%2C+and+Applications-p-9780470521564. [Accessed: 16-Dec-2019].
[62] W. Cochran *et al.*, “What is the fast Fourier transform?,” *IEEE Transactions on Audio and Electroacoustics*, vol. 15, no. 2, pp. 45–55, Jun. 1967, doi: 10.1109/TAU.1967.1161899.
[63] M. G. Simes and F. A. Farret, “POWER QUALITY ANALYSIS,” in *Modeling Power Electronics and Interfacing Energy Conversion Systems*, IEEE, 2017, pp. 227–253.
[64] “Power Electronics: Circuits, Devices & Applications, 4th Edition.” [Online]. Available: /content/one-dot-com/one-dot-com/us/en/higher-education/program.html. [Accessed: 16-Dec-2019].

Appendix A

Summary of Comparison Between PSCAD and Matlab-Simscape

Comparison Factor	PSCAD	Matlab-Simscape
Step Size	Fixed	Fixed & Dynamic
Computation	Parallel	Sequential
Computation Time	Low	High
Solver Type	EMTDC	Varying (ODE Family, Runge Kutta etc.)
Load Modelling	PQ	Constant Z
Ease of Use	Moderate	Complex
Input Parameter	Completely Adjustable	Completely Adjustable
Availability	Expensive and industry only	Academia, Industry
System Size	Large Scale	Small Scale
Inter-Platform Communication	Capable of Data Export	Capable of Data Export and Computation Within Same Software
Library	Power System	Power System and Various Other Libraries
Analysis Study	Steady State and Transient	Steady State and Transient
Performance	Faster	Slower

Appendix B

PSCAD Photovoltaic Array Input Parameters

Photovoltaic Array Input Parameters
Array Name
Number of modules connected in series per array
Number of module strings in parallel per array
Number of cells connected in series per module
Number of cell strings connected in parallel per module
Reference irradiation
Reference cell temperature

Photovoltaic Cell Input Parameters
Effective area per cell
Series resistance per cell
Shunt resistance per cell
Diode ideality factor
Band gap energy
Saturation current at reference conditions per cell
Short circuit current at reference conditions per cell
Temperature coefficient of photo current

Matlab-Simscape Photovoltaic Array Input Parameters

Photovoltaic Array Input Parameters
Parallel strings
Series-connected modules per string

Module Data
Maximum Power (cannot be changed dependent on input parameters)
Open circuit voltage
Voltage at maximum power point
Temperature coefficient of open circuit voltage
Cells per module
Short-circuit current
Current at maximum power point
Temperature coefficient of short circuit current
Irradiance
Temperature